university of groningen

Optimal Energetic Management of the Combined Heat and Power Plant by A2A in Cremona, Italy

Master Research Project IEM

Author:
M. Sissing

Supervisors:
Prof. Dr. Ir. J.M.A. Scherpen
Prof. Dr. Ir. M. Cao

Additional Supervisors:
Dr. J.E. Machado Martinez
Dr. M. Cucuzzella

April 9, 2022

Abstract

Multi-carrier energy systems are a useful resource in reducing primary energy consumption and greenhouse gas emissions. Nonetheless, the complexity of these systems ask for intelligent operation to maximise benefits. Coordinated operation of integrated electricity, natural gas, and heat system can improve operational flexibility and reduce costs. In this thesis, we consider modelling and control aspects of the thermal energy generation and management of the district heating plant of the Italian company, A2A Energia, for the purpose of hourly, operational optimisation for a two-day ahead demand profile.

The proposed model incorporates linear part-load efficiency curves. Also, thermal energy storage is considered which adds flexibility to the system. The heating plant of A2A has two energy generation technologies to be optimised, a gas-based CHP and four gas boilers. Apart from the load percentages of these devices, also the thermal energy storage is controlled to minimise the cost of matching heat supply and demand. In addition, the amount of dissipated heat in the event of productions surplus is optimised.

The model is validated via backtesting, perform simulations using historical demand profile data and compare with historical operational data of A2A. Ultimately, the case study outcomes illustrate the potential energy savings when implementing this optimisation, predictive control strategy.

Contents

1 Introduction **1**
- 1.1 Introduction to the Project . . . 1
- 1.2 Research Focus . . . 3

2 Literature Review **5**
- 2.1 District Heating Plant . . . 5
- 2.2 Control Methods . . . 8
- 2.3 Optimisation Problems . . . 9

3 System Model **13**
- 3.1 System Configuration . . . 13
- 3.2 Model Formulation . . . 14

4 Higher-Level Control **23**
- 4.1 Problem Formulation . . . 23
- 4.2 Property Analysis . . . 28
- 4.3 The Solver . . . 32

5 Algorithm Verification **36**
- 5.1 Base Case . . . 36
- 5.2 Scenario I.A . . . 38
- 5.3 Scenario I.B . . . 40
- 5.4 Scenario II . . . 41
- 5.5 Scenario III . . . 42

6 Algorithm Performance **45**
- 6.1 Integration of Linearly Dependent Company Data . . . 45
- 6.2 Tuning the Artificial Cost Factors . . . 49
- 6.3 Model Validation . . . 50
- 6.4 Discussion of Results . . . 61

7 Concluding Remarks **62**
- 7.1 Limitations . . . 62
- 7.2 Further Work . . . 62
- 7.3 Conclusion . . . 64

A Demonstration for Scenario I.B **73**

Nomenclature - Abbreviations

Abbreviations

BF	Biomass Furnace
CHP	Combined Heat and Power
DH	District Heating
DMNL	Dimensionless
EH	Energy Hub
GB	Gas Boilers
IPM	Interior Point Method
LD	Local Demand
LHS	Left Hand Side
LP	Linear Problem
LR	Lagrangian relaxation
MES	Multi-energy system
MILP	Mixed Integer Linear Problem
MINLP	Mixed Integer Nonlinear Problem
MIP	Mixed Integer Problem
MOO	Multi Objective Optimisation
MPC	Model Predictive Control
NLP	Nonlinear Problem
OPF	Optimal Power Flow
RHS	Right Hand Side
SHS	Sensible Heat Storage
SoC	State of Charge
TS	Thermal Storage
WF	Waste Furnace

Nomenclature - Variables

Variables[1][2]

g^{CHP}	the natural gas energy consumption by the CHP unit [in Joules].
g_i^{GB}	the natural gas energy consumption per boiler [in Joules].
g^{in}	the total natural gas energy consumption [in Joules].
h^{δ}	the thermal energy dissipated into the atmosphere [Joules].
h^{BF}	the thermal energy output of the biomass furnace [in Joules].
h^{CHP}	the thermal energy output of the CHP unit [in Joules].
h^{D}	the thermal energy demand [in Joules].
h_i^{GB}	the thermal energy output per boiler [in Joules].
h^{out}	the total thermal energy output delivered to the customers [in Joules].
h^{TS}	the thermal charging ($h^{TS} > 0$) or discharging rate ($h^{TS} < 0$) of the TS [in Joules].
h_{Δ}^{TS}	the value difference between the (dis)charging rates per timestep.
h^{WF}	the thermal energy output of the waste furnace [in Joules].
p^{CHP}	the electric energy output of the CHP unit [in Joules].
p_i^{GB}	the electric energy consumption per boiler [in Joules].
p^{in}	the total electric energy consumption [in Joules].
p^{LD}	the local demand (i.e., electric self consumption) of the CHP plant [in Joules].
p^{out}	the total electric energy output sold to the grid operator [in Joules].
W^{TS}	the level of thermal energy stored in TS [in Joules].
η^{CHP}	the general operating efficiency of the overall CHP [dmnl]. This efficiency is time dependent w.r.t. the operating mode and ambient temperature.
η_i^{GB}	the operating efficiency of each individual boiler [dmnl]. This efficiency is time dependent w.r.t. the operating mode and ambient temperature.

Vectors

x	Vector whose components are the collection of the optimisation variables.

[1] Note, the time dependency of the variables is not explicitly displayed in the mathematical descriptions in this report but when discussing variables the time dependency is implicitly present. Also, the general time dependent notation of a variable $y(t_k)$ is considered equivalent to y_k, i.e.; $y(t_k) =: y_k$.

[2] There is a unitary coefficient factor (per hour) such that it is possible to work with either power or energy units.

Nomenclature - Parameters

Parameters

α^{TS} the proportional constant associated with the initial state of charge [dmnl].
ϵ_i^{GB} the fixed amount of electric energy required to keep each boiler in operation [in Joules].
γ^{GB} the coefficient relating electric energy consumption and heat production of each boiler [dmnl].
μ^{TS} the thermal dissipation rate of the TS [dmnl].
b the ratio between the storage efficiency and storage capacity [smnl].
c weight used in optimisation problem [dmnl]. Subscripts are added to represent the corresponding optimisation variable;

Subscript	**Optimisation variable**
g	natural gas grid price
ets	fine on CO2 emissions when burning gas.
tee	grant for reduced CO2 emissions when burning clean gas.
p	electric grid price for boiler consumption.
δ	artificial cost for dissipating thermal energy into the atmosphere.
out	electric sales price.
ts	artificial sales weight for maximising storage level in the tank.
Δ	artificial penalty for differences in (dis)charging rates per timestep.
c_{share}	artificial penalty to enforce production sharing among boilers.

C^{CHP} the capacity of the CHP unit [in Joules].
C_i^{GB} the capacity of each boiler [in Joules].
C_{tot} the total operational cost over the optimisation period.
C^{TS} the capacity of the thermal storage tank [in Joules].

1 Introduction

1.1 Introduction to the Project

Global energy demand is constantly increasing as a result of population growth [1]. To illustrate, the global growth of the natural gas consumption is depicted in Figure 1. The increase in energy demand has led to the emergence of more complex energy systems [2]. Many solutions have been created to optimise the complex multi-energy systems (MES) of today. A promising option is the energy hub (EH) concept, which can be described as a centralised energy unit that integrates the conversion, production, storage and consumption of multiple energy carriers to meet different types of demand [3]. Multiple energy infrastructures are combined into one central interface where the different energy carriers and systems interact in a synergistic way.

EH models use multi-generation systems, such as a combined heat and power (CHP) system (see section 2.1.2). This leads to improved efficiency and a drop in primary energy consumption and costs [4]. Furthermore, a specific demand can also be met in various ways as multiple energy conversion technologies are integrated into one EH system. Hence, also the reliability of supply is improved. Hence, the main advantage of integrated energy infrastructures is the efficient use of multi-generation systems, which translates into optimal use of energy resources, higher efficiency and reduced emissions and costs [5].

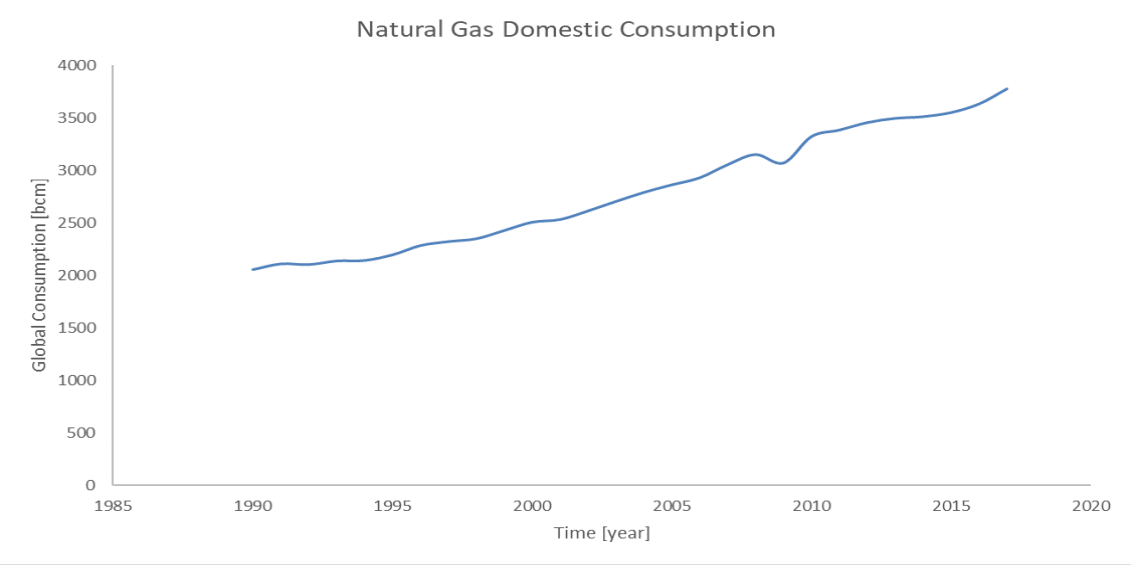

Figure 1: Growth pattern of the natural gas domestic consumption on global level [6]. The gas consumption is measured in billion cubic meters [bcm].

One type of energy hub is a district heating network. Heat is centrally generated by means of different energy carriers and transported to the domestic or industrial areas. To increase efficiency and supply demand economically often energy storage systems are implemented [7], [8]. This can provide crucial flexibility in balancing thermal energy, as excess heat can be easily stored in hot water tanks or backup energy can be provided in the event of production shortages [9]. In this thesis, A2A's district heating plant in Cremona is regarded. The Italian company, A2A Energia, generates and distributes energy services. For this research, the focus lays on their district heating service to the

end consumer in Cremona. Heating is generated by means of a CHP unit, natural gas based boilers, a waste furnace, and a biomass furnace. Apart from production devices, the company also manages thermal storage units, water tanks, which are operated in the event of production surplus or shortage. Transportation of the generated thermal energy happens through pipelines. The company has the desire to better tune its heat production to demand but at the same time wants to keep the costs low.

The case-study nature of this thesis contributes to the research field in a number of ways. Existing works typically focus on theoretical models (see [5] for a review and classification of existing research on EH models, and [10], [11] provide a review on optimisation of DH systems), while this project will focus more on the practical side by analysing real business data and forecasts. Moreover, the efficiencies of A2A's production devices will be incorporated in the model as linear dependent on the respective decision variables. While normally the efficiencies are considered as constants as done in [12], [13]. The inclusion of such a state dependency is beneficial because individual plant elements must be operated under these conditions most favourable for maximising its efficiency [14]. In fact, it is generally accepted that boiler load has a substantial impact on boiler efficiency. Taking this into account will better reflect reality and result in a cost reduction if efficiency is indeed maximised. Finally, this project can also potentially contribute to the research field with real-life experiments since it is possible to implement the results in A2A's plant and proof that solution works in practice.

Thesis Outline
A collaboration between the University of Groningen and the University of Pavia is established to focus on energy distribution networks. A2A came to the university of Pavia with their specific request to optimise their operation so that energy is used more efficiently, and production and demand are better balanced. This results in energy savings and minimises waste due to excess heat production. Therefore the problem statement is formulated as follows:

Problem Statement: *How to design an optimal operation scheme for A2A's District Heating plant which minimises operating costs and energy waste?*

The thesis is structured as follows, subsection 1.2 will structure the research by formulating research questions. Then section 2 elaborates on the current state of the literature of district heating networks and the control theories which are applied. In subsection 3.1 the system at A2A's plant in Cremona is configured and explained. subsection 3.2 goes more in depth about the model which is used to prioritise and optimise the energy flows in the plant. In section 4 a higher-level controller is introduced to find a solution to the optimal power flow problem. The cost function subject to (in)equality constraints is defined. In section 5 the algorithm is verified by testing hypotheses for multiple scenarios. section 6 elaborates on the integration of company data and the tuning of the artificial costs factors is explained. These both are required to check the performance of the algorithm by means of backtesting. The last sections, section 7 and subsection 7.3, show the limitation of the current research and the focus on further works to improve the energy distribution for A2A.

1.2 Research Focus

1.2.1 Research Goal

This research is highly case-specific as the optimisation model will be specifically designed for controlling A2A's DH plant, rather than analysing DH plants in general. As described earlier, A2A wants to better manage energy flows so that demand is met at all times at minimal cost. Therefore, the different components of A2A's DH plant must be integrated. The resulting mathematical model will be controlled using optimisation tools in MATLAB. Once the model is constructed, case studies are developed to verify the working of the operational optimisation method. Subsequently, the model is validated by comparing the solution of the developed optimisation problem with the available historical data of A2A (i.e., backtesting). The contribution of this case-specific project to the current knowledge base regarding DH plants, is to provide more insight in the operational implications of controlling DH plants. This insight is attained by the model and backtesting.

Research Goal: *To design a control strategy for the DH plant of A2A Energia aimed at hourly operational optimisation of thermal energy generation and storage for a two-day ahead schedule such that the operational costs of meeting heat demand are minimised.*

1.2.2 Research Questions

To achieve the research goal and structure the project, research questions are developed. A distinction can be made between knowledge and design questions [15]. Knowledge questions are recognised as questions that purely ask for knowledge about the world without any aim to improve it. Whereas, design questions aim for information directing towards a specific goal, in a specific situation. The questions are answered throughout the sections in chronological order.

1. What is the current state of DH plants in literature and what control methods are applied?
   This knowledge question will summarise the state of DH plants in literature. It will cover the different optimisation methods applicable for controlling the energy flows of a DH plant.

2. How is A2A's DH plant configured?
   This design question will map the layout of A2A's DH plant.

3. How will the simulation model of A2A's DH plant be designed?
   This design question will formulate the mathematical optimisation model based on the configuration of A2A's DH plant. The design choices will be motivated.

4. How will A2A's DH plant be controlled, taking into account future time steps?
   This design question will determine the higher level control strategy to create set-points for a two-day ahead schedule. This is based on the summary of optimisation methods applicable for DH plants.

5. Which case scenarios verify the model?
   This design question will formulate and analyse realistic case scenarios to test the working of the algorithm. This is an iterative process in which the algorithm is im-

proved and retested until satisfactory results are obtained that are consistent with the stated hypotheses.

6. What is the performance of the designed algorithm compared to A2A's historical data and what conclusions are drawn from these results?
   This knowledge question will validate the model via simulation with historical company data and analyse how the results add knowledge to the literature base.

2 Literature Review

2.1 District Heating Plant

A district heating (DH) network is a system that considers the distribution of heat being produced in a central location. This heat is then distributed to several end-users, who can be residential or commercial end-users. Transportation of the heat happens with (insulated) pipelines. A variety of energy supply technologies can be used for a DH system, such as: heat-only boiler, co-generation, heat pump, and thermal storage for buffer and seasonal purposes. To operate such devices either natural gas or biomass is used as fuel. Eventually, this integrated energy infrastructure facilitates space heating and/or provides hot water services. The benefit of integrating different energy types is the greater efficiency in the use of energy sources and environmentally friendliness compared to individual heating solutions [16], [17], [18]. A better efficiency implies reduced energy loss. As a result, less consumption and costs are incurred. Indirectly, also pollution is reduced. At the same time, DH systems also add complexity to the control of energy networks due to its intertwined energy nature. For instance, a CHP unit generates both electrical and thermal energy. As a result of this integration, the optimal operation must regard each energy vector [19].

A DH network, or more specifically, the connection facility of the integrated energy infrastructure can be referred to as the energy hub [5], [20]. Such an EH facilitates the energy production, conversion and storage. Therefore, the concept of an energy hub is briefly introduced in subsubsection 2.1.1. Furthermore, a DH network can be comprised of a variety of components. However, only these concepts that are present in A2A's DH plant are elaborated in subsections 2.1.2, 2.1.3, and 2.1.4.

2.1.1 The Energy Hub Concept

The energy hub concept was first introduced by Geidl and Andersson [3], [20], [21]. It is a centralised energy unit that integrates the conversion, storage, and distribution of multiple energy carriers [22], [23], [5]. This way, different energy infrastructures are combined in one central interface. An EH consumes power at the inlet ports supplied via a connection with, for instance, electricity and natural gas infrastructures. Subsequently, the energy is converted, conditioned and, when required, stored inside the hub. Eventually, the generated energy is supplied to the utility grid, intermediary, and/or end consumer [21]. A schematic visualisation of this process is depicted in Figure 2. The energy services are performed by the following basic elements: direct connections, converters, and storage devices. Direct connections simply ensure a connection between the input and output carrier without the interference of energy conversion processes. Whereas converters serve as couplings for different energy carriers by transforming power into other forms. Examples of converter elements are gas boilers, combined heat and power unit, combustion engines, and electric machines. The third element, storage devices, affect the energy stream due to the integral action. Storage units are employed in the event of an imbalance between production and demand [23]. Commonly, an EH also integrates renewable energy [24]. In the case of A2A, the plant is operated with renewable energy in the form of biomass waste. On top of that, other energy inputs are fossil fuels and waste energy.

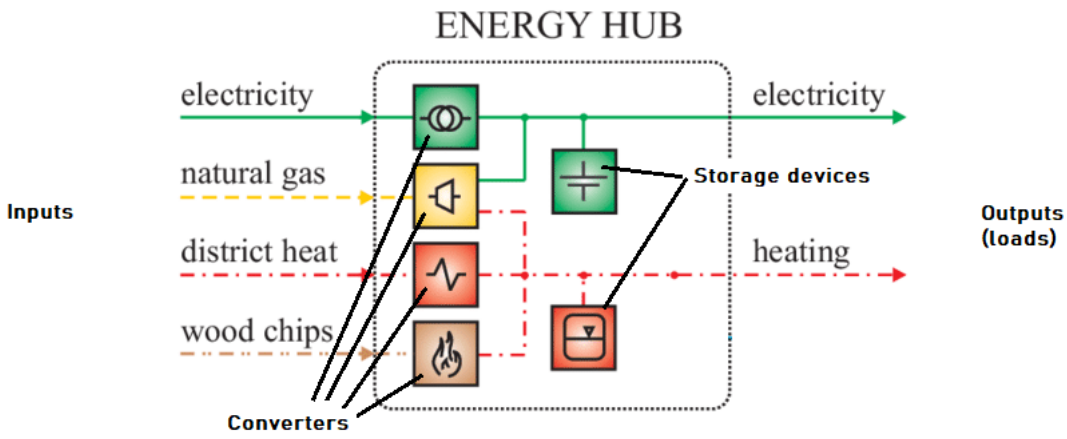

Figure 2: Schematic visualisation of an energy hub: a multi-source multi-product system [23].

2.1.2 Combined Heat and Power Unit

As the name suggests, a combined heat and power (CHP) system produces both heat and power. A simplified procedure of this process is depicted in Figure 3. In short, natural gas (or biogas) is converted into motive power by means of a burner and a turbine or engine. Subsequently, the motive power is converted into electricity by means of a generator. The electrical power is supplied or sold to the grid. In addition, energy losses are captured and supplied as thermal energy [25]. This way, less energy is lost and hence, the efficiency is increased. Typically, CHP production is controlled in accordance with the heat or electricity demand, i.e., heat-led or electricity-led strategy [26]. If for instance a CHP is applied in a district heating system, a heat-driven control strategy is usually employed [27]. Normally, water is then heated and the power output is a by-product used to suffice the local electricity demand. However, this may result in a mismatch between power supply and demand. This can be solved by selling excess power to the utility grid [28]. In addition, meeting local power demand can be ensured by constraining the CHP production in such a way. Whereas, in the event of a power-driven strategy, a storage tank can be included in the network to add flexibility in balancing thermal energy since excess heat can be stored easily in hot water tanks [29]. If preferred, the joint electricity and thermal production can be decoupled by means of such balancing measures [30], [31]. Apart from an output-driven strategy, it is also possible to control the CHP with a least-cost operating strategy [26]. In that case, the aim is to minimise the cost of meeting both the local electricity and heat demand. This is achieved by importing or exporting power depending on the electricity prices and the (dis)charging of the hot water storage tank is determined on a cost-optimal basis.

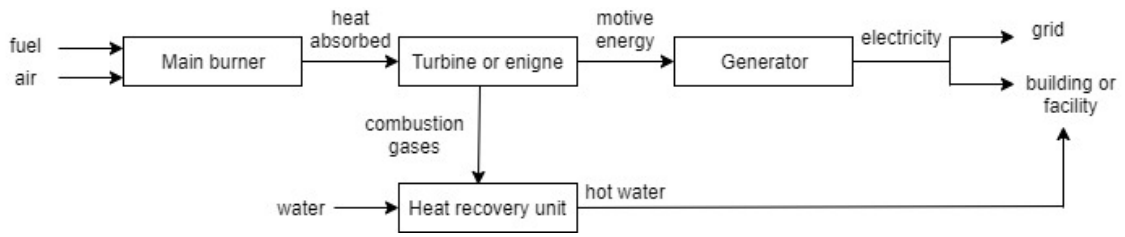

Figure 3: Simplified schematic of a CHP unit, inspired by [25].

2.1.3 Hot Water Storage Tank

Regularly, CHPs are installed together with a hot water tank for storage of thermal energy production. The tank stores the redundant energy or cheap energy and discharges when there is insufficient production or when the energy price is substantial [7]. Therefore, the tank functions as a temporary buffer to correct the imbalance between heat supply and demand [32]. In general, the minimum and maximum storage level depend on the mass of the storage material, m, the specific heat constant of the medium, c_p, and the difference between the room temperature and the minimum (maximum) temperature of the medium, $\Delta T_{m(M)}$ [29]. Specifically, for the water medium, the formula is given as follows,

$$W^{TS}_{m(M)} = m_{H2O} c_{p_{H2O}} \Delta T_{m(M)} \tag{1}$$

Water is one of the most commonly used storage media as it is inexpensive and has a high specific heat of $c_{p_{H2O}} = 4.18$ [kJ/(kg $^\circ C$)] [33]. According to [34], thermal losses of the storage are negligible. Apart from hot water storage, there are also other types of (thermal) energy storage methods. These, together with a discussion on design characteristics, can be reviewed in [35], [36], [37]. These are both beyond the scope of this study.

2.1.4 Natural Gas Boilers

Natural gas fired water boilers produce heat by boiling water. Thermal energy is supplied by burning natural gas which heats the water. In general, a boiler can be divided into two parts, the combustion chamber and heat exchanger. This is schematically represented in Figure 4. Within the combustion chamber (i.e., the burner), the natural gas reacts with dry air. When burning natural gas, the combustion products are carbon dioxide and water vapor. Subsequently, the water vapor heats the backwater from the heating system via a heat exchanger [38], [39]. The by-products are flue gas and heat loss. A more detailed performance study regarding burner types is present in [39].

The burner and heat exchanger are also the major contributors to energy loss within the conversion process. As a result, the energy input is always more than the output. Typically, the thermal efficiency of gas boilers is in the range of $70 - 80\%$ [38]. Apart from conversion losses, also heat is lost from the boiler's outer surface to the environment [17]. In the summer months, gas boilers are only operated to a small extent as heat demand is low during the warm summer months.

An detailed study regarding the boiler's thermal efficiency is provided in [40], where a mathematical model is compared with an actual boiler room. Furthermore, a review regarding boiler usage, techniques for evaluating the energy efficiency, and ways to reduce energy losses is provided in [41].

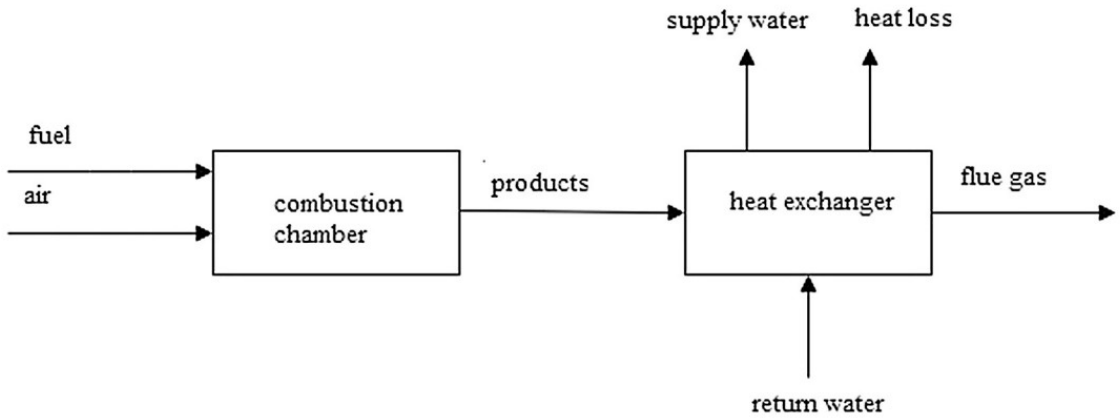

Figure 4: Schematic of a natural gas fired water boiler [17].

2.2 Control Methods

It is prevalent to employ one of the following methods when solving management and control problems in energy hubs: optimisation [5], game theory [42], bidding [43], or machine learning when considering smart energy hubs [44]. A brief description of each method is provided below for general understanding.

Optimisation: this method aims to optimise an objective function which is subject to (in)equality constraints, given a set of unknown optimisation variables [45]. This is referred to as the optimisation problem, where the constraints and the objective can either be linear or nonlinear. Energy management of DH networks is commonly regulated via optimisation [5]. As this is the aim of this research, a brief elaboration on the types of optimisation problems tailored to this study is provided in subsection 2.3.

Game theory: this method employs a cooperative framework. It determines the optimal solution by incorporating the relationship between the agents in a model. Particularly, game theory considers non-cooperative behaviour of the agents in the system. The challenge with this method is to obtain the assurance that the local optimum of each agent is also the global optimum. This study will focus on solving the problem in a centralised fashion disregarding network collaborations. Therefore, game theory will not be used in this study.

Bidding: this method focuses on maximising energy sales by finding the optimal bid that an energy hub can submit on the day-ahead market for both selling and buying of energy. This contributes to optimising the costs. This approach is not considered in this study as the energy market is not included in the scope.

Machine learning: this method formulates algorithms that continuously improve control systems by learning from empirical data. This data is used for forecasting so that future decision-making is improved. This method is useful for energy systems using intelligent technologies, such as a smart energy hub. A prerequisite for machine learning is the access to a substantial amount of data so that algorithm learning is enhanced. As the company has a limited data records and updates, this method will not be used in this study.

2.3 Optimisation Problems

Optimisation problems in DH networks are commonly solved by using one or a combination of the following mathematical tools: convex programming [46], [47], dynamic programming [48], [49], stochastic programming [12], [13], robust programming [22], [49], particle swarm optimisation [50], [51], and interior-point optimisation [52], [53]. This study will use the inter-point method (IPM) for optimising the problem. IPMs are suitable for nonlinear constrained optimisation problems, similar to the problem that will be defined in section 4. Furthermore, the solver[3] that will be used to solve this problem uses an interior-point approach (elaborated in section 4.3).

Apart from that, an optimisation problem can be cast in various ways, such as: linear problem (LP), nonlinear problem (NLP), mixed-integer linear problem (MILP), mixed-integer nonlinear problem (MINLP). In addition, when positioning such an optimisation problem different approaches can be used, for instance: Lagrangian relaxation (LR), centralised vs decentralised, and model predictive control. A brief elaboration, tailored to the relevance for this study, is provided in this subsection.

2.3.1 Linear vs Nonlinear Program

A system is considered to be nonlinear when the change in output is not proportional to the change in input. Although most real-life processes are nonlinear in nature, it is also common to implement linear models as a linear program (LP) can easily be derived from process data and lead to accurate results when operating near the operating point [54]. Furthermore, LPs are computational attractive due to the robust formulation and affine nature but the design may be conservative as opposed to nonlinear programs (NLP) [13]. However, if a NLP with great complexity is studied, it may be convenient to linearise the nonlinear equations around the optimum x^*. In general, a scalar nonlinear function $g(x)$ can be linearly approximated around the point x^* by employing the following equation,

$$g(x) \approx \frac{\delta g(x)}{\delta x} \Big|_{x=x^*} (x - x^*) \tag{2}$$

Note that in case $g(x)$ is not a scalar but $x \in \mathbb{R}^n$ then instead of computing the derivative, it is required to take the gradient,

$$g(x) \approx \nabla g(x)^T (x - x^*) \tag{3}$$

2.3.2 Mixed Integer Program

Mixed integer problem (MIP) is a type of program that explicitly considers the binary nature of a problem. This is incorporated by means of binary variables that indicate whether a device is running or not. This program is described in more detail in [55]. To illustrate the effect of mixed integer consideration, if for instance, a quadratic program[4] (QP) is compared with a mixed integer quadratic program (MIQP), then it turns out that the MIQP provides better solutions for the objective function, while the QP method is faster. The latter is logic as the MIQP explicitly considers the on-off behaviour [56]. Apart from, mixed-integer nonlinear problems (MINLP) such as a quadratic program, it is also

[3] A solver is considered a software package that contains one or more algorithms for finding solutions to a problem.

[4] The use of a linear model together with a quadratic objective function. Such a QP gives rise to a convex problem [54].

possible to employ the mixed-integer problem on linear programs (MILP). For example, in [57], [58], and [23] the operation of EHs is posed as a MILP, while in [59] and [60] this is formulated as a MINLP. Solvers suitable for mixed-integer problems are discussed by [61].

2.3.3 Lagrangian Relaxation and Duality

A general static optimisation problem is introduced to briefly discuss two concepts from convex optimisation, the Lagrange dual function and duality. Note that a more elaborate description of this theory can be found in [46].

The following primal problem is considered with cost F(x): $\mathbb{R}^n \to \mathbb{R}$ associated with the given variable $x \in \mathbb{R}^n$, the inequality constraints $g_i(x) \leq 0$, and equality constraints $h_j(x) = 0$ where $g_i, h_j : \mathbb{R}^n \to \mathbb{R}$. In other words, the primal problem is defined as

$$\begin{aligned} &\text{minimise} && F(x) \\ &\text{subject to} && g_i(x) \leq 0, \quad i = 1, ..., m, \\ &&& h_j(x) = 0, \quad j = 1, ..., p. \end{aligned} \tag{4}$$

The optimal solution with associated optimal value of (4) is denoted by $F(x^*)$. The solution is optimal when a feasible minimum solution is found. Furthermore, a point belongs to the feasibility set if the hard constraints are satisfied, i.e. any feasible point $\tilde{x} \in X$ with $X := \{x | g_i(x) \leq 0, h_j(x) = 0\}$. However, solving a primal problem implies that the constraints must be solved explicitly to find the optimal value x^*. When it is not required or not deemed possible to precisely meet the strict constraints, Lagrangian relaxation (LR) can be employed to provide more flexibility to the solution [29]. This is an effective means of reducing the solution complexity by relaxing the constraints of the primal problem with Lagrangian multipliers. This requires the introduction of the Lagrange dual function that takes into account not only the objective cost function but also Lagrangian multiplier vectors associated with the inequality and equality constraints (5). These Lagrangian multipliers, v_i and λ_j, have the interpretation of price and arise when the constraints are violated. Therefore, $v_i \geq 0$ because when $g_i(x) \leq 0$, implying that the inequality constraint is satisfied, the associated Lagrangian multiplier should contribute to a reduction of $L(x, v, \lambda)$. Whereas this multiplier should act as a penalisation such that it enlarges $L(x, v, \lambda)$ when the inequality constraint is violated, i.e., $g_i(x) > 0$. Alternatively, $h_j(x)$ should be penalised when it is unequal to zero and hence, λ_j can be both positive and negative. The primal problem is reduced to the unconstrained relaxed case, when all constraints are no longer strict but relaxed, $v_i = v_1, ..., v_m$ and $\lambda_j = \lambda_1, ..., \lambda_p$.

$$L(x, v, \lambda) = F(x) + \sum_{i=1}^{m} v_i g_i(x) + \sum_{j=1}^{p} \lambda_j h_j(x) \tag{5}$$

It follows that when the constraints are violated this imposes an extra cost proportional to the degree of violation. Moreover, to converge more quickly to a solution (i.e., enhance algorithm performance), the square of the constraint terms can be included in the objective function, which means that violation of the constraints is more heavily penalised [62], [63].

Finding the minimum of the Lagrange dual function in (5), for fixed v and λ implies finding a lower bound for the optimal value of F*. To illustrate, for any feasible point $\tilde{x}$

that does not violate the constraints, it follows that

$$\inf_{x\in\mathbb{R}^n} L(x,v,\lambda) \leq \inf_{\tilde{x}\in X} L(\tilde{x},v,\lambda) \tag{6a}$$

$$L(\tilde{x},v,\lambda) \leq F(\tilde{x}) \tag{6b}$$

This holds because the Lagrangian multiplier terms in (5) are respectively negative and equal to zero at $\tilde{x}$[5]. Ultimately, finding the best lower bound is referred to as the dual problem [29] and is defined as

$$L^* = \sup_{v_i\geq 0,\lambda} \inf_{x\in\mathbb{R}^n} L(x,v,\lambda) \tag{7}$$

where L* is referred to as the optimal value of the dual problem. It follows from (6b) that the optimal value of the primal problem can be expressed in terms of the Lagrange function

$$F^* = \inf_{x\in\mathbb{R}^n} \sup_{v_i\geq 0,\lambda} L(x,v,\lambda) \tag{8}$$

because $\sup_{v_i\geq 0,\lambda} L(x,v,\lambda) = F(x)$ when x is feasible and $\sup_{v_i\geq 0,\lambda} L(x,v,\lambda) = \infty$ when x is not feasible [29]. Continuing on this, the duality gap is defined as the distance between the solution of the Lagrangian dual problem and the solution of the primal problem, i.e., $L^* \leq V^*$. This is denoted as weak duality, when the duality gap is nonzero. This definition always holds regardless of the convexity of the primal problem.

2.3.4 Centralised, Decentralised vs Distributed Approach

If the optimisation problem is positioned in a centralised nature, only one decision-making agent is considered. A centralised algorithm uses global information. While in a decentralised network, multiple decision agents are considered each with its own local information. The agents operate a device on the basis of local information about the system. The centralised strategy offers optimal performance but is computational complex, while decentralised control has ease of implementation but also lower performance [64]. As a third approach, the benefits of both are combined in distributed control based on dual-decomposition and sub-gradient iterations. In that case, information sharing among the agents in the network is incorporated. Commonly, the information sharing is done between neighbouring agents in accordance with the information structure. The agents locally control system parts on the basis of this neighbouring information. Therefore, distributed networks are more robust to topological failures [65]. Hence, it has advantages with respect to robustness, energy delivery reliability, computational scalability, and as a result, the cost. However, the computational effort and system complexity increase as well when considering distributed networks.

2.3.5 Model Predictive Control

A Model Predictive Control (MPC) framework is useful when the DH network has to continually anticipate on the future situation in the form of updated forecast information [29], [66]. This framework incorporates predictions about the demand and technical constraints from the devices that need to be controlled [67], [68]. The MPC algorithm optimises with

[5]The Lagrangian multiplier associated with the equality constraints cancels out as the equalities are satisfied for any feasible point $\tilde{x}$, i.e., $h_j(\tilde{x}) = 0$. Similarly, the inequality constraints are met as well, i.e., $g_i(\tilde{x}) \leq 0$. As a result, $v_i g_i(\tilde{x}) \leq 0$ and possibly reduces the value of L. Therefore, $L(x) \leq L(\tilde{x})$ and also, $L \leq F$ for any feasible point $\tilde{x}$.

a receding horizon approach [69], which implies the problem is solved repeatedly taking into account future timesteps based on the model predictions. More specifically, with each iteration, the time horizon shifts one time instant forward. To clarify this with an example: in the first iteration, the problem is optimised for the next T hours, from t to t+T, while in the next solution step (t+1), the problem is solved over the time horizon from t+1 to t+T+1. At each iteration only the setpoints of the first time instant are implemented. Thereafter, the model predictions are updated based on the implemented setpoints and shifting one timestep forward. On the basis of the updated model prediction and updated time horizon, again the problem is solved with only the setpoints of the first time instant being implemented. For that reason, MPC can be viewed as the synergy of optimisation and machine learning. The benefit of MPC is that the solution is updated with each time instant to account for constantly changing circumstances in the system as time progresses [9]. Examples of studies that employed MPC in optimal energy management of EHs are [64], [70], [71].

3 System Model

First, this section will answer the research question *"How is A2A's DH plant configured?"*. The configuration and interconnections of the plant must be identified before establishing the mathematical model. Secondly, the mathematical model will be developed by answering the research question *"How will the simulation model of A2A's DH plant be designed?"*.

3.1 System Configuration

This section will provide an answer to the question *"How is A2A's DH plant configured?"*. In conjunction with subsubsection 2.1.1, the layout of the DH plant in Cremona can be considered as an energy hub. When developing an energy hub, two questions are fundamental: (1) in what way should the hub structure be designed, and (2) how to coordinate the hub operation with storage system interaction [21]. In the case of A2A, it is of interest to find an improved answer to the second question. The aim is to better manage the energy flows and storage schedule such that the costs of meeting heat demand are reduced to minimum. Therefore, the energy flows have to be described first. This is done by configuring the DH plant as an energy hub, which requires the identification of the inlet ports, conversion processes, and outlet ports.

3.1.1 Structure of A2A's DH Plant

There are multiple devices that contribute to the heat supply of A2A's DH plant in Cremona. The company produces heat by means of a combined heat and power (CHP) unit and eight gas boilers (GB). Both devices consume natural gas from a gas grid. In addition, the GB requires electric energy consumption from the grid to operate hydraulic pumps and other equipment such as valves. Furthermore, also external heat is delivered to the company which is supplied by a biomass furnace (BF) and waste furnace (WF). These four thermal energy sources cover the peak heat demand throughout the year. Apart from production, there is also local energy consumption. More precisely, the electric power produced by the CHP unit is used for the plant's own electricity consumption, referred to as local demand (LD). When the electricity produced by the CHP is redundant (i.e., production is greater than local demand), it is sold to the utility grid. The DH plant also houses a hot water storage tank to correct any imbalance between heat supply and demand. In the event of production surplus with a full storage tank, it is possible to dissipate the heat into the atmosphere, which is considered undesirable because potential revenue is wasted.

This structure and associated energy flows are depicted in Figure 5. The model mainly considers unidirectional coupling with a bidirectional link for the storage system. The main goal is to develop an automatic solution for the optimal energy management of the plant. Therefore, the model is examined at higher-level as it is mainly of interest to identify the required power input for each of the sources and the associated energy flows.

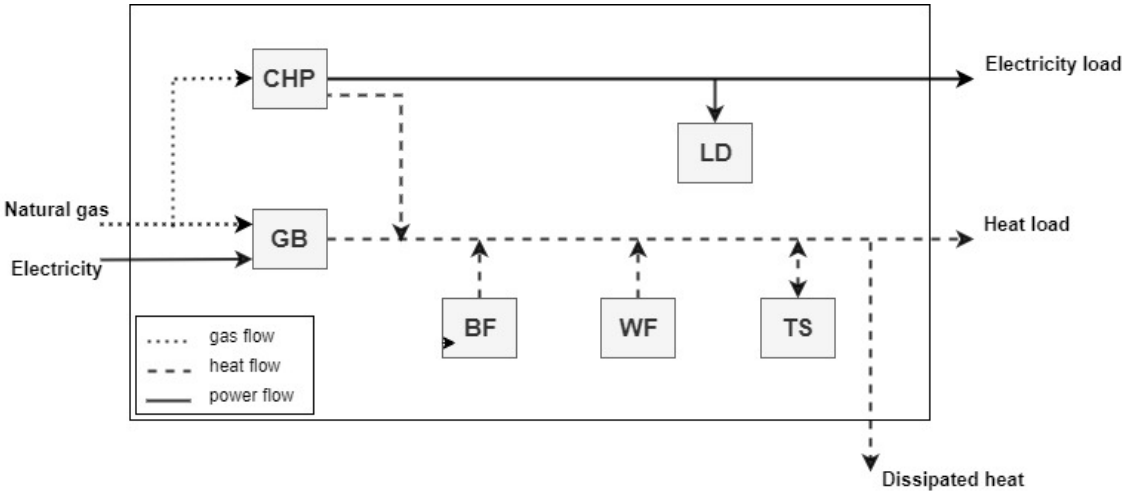

Figure 5: Topology of the DH plant in Cremona, inspired by the schematics in [13] and [12]. The inputs are natural gas and electricity from the grid, waste and biomass furnaces. The outputs are electricity (to the utility grid), heat supply, and heat dissipation. The following components are considered: Combined Heat and Power unit (CHP), Gas Boilers (GB), Biomass Furnace (BF), Waste Furnace (WF), Local Demand (LD), and Thermal Storage (TS).

The aim is to ensure that the overall heat demand is fulfilled. That is, the overall heat production minus the dissipated heat must match the heat load at all times. First it is noticed that, under the assumption that the considered DH plant is well dimensioned, a solution to this problem is always feasible due to the direct connection to the gas grid. Furthermore, the heat produced by the biomass and waste furnaces is assumed to be known. Also, the plant's electricity consumption, referred to as local demand, and the heat demand are assumed to be known. Furthermore, the capacities of the devices displayed in Figure 5 are known as well. These devices operate with a certain efficiency that vary with the degree of loading. However, such nonlinearity of part-load efficiency curves can be linearised at each optimisation step if preferred [72], [32]. Instead, historical company data can be provided from which the state dependent relations can be identified using techniques such as curve fitting. This is covered in subsection 6.1.

Note that the district heating network itself (i.e., grid connections) is excluded from the configuration. To this end, the following simplifying assumptions are in place: (1) there are no thermal losses within the distribution network and (2) heat supply is instantly delivered to the demand without the consideration of transportation delays. In fact, the latter can be relaxed as the demand prediction provided by A2A will be the profile at the consumer end. Therefore, the thermal lag and network losses are already accounted for in this production profile.

3.2 Model Formulation

This section will answer the research question *"How will the simulation model of A2A's DH plant be designed?"*. The mathematical model formulation is inspired by [13] and [12]. For general analysis on system level, steady state energy flow models are appropriate to use [21]. To clarify the formulation below, an extensive list of variables is introduced in the Nomenclature (see p. ii, iii). In Figure 6, these variables are linked to the topology of the plant.

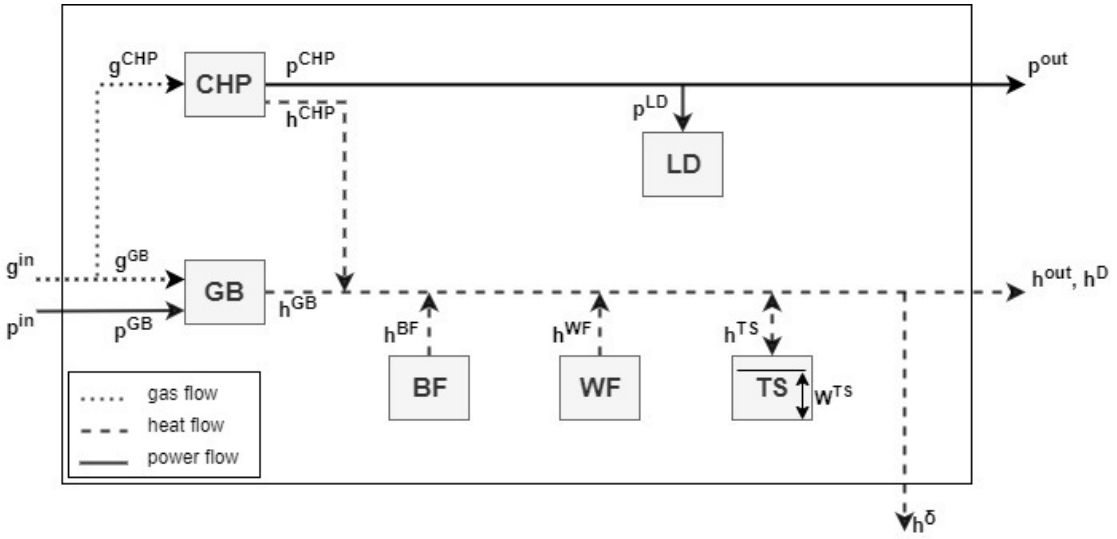

Figure 6: Representation of the main variables of the DH plant in Cremona.

3.2.1 Energy Balancing Conditions

The flows through the energy conversion devices can be modelled by defining the energy efficiency (i.e., the coupling) as the ratio of steady state energy output and energy input [32], [22], [24]. It is assumed that energy losses occur only in the conversion devices. Based on the topology presented in Figure 6, the energy flows and storage dynamics of A2A's DH plant at each time interval of 1 hour can be constructed as follows,

$$h^{\text{out}} = h^{D} \tag{9a}$$

$$h^{\text{out}} = h^{CHP} + \sum_{i}^{4} h_i^{GB} + h^{WF} + h^{BF} - h^{TS} - h^{\delta} \tag{9b}$$

$$p^{\text{out}} = p^{CHP}(h^{CHP}) - p^{LD}(h^{CHP}) \tag{9c}$$

$$g^{CHP} = \frac{h^{CHP}}{\eta^{CHP}(h^{CHP})} \tag{9d}$$

$$g_i^{GB} = \frac{h_i^{GB}}{\eta_i^{GB}(h_i^{GB})}, \qquad i = 1, ..., 4 \tag{9e}$$

$$p_i^{GB} = \epsilon_i^{GB} + h_i^{GB}\gamma_i^{GB}, \qquad i = 1, ..., 4 \tag{9f}$$

$$p^{in} = \sum_{i}^{4} p_i^{GB} \tag{9g}$$

$$g^{\text{in}} = g^{CHP} + \sum_{i}^{4} g_i^{GB} \tag{9h}$$

$$W_{+}^{TS} = W^{TS}(1 - \mu^{TS}) + bh^{TS}; \qquad W^{TS}(0) = \alpha^{TS} \tag{9i}$$

where

a. Equality (9a) ensures heat demand is met at every time step. There is no such restriction for electricity, because all that is produced by the CHP can be supplied to the electricity grid.

b. The heat balance condition is stated in (9b). The heat output of the DH plant, which is equal to the heat demand, is defined as the sum of all heat produced by the devices and thermal storage discharge minus the heat that is eventually dissipated into the atmosphere h^{δ}. At first sight it might seem as if the discharged thermal energy h^{TS} is subtracted from the total heat supply, while in fact it is the reverse. If the system was to extract thermal energy from the storage, this is indicated by the discharging rate $h^{TS} < 0$. Resultantly, in equation (9b) the discharging rate will be added to the total heat supply. On the other hand, if the storage tank is being charged (i.e., $h^{TS} > 0$) this amount is subtracted from the total heat production. Note that A2A operates a total of eight boilers, of which only the main four are considered in this study, as the other four boilers serve as backup boilers and are almost never operated[6]. Hence, these are disregarded in the problem formulation. Another annotation regarding equation (9b) concerns the variable h^{δ}. In the event of heat production surplus and if it exceeds the remaining space in the storage tank, a certain amount of heat needs to be flared [73] which is indicated by h^{δ}. This way, heat flaring corrects the imbalance between heat load and production.

c. The electric energy balance condition for the CHP plant is stated in (9c). The electrical energy generated by the CHP (p^{CHP}) is used for the plant's own consumption (p^{LD}), and the electrical redundancy is sold to the grid (p^{out}). For that reason, p^{out} must be non-negative at all times. Note that the electricity production and heat production of the CHP are linearly coupled. Similarly, the local electricity demand is also linearly dependent on the heat load. These two linear state dependent relations are derived from historical company data in section 6.1. Apart from that, the CHP will be controlled via a least-cost operating strategy, which was explained in more detail in section 2.1.2.

d. The overall input-output relation of the CHP with thermal efficiency[7] $\eta^{CHP} \in (0, 1]$, is provided in (9d). The thermal efficiency is linearly dependent on the heat load. This relation is derived from historical company data in section 6.1. The total CHP output consists of both thermal and electric energy but with one degree of freedom as these variables are coupled. This means that only one of these two outputs can be considered a decision variable, the other is accordingly co-determined via the coupling relation, defined in section 6.1. Once again, as the priority lies on heat production, it is decided to express the equation in terms of h^{CHP}. If there is excess heat, this can be stored in the storage tank.

e. Similarly, the input-output relation of the individual boilers is given in (9e) with efficiency, $\eta_i^{GB} \in (0, 1]$. The boiler efficiency differs with the heat load. The rela-

[6]These four boilers are close to the CHP plant and therefore cause a contribution to CO2 emissions when activated, leading to a fee for A2A.

[7]The thermal efficiency decreases and power efficiency increases with increasing CHP production, as demonstrated in section 6.1.

tion is derived from historical company data in section 6.1. The varying efficiency factor considers the heat exchange between gaseous fuel and boiling water, and normally also accounts for heat exchange between the boiler's external surface to the environment [40], [41].

f. The boilers consume electric energy, which is bought from the power grid. This is specified in (9g). It is expected that the power consumption of the boilers is going to be small compared to the gas consumption. Note that the electric demand of the boilers is twofold: *i*) a fixed amount of electric energy ϵ_i^{GB} is required at all times to keep the boiler in service and connected to the control room, and *ii*) a second portion of electric consumption is required to activate for instance the pumps and is thus related to the heat production via the coefficient γ_i^{GB}.
g. The gas balancing condition is provided in (9h), where the natural gas entering the DH plant is equal to the sum of the gas used by the CHP and by each of the boilers.
h. Equation (9i) describes the normalised thermal storage dynamics. The storage tank is used to answer heat fluctuations in demand and supply. A more detailed explanation can be found in the next subsubsection 3.2.2.

3.2.2 Thermal Energy Storage Dynamics

A2A operates a sensible heat storage tank. The energy carrier used for (dis)charging is water and also the heat storage medium is water. More specifically, the thermal energy is stored in a water tank by heating or cooling the water storage medium, depending on the charging or discharging operation mode [36], [37]. In equation (9i) the normalised state of charge is denoted by $W^{TS} \in [0, 1]$ representing the storage level at each time instant, where $W^{TS} = 1$ is a fully charged storage tank, and $W^{TS} = 0$ completely discharged. Furthermore, W_+^{TS} represents the storage level after (dis)charging energy while W^{TS} depicts the storage level before (dis)charging energy at time t. The normalised initial state of charge $W^{TS}(0)$ is specified as proportion of the thermal storage capacity with $\alpha^{TS} \in [0, 1]$. The storage level decreases not only due to discharge, but also due to thermal losses over time [12], [74]. Basically, thermocline decay is mainly caused by thermal losses to the ambient as stated by [75] and [76]. This is represented by μ^{TS} in (9i), the thermal dissipation rate of the storage tank. Similar to the approach taken in [73], in agreement with A2A it is assumed that there are no thermal losses in the storage system but for completeness this term is considered in the equation. Hence, $\mu^{TS} = 0$. Please note that in the storage dynamics it is assumed that there is no water leakage over time as A2A requires this to be disregarded.

Charging and discharging of the tank cannot happen simultaneously. More specifically, the variation in storage level during the considered time interval is described by h^{TS}, where $h^{TS} > 0$ is the amount of energy stored in the storage tank, while $h^{TS} < 0$ is the amount of energy extracted from the storage tank within the considered time interval. Furthermore, $b = 1/C^{TS}$ is the capacity ratio with $C^{TS} > 0$ to normalise the (dis)charging rate.

It is assumed that there are no losses during (dis)charging because normally these would occur due to the conversion of energy from the energy carrier to the storage medium. However, for the hot water storage tank there is no such conversion as both the energy carrier and storage medium are water. More specifically, the storage level is adjusted by adding hot or cold water, so no heat exchanger or other type of conversion device is involved. As a result, a lossless storage is assumed and hence, a thermal efficiency is neglected [32]. This simplification is justified because the model does not view the storage

dynamics at a lower level. If a more complex model needs to be implemented, this can be adapted by also considering a charging efficiency $f(h^{TS}) = \eta_c$ and discharging efficiency $f(h^{TS}) = 1/\eta_d$ [12], [13]. In other words, more energy than required is discharged, while during charging less energy is stored than that in fact is charged to account for energy losses.

In practical sense, the course of A2A's storage tank as defined in (9i) is synchronised with demand: discharging phase takes place in the mornings when there is peak demand, the charging phase takes place at night when demand is relatively low and excess heat is produced. This way, the storage tank contributes to reducing the extent to which excess heat has to be dissipated to the atmosphere. In other words, the (dis)charging rate represents the imbalance in heat supply and demand, which can mathematically be expressed as $h^{TS} = h^{CHP} + h^{GB} + h^{BF} + h^{WF} - h^{\delta} - h^{D}$. It is expected that in practice $h^{delta} = 0$ as long as $h^{TS} \neq 0$. In other words, when the storage is discharged, it is done at a controlled rate, so no heat dissipation is required. On the other hand, when the storage is charged, it is done at a rate fast enough to cause no heat dissipation unless the tank is completely filled.

Remark. *Note that, if indeed a thermal efficiency was to be considered ($\eta_d, \eta_c < 1$), the problem has to be translated to a mixed-integer problem (MIP) as two separate variables have to be introduced: one for charging and one for discharging. This is required to account for different charging and discharging efficiencies [32], [24]. In addition, it must be specified that charging and discharging cannot happen simultaneous. This complementarity can be strictly imposed via binary variables [12]. When considering MIP, the normalised storage dynamics would become as follows,*

$$W_{+}^{TS} = W^{TS}(1 - \mu^{TS}) + \frac{h_c^{TS}\eta_c^{TS} - h_d^{TS}/\eta_d^{TS}}{C^{TS}}$$

3.2.3 Constraints on the Performance of the Energy Devices

All the devices operate between lower and upper limits. As for the heat dissipation, an upper bound is installed to prevent excessive waste of heat. The operational variables introduced in subsubsection 3.2.1 are bounded by at most the capacity limits of the devices, where the capacities are non-negative: $C^{CHP} > 0, \quad C^{TS} > 0, \quad C^{GB} > 0$. The latter is written for convenience, even though it will not affect the optimisation problem since the capacities are known and positive. Basically, the proper functioning of the DH plant in Cremona is subject to the following set of constraints,

$$h_m^{CHP} \leq h^{CHP} \leq h_M^{CHP} \tag{10a}$$

$$h_{i,m}^{GB} \leq h_i^{GB} \leq h_{i,M}^{GB}, \qquad i = 1, ..., 4 \tag{10b}$$

$$W_m^{TS} \leq W^{TS} \leq W_M^{TS} \tag{10c}$$

$$-h_M^{TS} \leq h^{TS} \leq h_M^{TS} \tag{10d}$$

$$0 \leq h^{\delta} \leq h_M^{\delta} \tag{10e}$$

where

a. The inequalities in (10a) indicate the bounds on the thermal energy produced by the CHP unit. The bounds will be specified by A2A but are at least greater than zero due to the coupling of the heat and power output of the CHP. A certain minimum power output is required to ensure the CHP remains in operation because once activated in the winter months, the CHP is not shut down (it is too inefficient and requires transmission time[8]). Hence, the local electricity demand will be greater than zero and thus, $p_m^{CHP} \leq p^{CHP}$. As a result of the output coupling, the heat output will also be greater than zero, $h_m^{CHP} > 0$. The heat can be stored or dissipated into the air when redundant. A2A will provide per month the actual lower bound for the required amount of CHP production.
b. The inequalities in (10b) indicate the bounds on the thermal energy produced by each individual boiler, with $i = 1, ..., 4$. The bounds will be provided by A2A.
c. The inequalities in (10c) indicate the normalised bounds on the thermal storage level. The storage level is controlled by adding hot or cold water to the tank to regulate the inner temperature. The company operates within a fixed temperature range, [T_m, T_M]. This way, by considering the fixed temperature range ΔT and the capacity of the storage tank C^{TS}, it is possible to determine the minimum and maximum thermal storage level. Therefore, these bounds are calculated by substituting the company data into equation (1).
d. The inequalities in (10d) indicate the maximum amount of thermal energy that can be stored into or extracted from the tank within one time interval.
e. In (10e) the thermal energy dissipated into the atmosphere is imposed to be non-negative and smaller than a predefined value.

Remark. *Based on the simulations performed, it was decided not to consider positivity limits for the dissipation. This is more convenient for this study because it gives more flexibility to the solution. In the case where the maximum production is lower than the demand, still a solution can be provided instead of declaring convergence problems. To clarify, the dissipation becomes negative ($h^{delta} < 0$) to compensate for the production shortfall, so that mathematically the demand is still met (see equations (9a) and (9b)). To this end, A2A may decide to manually deviate from meeting demand and activate its remaining four backup boilers, which are excluded from the problem formulation, to supplement the residual of total production. For completeness, heat dissipation limits are not excluded from the model formulation.*

3.2.4 Prioritising the Gas Boiler Devices

Before further formulating the optimisation problem, the GB component has to be addressed first. This component is comprised by a set of five devices. However, the GB devices of A2A all operate in a different fashion with varying efficiency and hydraulic capacity. Some of these operating conditions are more preferable than others and hence, some devices must be prioritised with respect to others when optimising. Multiple procedures exist for optimising in a prioritised manner. In the paragraphs below, a brief review on prioritisation procedures is provided. This section finalises with the proposed solution to prioritise the boilers.

[8]Note that the transmission time for scaling up and down the CHP is neglected in the model. This could be included by imposing additional constraints that limit the rate at which the CHP can ramp up or down in a timestep

Prioritisation Procedures

Weighting the elements: As a first procedure, the elements of interest for the optimisation can be weighted differently, which results in a scalar objective function to be optimised. There are different types of weight that can be assigned, for instance: equal weights, rank order centroid weights, and rank-sum weights [77]. Assigning a type of weight depends on the type of relative importance. For example, if all elements are of equal importance, it is convenient to consider equal weight factors.

Multi-objective optimisation: Another way of formulating the problem is by means of multi-objective optimisation (MOO), which implies optimising multiple objectives in a prioritised manner. For example, [78] employed an algorithm that operates in this fashion. Similarly, [77] provides a review on MOO and proposes two mathematical methods: Pareto and scalarisation. The former keeps the elements of the optimal solution vector independent and solutions are differentiated by dominance and non-dominance. Pareto optimality is achieved when one objective function cannot be optimised further without having a detrimental effect on the other objective functions. Whereas in the scalarisation method, weights are assigned to the individual objectives prior to optimisation. This results in the formulation of a scalar function which is incorporated in the fitness function. More information regarding the state-of-the-art methods applicable for MOO problems is provided by [79]. Besides, the problem can also be formulated without explicitly weighting the objectives. In that case, the objectives can simply be ordered in the preferred sequence of optimisation. To clarify with an example tailored to this study: always employ the full capacity of the boiler with greatest preference first, then the full capacity of the boiler with second greatest preference, and so forth. Approaching the prioritisation in this way guarantees that the lower priority objectives are optimised if and only if this does not affect the higher priority objectives (i.e., non-Pareto optimal solution) as demonstrated by [80]. This way, it is possible to eliminate or rearrange objectives without rebalancing the problem. However, it is required that the first n-1 objectives are not strictly convex. Otherwise, the lower priority objectives would become obsolete in the existence of a unique solution.

Mixed-integer problem: A more sophisticated approach would be considering the problem as mixed-integer. This way, switching devices on and off is hard-coded by means of integer constraints [81]. Although the outcome might be realistic, the complexity and computational effort of the problem solving is increased when considering mixed-integer [56]. For more information see subsubsection 2.3.2.

Solution for Boiler Prioritisation

Operator Experience

Despite these different methods, this study will opt for a more simplified approach. Crucially, A2A prefers to operate the boilers with greatest hydraulic capacity to ensure that hot water is pumped from the source to the destination. A secondary prioritisation, if two boilers have the same hydraulic capacity, is based on the efficiency. Apart from these prioritisation rules, the order of activation is ultimately controlled based on the operator's experience, such as, which boilers are located closest to the demand.

Consequently, boiler operation does not adhere to strict priority rules, making it difficult to account for individual priority variables. In fact, the company has constrained not to control which boiler is used. However, if no distinction is made between individual

boilers[9], some crucial characteristics (individual efficiency and hydraulic capacity) will not be captured, resulting in a less accurate representation of A2A's situation.

Heat Sharing Approach
To this end, it is decided to opt for a weighted heat production sharing approach among all boilers. The variable representing the boiler's heat production ($h_i^{GB}|_{i=1}^4$) is multiplied with a weight (w_i) representing the frequency of operation (i.e. the boiler's respective hydraulic capacity). To force production sharing scaled to the frequency of operation, which we infer from historical company data, the individual boiler expressions should be equal to one and another,

$$\begin{aligned} w_i &= \frac{1}{C_i} \\ w_i h_i^{GB} &= w_j h_j^{GB}, \quad i \neq j \end{aligned} \tag{11}$$

To illustrate the implication of this heat sharing approach: when boiler 1 has a greater hydraulic capacity than boiler 2 (i.e., $C_1 > C_2$), then according to (11) boiler 1 has to produce more than boiler 2 (i.e., $h_1^{GB} > h_2^{GB}$) to ensure that expression (11) holds, i.e., $\frac{1}{C_1} h_1^{GB} = \frac{1}{C_2} h_2^{GB}$. This way, the solution does account for the boilers' individual characteristics, i.e., frequency of operation as a function of hydraulic capacity and the associated coupling (i.e., boiler efficiency). This gives a better representation of A2A's actual situation. While simultaneously, A2A's operators are provided with the freedom to control which specific boilers to switch on or ramp up in practice and to which extent. The latter is possible, because the overall heat production of the boilers (instead of individual boiler production) will be provided to the company: $h^{GB} = \sum_{i=1}^4 h_i^{GB}$.

When regarding (11) as strict equality constraints, this may give rise to an infeasible solution in some situations as there is a lower and upper bound as to how much each boiler can generate. Therefore, Lagrangian relaxation is employed on these constraints (see subsubsection 2.3.3). This way, more flexibility in the solution is provided as it is sufficient to approximate this heat sharing behaviour.

Note that it is also possible to find an equivalent representation of these constraints using graph theory [82]. In that case, the boilers are regarded as nodes and the heat sharing among the boilers are denoted as edges in the graph. This graph representation makes it possible to express the heat sharing constraints mathematically via the incidence matrix, B. The rows of the incidence matrix represent the amount of nodes (n), while the columns represent the links (m). Hence, $B \in \mathbb{R}^{n \times m}$ with the matrix elements being,

$$b_{ij} = \begin{cases} +1, & \text{if } n_i \text{ is the source of } m_j \\ -1, & \text{if } n_i \text{ is the sink of } m_j \\ 0, & \text{otherwise} \end{cases} \tag{12}$$

In case of an undirected graph, an arbitrary direction for each link can be chosen. To illustrate how to use this incidence matrix for the heat sharing, an elaboration is provided below. First, the heat sharing constraints are provided,

[9] One possible solution could be aggregating the boilers. This would require to approximate an overall boiler efficiency and production.

$$w_1 h_1^{GB} = w_2 h_2^{GB}$$
$$w_2 h_2^{GB} = w_3 h_3^{GB}$$
$$w_3 h_3^{GB} = w_4 h_4^{GB}$$

This way, all boilers indirectly adhere to weighted heat sharing with each other. On the basis of these constraints and the graph representation in Figure 7, the corresponding incidence matrix and constraint expression can be composed,

$$B^T = \begin{bmatrix} 1 & -1 & 0 & 0 \\ 0 & 1 & -1 & 0 \\ 0 & 0 & 1 & -1 \end{bmatrix}$$
$$B^T \mathbf{h^{GB}} = 0$$

with $\mathbf{h^{GB}} = [h_1^{GB}, h_2^{GB}, h_3^{GB}, h_4^{GB}]^T$.

When writing these strict heat sharing constraints in matrix format, still Lagrangian relaxation can be used when formulating the optimisation problem. Note that, when an augmented Lagrangian penalty term in matrix format is added to the cost function, the transpose must be considered for squaring, BB^T. In fact, this results in the Laplacian matrix: $L = BB^T$. More information on graph theory can be found in [82].

Despite this equivalent matrix representation, the constraints will be explicitly coded so that the concept is easier to grasp. Also, the speed of convergence for some solvers may depend on the connectivity of the underlying graph defining the Laplacian matrix [83], [84]. Therefore, the heat sharing will be coded explicitly to avoid any ambiguity on how to define the graph.

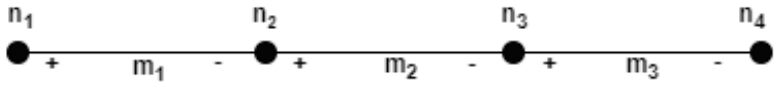

Figure 7: Graph representation of heat production sharing with four boilers.

4 Higher-Level Control

This section will answer the research question *"How will A2A's DH plant be controlled, taking into account future time steps?"*. To this end, a higher-level model is considered as the focus is on optimal energy management of the plant. Furthermore, optimisation can be executed in a static manner as the company requested offline optimisation. The static problem of A2A will be translated into a conventional optimisation problem: solving a set of optimisation variables with respect to inequality and equality constraints.

First, the multi-variable optimisation problem is formulated and analysed using multiple criteria: energy cost, carbon emissions, energy waste, storage usage, and production sharing among boilers. These different criteria are combined in one objective function. This way, the problem is described as a multi-objective optimisation [21]. Eventually, the optimal dispatch strategy is determined on the basis of the collection of the following data: device parameters, linear device variable relations, electricity price, gas tariff, forecast of external heat input from the furnaces, and heat demand forecast. Ultimately, this optimal dispatch strategy will be compared with A2A's historical energy consumption data. This comparison is covered in the section 6.

Remark. *An offline optimisation approach is considered because at the specific time of the optimisation no data is received: no system feedback and low update frequency. Consequently, the solver does not react to disturbances and changes in actual demand. Instead, it uses profile predictions of the next 48 hours and solves the static optimisation problem every 24 hours. However, if setpoints were calculated more frequently and if at the time of calculation the setpoints of the previous solution and (more importantly) the updates of system data at that specific time are used, then it would be considered online optimisation.*

4.1 Problem Formulation

Although this research is focused on thermal heat management, it is comparable to the Optimal Power Flow (OPF) problem [85]. This type of problem is focused on determining the optimal power generation from large power plants given the line power constraints [29]. The objective is to minimise generation cost whereas the balance problem is included as a hard constraint. A similar objective is applicable for A2A with the only difference being the energy focus, heat instead of power. It is a steady state optimal control problem. Moreover, the problem will be solved in a centralised fashion which makes it easier to include predictions of the future situation of the network as there is one decision-making agent possessing and sharing all information.

The main goal is to minimise the costs of heat generation and to maximise the associated revenues, such that supply and demand are matched. The priority of each minimisation and maximisation term is reflected by the weighting factor used on that term. In addition, the matching of supply and demand is specified as a hard constraint[10] and this is possible due to usage of conventional energy sources (i.e., no uncertainty from renewables).

[10] If it is not deemed possible to impose a hard constraint, Lagrangian relaxation may be applied [46].

4.1.1 Preliminary Cost Function

The preliminary[11] cost function is defined in (15) where the daily operation cost is composed of the following parts: natural gas purchases (c_g), carbon emission fee associated with gas burning at the CHP plant location (c_{ets}), and net electricity purchases (c_p). In addition to the costs, a grant is provided for burning gas of clean-quality as this results in reduced CO2 emissions (c_{tee}). Also, CHP electricity sales are generated when sold to the grid (c_{out}). Optimising revenue generation is employed in a similar fashion as done in [86]. However, maximising revenue is similar to minimising the negative value of revenue. As a result, the multi-objective optimisation problem reads as follows,

$$
\begin{aligned}
\min \quad & C_{\text{tot}} = \sum_{t_k=1}^{K} \Bigg(c_g(g^{CHP} + \sum_{i=1}^{4} g_i^{GB}) + c_{\text{ets}} g^{CHP} + c_p \sum_{i=1}^{4} p_i^{\text{in}} - c_{\text{tee}} p^{CHP} - c_{out} p^{\text{out}} \\
& \qquad - c_{\text{ts}} W^{TS^T} W^{TS} C^{TS} + c_\Delta h_\Delta^{TS^T} h_\Delta^{TS} + c_\delta h^{\delta^T} h^\delta \\
& \qquad + c_{\text{share}} \sum_{i=1}^{3} \sum_{j=2}^{4} (w_i hi^{GB} - w_j hj^{GB}) \Bigg), \qquad i \neq j \\
\text{s.t.} \quad & \text{Energy balance constraints (9a)-(9h)} \\
& \text{Thermal storage dynamics (9i)} \\
& \text{Capacity constraints (10a)-(10e)}
\end{aligned}
\tag{15}
$$

where the time horizon K is equal to 48 hours with 1 hour as a calculation period. The algorithm optimises the problem hourly for a two-day ahead schedule using forecasts of heat demand and supply from the biomass and waste furnaces.

Apart from energy purchases, artificial cost factors are included as well to penalise fluctuating (dis)charging rate behaviour over the time horizon (c_Δ), to enforce minimisation of lost revenues from dissipated energy (c_δ), and to encourage production sharing among the boilers (c_{share}) as explained in subsubsection 3.2.4. Note that this set of equality constraints for weighted boiler sharing is appended to the objective function using Lagrangian relaxation (see section 2.3.3), as it is attempted to approximate the frequency of operation but not required to precisely capture it. The motivation for minimising the (dis)charging rate differences is to ensure stable and smooth rather than fluctuating and angular results for the optimised variables. Moreover, minimisation of the dissipated heat is adopted from the reverse approach of [13], where efforts are made to minimise the amount of load shedding because there is no guarantee of sufficient production due to uncertainty of renewables. In this case it is likely to be the other way around: dependence on fossil sources makes a production surplus more likely than a deficit [9]. Therefore, equation (15) tries to minimise reverse load shedding, i.e., minimise the amount of excess heat. As the company is focused on generating profit, the aim is to either sell or store heat and by all means not to waste it. Hence, it is reasonable that c_δ will be set to a large value to avoid heat loss when possible. Furthermore, an artificial weighting term is included to maximise the amount of stored energy over the time horizon (c_{ts}). The latter is installed to encourage back-up supply as a buffer for uncertainties, such as sudden changes in demand or supply.

[11] It is denoted as the preliminary cost function because the optimisation variables, over which the problem should be optimised, have not yet been defined.

In the current model, uncertain factors are disregarded as the storage tank is expected to mitigate the negative impact of a sudden malfunctioning production device or a sudden peak in demand. In conjunction with this, a sudden drop in demand can also be answered by the storage tank. In case the tank is fully charged, excess heat can be dissipated to the atmosphere. Also, gas supply from the grid is fairly unlimited and hence, in principal demand is met at all times.

Remark. *A2A considers an optimisation horizon of 48 hours because the demand forecast is accurate enough. If the data is available, then in principal better results can be expected when extending the optimisation horizon. The latter holds because the solution of the current timestep accounts for what is going to happen in the future. Especially, since the operation is more or less cycling with a comparable demand profile for each day. However, care should be taken that the longer the predictions are away in the future also the predictability becomes less reliable, principally since demand forecast depends on weather. Hence, the consideration of $T = 48$ with accurate demand forecast.*

4.1.2 Identifying the Optimisation Variables

The preliminary objective in (15) is defined in terms of the unknown inputs and outputs of the energy hub on device level (see Figure 6), except for the matching of supply and demand which is specified as a hard constraint. These unknowns are collected as components in the control vector $\mathbf{x}$, specified in (16). Optimisation implies finding the optimal feasible point of the vector $\mathbf{x}$: the point that satisfies all constraints and minimises the objective function [46].

$$\mathbf{x} = \left[(\mathbf{h^{CHP}})^T, (\mathbf{h_1^{GB}})^T, (\mathbf{h_2^{GB}})^T, (\mathbf{h_3^{GB}})^T, (\mathbf{h_4^{GB}})^T, (\mathbf{W^{TS}})^T, (\mathbf{h^{TS}})^T, (\mathbf{h}^{\delta})^T\right]^T \tag{16}$$

In fact, for the larger part of the components, it is a set of non-negative real numbers, $\mathbb{R}^+ = [0, \infty)$. The exceptions to this are the normalised state of charge $W^{TS} \in [0, 1]$ and the rate of (dis)charge $h^{TS} \in \mathbb{R}$. The latter is a real number as it can be positive or negative, depending on charging or discharging the storage tank. The control variables are displayed in bold to indicate that it is the collection of the variable at each time step of the optimisation horizon. To clarify by means of an example: $\mathbf{h^{CHP}} = \left[h^{CHP}(t_1), h^{CHP}(t_2), ..., h^{CHP}(t_n)\right]^T$, with $n = K = 48$. Note that the general time dependent notation $y(t_k)$ is equivalent to y_k, i.e.,

$$y(t_k) =: y_k$$

A couple of remarks regarding the components of the control vector $\mathbf{x}$ in (16) in relation to the preliminary objective to be optimised in (15):

- The first component, h^{CHP}, is the optimisation variable for the gas input to the CHP: g^{CHP} of the objective in (15). The CHP gas consumption is associated with gas purchase costs and a fine on CO2 emissions. In addition, a subsidy is granted to A2A for reduced CO2 emissions when producing CHP electricity. This is maximised by also optimising h^{CHP}, because $p^{CHP}(h^{CHP})$. In addition, h^{CHP} is also collected in $\mathbf{x}$ to maximise the electrical energy sold to the grid, p^{out}. To clarify, p^{out} is defined in terms of the unknown variables $p^{LD}(h^{CHP})$ and $p^{CHP}(h^{CHP})$. This was defined in equation (9c).
- The second component, h_i^{GB}, are the optimisation variables for each gas boiler. This variable is regulated to minimise both the gas and electricity consumption of each

boiler, g_i^{GB} and p_i^{GB} of the objective in (15). In addition, this optimisation variable is also controlled to enforce heat production sharing among all boilers.

- The third and fourth component, h^{TS} and W^{TS}, are collected in (16) to control the storage tank when matching supply and demand at minimum cost. Despite both variables being related to the storage tank, they are independent of one another. Therefore, both need to be optimised separately and the constraints on the state of charge (W^{TS}) and on the rate of charge (h^{TS}) have different bounds. It is a dynamic portion with h^{TS} an independent control input and W^{TS} an independent variable. Indeed by controlling h^{TS}, W^{TS} is manipulated but a trajectory is needed to select a specific value for W^{TS}. More specifically, with h^{TS} only the future value of W^{TS} can be adjusted not the value at the current instant of time. Therefore, the optimisation should be distinguished. The storage level can be maximised to ensure a buffer for sudden changes in demand or production. Whereas the differences in (dis)charging rates are minimised to ensure the behaviour of the optimisation variables is stable and smooth rather than fluctuating and angular. The weights associated with these terms are small with respect to the other cost factors to keep flexibility in (dis)charging and prioritise optimisation of the actual costs. In fact, the storage level maximisation weight is set to zero since A2A does not require back-up supply.
- The final component, h^{δ}, is the control variable for minimising the heat dissipated into the atmosphere. This is similar to the variable considered in the preliminary objective in (15).

Remark. *Artificial quadratic terms for the storage are added to the objective due to the observed issue of fluctuating and edgy chart behaviour of the optimisation variables when the storage is not included in the objective. These fluctuating edgy results are irrespective of whether the input variables are static. A conclusive explanation for this phenomenon could not be found, only a hypothesis is provided. The stored heat is a free parameter within its bounds when it is not considered in the objective. Consequently, the solver provides a free solution for the storage tank within its bounds when demand does not approach or exceed production capacity or when energy prices are fixed. Therefore, as a solution, small quadratic optimisation terms for the storage are added to the objective to enforce optimised storage usage. Note that these terms will be chosen considerably small so that the solver is primarily focused on optimising the terms related to the actual costs.*

4.1.3 Explicit Cost Function

The preliminary objective in (15) can be expressed in terms of $\mathbf{x}$ in (16). Therefore, the explicit cost function based on the relationships defined in (9c) till (9h), reads as follows,

$$\begin{aligned} C_{\text{tot}}(f(\mathbf{x})) = \sum_{t_k=1}^{K} \Bigg(& c_g \left(\frac{h^{CHP}}{\eta^{CHP}(h^{CHP})} + \sum_{i=1}^{4} \frac{h_i^{GB}}{\eta_i^{GB}(h_i^{GB})} \right) + c_{\text{ets}} \left(\frac{h^{CHP}}{\eta^{CHP}(h^{CHP})} \right) \\ & + c_p \left(\sum_{i=1}^{4} (\epsilon_i^{GB} + h_i^{GB} \gamma_i^{GB}) \right) - c_{\text{tee}} p^{CHP}(h^{CHP}) \\ & - c_{out}(p^{CHP}(h^{CHP}) - p^{LD}(h^{CHP})) - c_{\text{ts}} W^{TS^T} W^{TS} C^{TS} + c_{\Delta} h_{\Delta}^{TS^T} h_{\Delta}^{TS} \\ & + c_{\delta} h^{\delta^T} h^{\delta} + c_{\text{share}} \sum_{i=1}^{3} \sum_{j=2}^{4} (w_i hi^{GB} - w_j hj^{GB}) \Bigg) \qquad i \neq j \end{aligned} \tag{17}$$

Furthermore, the control variables in (16) are imposed with inequality constraints as specified in (10a) till (10e). These constraints can be written more compactly in the form $M\mathbf{x} \leq b$, with $M \in \mathbb{R}^{16\times 8}$ a matrix with the coefficients, $\mathbf{x} \in \mathbb{R}^{8\times 1}$ a column vector of the constrained control variables, and $b \in \mathbb{R}^{16\times 1}$ a column vector of the bounds. Note, the lower bound constraints are converted to upper bound constraints by multiplying both sides of the constraint with factor -1,

$$M = \begin{bmatrix} -1 & 0 & 0 & 0 & 0 & 0 & 0 & 0 \\ 1 & 0 & 0 & 0 & 0 & 0 & 0 & 0 \\ 0 & -1 & 0 & 0 & 0 & 0 & 0 & 0 \\ 0 & 1 & 0 & 0 & 0 & 0 & 0 & 0 \\ 0 & 0 & -1 & 0 & 0 & 0 & 0 & 0 \\ 0 & 0 & 1 & 0 & 0 & 0 & 0 & 0 \\ 0 & 0 & 0 & -1 & 0 & 0 & 0 & 0 \\ 0 & 0 & 0 & 1 & 0 & 0 & 0 & 0 \\ 0 & 0 & 0 & 0 & -1 & 0 & 0 & 0 \\ 0 & 0 & 0 & 0 & 1 & 0 & 0 & 0 \\ 0 & 0 & 0 & 0 & 0 & -1 & 0 & 0 \\ 0 & 0 & 0 & 0 & 0 & 1 & 0 & 0 \\ 0 & 0 & 0 & 0 & 0 & 0 & -1 & 0 \\ 0 & 0 & 0 & 0 & 0 & 0 & 1 & 0 \\ 0 & 0 & 0 & 0 & 0 & 0 & 0 & -1 \\ 0 & 0 & 0 & 0 & 0 & 0 & 0 & 1 \end{bmatrix} \tag{18}$$

$$\mathbf{x} = \begin{bmatrix} h^{CHP} \\ h_1^{GB} \\ h_2^{GB} \\ h_3^{GB} \\ h_4^{GB} \\ W^{TS} \\ h^{TS} \\ h^{\delta} \end{bmatrix}; \qquad b = \begin{bmatrix} -h_m^{CHP} \\ h_M^{CHP} \\ -h_{1,m}^{GB} \\ h_{1,M}^{GB} \\ -h_{2,m}^{GB} \\ h_{2,M}^{GB} \\ -h_{3,m}^{GB} \\ h_{3,M}^{GB} \\ -h_{4,m}^{GB} \\ h_{4,M}^{GB} \\ -W_m^{TS} \\ W_M^{TS} \\ h_M^{TS} \\ h_M^{TS} \\ 0 \\ h_M^{\delta} \end{bmatrix}$$

This implies that the problem should not only be optimised over $\mathbf{x}$ but also solved with respect to $\mathbf{x}$. As a result, the static problem can be cast as a conventional optimisation,

$$\begin{aligned} \min_{\mathbf{x}} \quad & f(\mathbf{x}) \\ \text{s.t.} \quad & \mathbf{x} \in X \end{aligned} \tag{19}$$

where X is the set of feasible points satisfying the matching of supply and demand in (9a), the storage dynamics specified in (9i), and the constraints $M\mathbf{x} \leq b$ defined in (18).

Mathematically, the feasibility set is defined as follows,

$$\begin{aligned} X :=\{\mathbf{x}|h^{CHP} + \sum_{i=1}^{4} h_i^{GB} + h^{WF} + h^{BF} - h^{TS} - h^{\delta} = h^{D}, \\ W_{k+n}^{TS} - W_k^{TS}(1-\mu^{TS}) - b\sum_{i=1}^{n} h_{k+i}^{TS} = 0, M\mathbf{x} - b \leq 0\} \end{aligned} \tag{20}$$

The dynamics of the storage tank can be included in this manner when translating the dynamical storage equation into a set of equality constraints depending on time[12],

$$\begin{aligned} W_{k+1}^{TS} &= W_k^{TS}(1-\mu^{TS}) + bh_{k+1}^{TS} \\ W_{k+2}^{TS} &= W_{k+1}^{TS}(1-\mu^{TS}) + bh_{k+2}^{TS} \\ &\vdots \\ W_{k+n}^{TS} &= W_{k+n-1}^{TS}(1-\mu^{TS}) + bh_{k+n}^{TS} \end{aligned}$$

where W^{TS} stands for the state of charge at the considered time instant, and h^{TS} represents the collection of the thermal energy over the considered time step. To illustrate the latter with an example: h_{k+1}^{TS} is the (dis)charging rate from time k to $k+1$. These equality constraints can be taken together by writing each of the equations in terms of the preceding one. Eventually, this results in the aggregated equation,

$$W_{k+n}^{TS} = W_k^{TS}(1-\mu^{TS}) + b\sum_{i=1}^{n} h_{k+i}^{TS} \tag{21}$$

This shows that the dynamic portion is only dependent on the initial state of charge (as $k=0$, and thus $W_k^{TS} = W^{TS}(0)$) and the (dis)charging rate at each of the considered time instants.

4.2 Property Analysis

As stated by [87], optimisation problems are classified based on the qualitative properties of the considered equations. Therefore, the mathematical structure of the problem should be analysed to support why an algorithm is appropriate to use [55].

4.2.1 Differentiability Analysis

A twice differentiable function $f : \mathbb{R}^n \to \mathbb{R}$ is said to be convex if and only if the second-order derivative is positive semi-definite $f"(x) \geq 0$ for all x in the interior of an open interval. When analysing partial derivatives, the Hessian matrix has a useful property for assessing the (strict) convexity of an equation [88]. More specifically, a twice partial differentiable function $f : \mathbb{R}^n \to \mathbb{R}$ is said to be convex if $\mathbf{H}_{f(x)} \geq 0$ for all $x \in \mathbb{R}^n$, and strictly convex if $\mathbf{H}_{f(x)} > 0$ for all $x \neq 0$. The benefit of having a convex problem is that any optimal local solution is also the global solution. Hence, global minima or maxima (depending on the type of objective: cost or utility function) can be guaranteed.

Apart from analysing the twice differentiability, it is also useful to analyse whether the equations are poor or well-defined. If the convexity of a problem cannot be guaranteed

[12]Recall that the following time dependent notations of the variable are equivalent $W^{TS}(t_k) =: W_k^{TS}$.

this is not by definition problematic, it depends on whether the nonlinearity is well-defined.

The differentiability analysis can be structured by means of two types of matrices: the first-order partial derivatives can be collected in the Jacobian matrix according to equation (22), while the second-order partial derivatives can be arranged in the Hessian matrix according to equation (23).

$$\mathbf{J}_f = \begin{bmatrix} \dfrac{\partial \mathbf{f}}{\partial x_1} & \cdots & \dfrac{\partial \mathbf{f}}{\partial x_n} \end{bmatrix} = \begin{bmatrix} \nabla^T f_1 \\ \vdots \\ \nabla^T f_m \end{bmatrix} = \begin{bmatrix} \dfrac{\partial f_1}{\partial x_1} & \cdots & \dfrac{\partial f_1}{\partial x_n} \\ \vdots & \ddots & \vdots \\ \dfrac{\partial f_m}{\partial x_1} & \cdots & \dfrac{\partial f_m}{\partial x_n} \end{bmatrix} \tag{22}$$

$$\mathbf{H}_f = \begin{bmatrix} \dfrac{\partial^2 f}{\partial x_1^2} & \dfrac{\partial^2 f}{\partial x_1 \partial x_2} & \cdots & \dfrac{\partial^2 f}{\partial x_1 \partial x_n} \\ \dfrac{\partial^2 f}{\partial x_2 \partial x_1} & \dfrac{\partial^2 f}{\partial x_2^2} & \cdots & \dfrac{\partial^2 f}{\partial x_2 \partial x_n} \\ \vdots & \vdots & \ddots & \vdots \\ \dfrac{\partial^2 f}{\partial x_n \partial x_1} & \dfrac{\partial^2 f}{\partial x_n \partial x_2} & \cdots & \dfrac{\partial^2 f}{\partial x_n^2} \end{bmatrix} \tag{23}$$

The equations of interest to analyse are the ones defining the optimisation problem: the objective function (equation (17)) and the set of (in)equality constraints (equation (20)) with respect to the set of optimisation variables (equation (16)).

Equality Constraints

The equality constraints in (24) are all linear as the change in output is proportional to the change in output and hence, these equations are well-defined. Although the storage dynamics are considered, it is piecewise linear at each optimisation step.

$$\begin{aligned} h^{CHP} + \sum_{i=1}^{4} h_i^{GB} + h^{WF} + h^{BF} - h^{TS} - h^{\delta} &= h^{D} \\ W_{k+n}^{TS} - W_k^{TS}(1-\mu^{TS}) - b\sum_{i=1}^{n} h_{k+i}^{TS} &= 0 \end{aligned} \tag{24}$$

The individual first-order partial derivatives with respect to the control vector $\mathbf{x}$ for the equality constraints is provided below,

$$\frac{\partial h_D}{\partial \mathbf{x}} = \begin{bmatrix} 1 & 1 & 1 & 1 & 1 & 0 & -1 & -1 \end{bmatrix} \tag{25a}$$

$$\frac{\partial W^{TS}}{\partial \mathbf{x}} = \begin{bmatrix} 0 & 0 & 0 & 0 & 0 & 1-\mu^{TS} & -bn & 0 \end{bmatrix} \tag{25b}$$

When adding these vectors together, this leads to the following Jacobian matrix of first-order partial derivatives with respect to the control vector $\mathbf{x}$,

$$\mathbf{J} = \begin{bmatrix} \dfrac{\partial \mathbf{f}}{\partial h^{CHP}} & \dfrac{\partial \mathbf{f}}{\partial h_1^{GB}} & \dfrac{\partial \mathbf{f}}{\partial h_2^{GB}} & \dfrac{\partial \mathbf{f}}{\partial h_3^{GB}} & \dfrac{\partial \mathbf{f}}{\partial h_4^{GB}} & \dfrac{\partial \mathbf{f}}{\partial W^{TS}} & \dfrac{\partial \mathbf{f}}{\partial h^{TS}} & \dfrac{\partial \mathbf{f}}{\partial h^{\delta}} \end{bmatrix}$$

$$= \begin{bmatrix} 1 & 1 & 1 & 1 & 1 & 0 & -1 & -1 \\ 0 & 0 & 0 & 0 & 0 & 1-\mu^{TS} & -bn & 0 \end{bmatrix} \tag{26a}$$

Resultantly, the Hessian matrix of second-order partial derivatives for the equality constraints will be a zero matrix. Resultantly, the Hessian is positive semi-definite as all eigenvalues of the Hessian will be zero. Hence, the equality constraints are convex.

Inequality Constraints

Secondly, the set of inequality constraints can be analysed, $Mx-b \leq 0$. Set $g(x) = Mx-b$, then $g(x)$ is convex if each of the components $g_i(x)$ has a positive semi-definite Hessian.

$$g(x) = \begin{bmatrix} -h^{CHP} - h_m^{CHP} \\ h^{CHP} + h_M^{CHP} \\ -h_1^{GB} - h_{1,m}^{GB} \\ h_1^{GB} + h_{1,M}^{GB} \\ -h_2^{GB} - h_{2,m}^{GB} \\ h_2^{GB} + h_{2,M}^{GB} \\ -h_3^{GB} - h_{3,m}^{GB} \\ h_3^{GB} + h_{3,M}^{GB} \\ -h_4^{GB} - h_{4,m}^{GB} \\ h_4^{GB} + h_{4,M}^{GB} \\ -W^{TS} - W_m^{TS} \\ W^{TS} + W_M^{TS} \\ -h^{TS} + h_M^{TS} \\ h^{TS} + h_M^{TS} \\ -h^{\delta} \\ h^{\delta} + h_M^{\delta} \end{bmatrix} \tag{27}$$

When analysing equation (27), it appears that only linear terms are present. Hence, it follows that the Hessian of inequality constraints is a zero matrix. Resultantly, the Hessian is positive semi-definite as all eigenvalues of the Hessian will be zero. Hence, the set of inequality constraints are convex. Furthermore, these inequalities are well-defined within their bounds.

Objective Function

Proceeding with the objective (17), which is nonlinear as it is explicitly defined in terms of the nonlinear input-output relations of the CHP and GB, equations (9d) and (9e), respectively. The other terms considered in the objective function are either linear or quadratic.

The efficiencies are linearly dependent on the heat load as will be defined in section 6.1. Hence, the nonlinearity is well-defined within the operating range of the devices as long as $h^{CHP} \neq \frac{-\beta}{\alpha}$ and $h_i^{GB} \neq \frac{-\beta_i}{\alpha_i}$, respectively. However, this would imply an efficiency of zero which is most unlikely. Hence, numerical instability is not anticipated.

The Hessian of the objective is given as a diagonal matrix $\mathbf{H} \in \mathbb{R}^{8\times 8}$ where in fact only the first five diagonal elements are non-zero entries. The diagonal elements are,

$$H(1,1) = \frac{\partial^2 g^{CHP}}{\partial h^{CHP^2}} = \left(\frac{-2\alpha}{(\alpha h^{CHP} + \beta)^2} + \frac{2\alpha^2 h^{CHP}}{(\alpha h^{CHP} + \beta)^3} \right) \tag{28a}$$

$$H(i+1, i+1) = \frac{\partial^2 g_i^{GB}}{\partial h_i^{GB^2}} = \left(\frac{-2\alpha_i}{(\alpha_i h_i^{GB} + \beta_i)^2} + \frac{2\alpha_i^2 h_i^{GB}}{(\alpha_i h_i^{GB} + \beta_i)^3} \right), \quad i = 1, ..., 4 \tag{28b}$$

$$H(6,6) = 0 \tag{28c}$$
$$H(7,7) = 0 \tag{28d}$$
$$H(8,8) = 0 \tag{28e}$$
$$\tag{28f}$$

In order for the Hessian to be positive semi-definite, $\mathbf{H} \geq 0$, all of its eigenvalues have to be non-negative, $\lambda(\mathbf{H}) \geq 0$. A useful property of the diagonal matrix is that all its eigenvalues appear on the diagonal. Hence, for the Hessian to be positive semi-definite, it has to be guaranteed that also diagonal elements 1 until 5 are greater than or equal to zero. In fact, λ_1 cannot become negative as h^{CHP} is defined to have a positive lower bound (see section 3.2) and also the denominators defining the linearly dependent efficiencies will be positive (see section 6.1), especially since it is practically not likely to have a negative efficiency nor an efficiency of zero. The latter implies that the equation is well-defined despite the nonlinearity. Also, as long as $h^{CHP} > 0$ then by convention $2\alpha_i^2 > -2\alpha_i$ and hence, $\lambda_1 > 0$.

On the other hand, h_i^{GB} is defined to have a non-negative lower bound (see section 3.2) but the denominators defining the linearly dependent efficiencies will be positive (see section 6.1). When $h_i^{GB} = 0$, then the second term will cancel out and hence, $\lambda_{i+1} = \dfrac{-2\alpha_i}{(\alpha_i h_i^{GB} + \beta_i)^2}$ which leads to $\lambda_{i+1} < 0$ due to the positive denominator.

As a result, all diagonal entries and hence, all eigenvalues of the Hessian are only greater than or at least equal to zero as long as $h_i^{GB} > 0$. Hence, the Hessian of the objective function is not said to be positive semi-definite. Therefore, convexity of the objective function cannot be guaranteed.

4.2.2 Convexity Analysis

Ultimately, since the objective is nonlinear the optimisation problem is regarded as a nonlinear program (NLP) [87]. Furthermore, the constraints that enter as (in)equalities to the problem (the feasibility set (20)) are all linear. Despite the convex constraints, convexity of the overall optimisation problem cannot be guaranteed due to its nonlinear nature. However, the nonlinearity is well-defined within the operating range of the respective devices as an efficiency of zero is in practical sense unlikely. Hence, no convergence problems are expected in finding feasible minimum solutions. Furthermore, the solver used for this problem (introduced in section subsection 4.3) can handle both linearity as well as nonlinearity. Ultimately, the simulation results will show that indeed the solutions converge to a minimum despite the nonlinearity (see section 6). However, if problems may arise then the nonlinear equations can be linearised around the optimum as demonstrated above.

Apart from that, for the nonlinear problem it is possible to compute the Hessian and check if it is positive definite at the optimal solution [88]. If so, then the solution is a local minimum but still no guarantees on global optimality can be given as it cannot be determined whether the Hessian is positive definite for all x.

4.3 The Solver

4.3.1 The Software

The simulations are performed using MATLAB R2021b. The optimisation problem can be solved by a variety of solvers, where a solver is considered a software package that contains one or more algorithms for finding solutions to a problem. The choice of preference depends on the properties of the problem, such as linear or non-linear, convex or non-convex. For instance, the problem can be modelled and solved using the free Matlab toolbox YALMIP which is a useful programming language for advanced modelling of both convex and non-convex optimisation problems [89]. Another commonly used solver, present within the Matlab environment, is fmincon. This solver aims at finding the minimum of a constrained nonlinear multivariable function [90]. Also external solvers are available, such as Gurobi Optimiser [91]. For this research, the Matlab solver 'fmincon' will be employed as it is embedded in the Matlab environment and capable of handling nonlinear programs just as the problem defined in section 4.1.

4.3.2 The Algorithm

The Matlab solver 'fmincon' is suitable for (non)linear constrained optimisation problems and is a gradient based method. This is a fast solver. However, the downsides are the possible local minima and the functions are required to be continuous. The fmincon solver has five algorithm options in Matlab that can be chosen [90]:

- interior-point (default option)
- trust-region-reflective
- sqp
- sqp-legacy
- active-set

The interior-point method is the default option. This algorithm is capable of handling both small-scale and large-scale problems, as well as linear and nonlinear optimisation problems. The interior-point method operates in the interior of the feasible region, instead of obtaining a solution from outside the feasible region as is the case for exterior point approaches [52]. The IP algorithm performs fast enough for this problem. Hence, the default algorithm is employed. In fact, the problem is solved twice. First, the faster sqp-algorithm is used to calculate the initial solution for each setpoint, so that a good initial guess of the optimisation variables, x_0, can be provided when resolving the problem using IPM. Hence, the setpoints outputted by the sqp are entered as initial guess to the IP algorithm, better conditioning the problem. This makes the iterations more productive when resolving the problem with more accurate initial conditions, close to the solution.

In the default option of the IP algorithm, fmincon estimates gradients of the nonlinear constraints and the objective function by finite differences [92]. However, the IP algorithm is improved by manually providing the Jacobian and Hessian upfront using symbolic Matlab equations. This saves computational time for the algorithm when iterating in finding a feasible solution for each timestep, making the solution process more robust by obtaining faster, more accurate solutions.

More specifically, the Jacobian is computed for all (in)equality constraints (equation (20)) and the objective function (equation (17)) with respect to $\mathbf{x}$, the vector of optimisation variables (equation (16)). In addition, also the Hessian of the objective function with

respect to $\mathbf{x}$ is computed symbolically. Note that all equality and inequality constraints are linear with respect to the optimisation variables. The equality constraints are written as $A_{\text{eq}} \cdot x = b_{\text{eq}}$ and inequality constraints as $A_{\text{ineq}} \cdot x \leq b_{\text{ineq}}$. Hence, the Hessian matrices of each component of these constraints is going to be zero. Therefore, it is sufficient to compute the Hessian of the objective function. Once fmincon has found a solution, it automatically checks the Hessian to determine whether the solution is a local minimum.

Interior Point Method

When fmincon employs the IPM, it solves the inequality constrained minimisation problem by repeatedly solving a sequence of approximate equality constrained minimisation problems using a logarithmic barrier function following a central path [93] [46]. Consider the following original inequality constrained problem,

$$\begin{aligned} \min_{x \in \mathbb{R}^n} \quad & f(x) \\ \text{s.t.} \quad & h(x) = 0 \\ & g_i(x) \leq 0, \qquad i = 1, ..., m \end{aligned} \tag{29}$$

which is translated into an approximate equality constrained problem to which the Newton-Raphson method [94] can be applied. The inequalities are appended implicit in the objective function by introducing the logarithmic[13] barrier function that takes these inequality constraints as argument,

$$\begin{aligned} \min_{x \in \mathbb{R}^n} \quad & f(x) - \frac{1}{t} \sum_{i=1}^{m} \log(-g_i(x)) \\ \text{s.t.} \quad & h(x) = 0 \end{aligned} \tag{30}$$

where $t > 0$ is the barrier parameter that appoints the accuracy of the approximation[14], and $\log(-g_i(x))$ is the differentiable logarithmic barrier[15] with as domain the set of points strictly satisfying the inequality constraints of 29. When initialising at a feasible point (which is a prerequisite for IPMs) and the optimiser iterates in finding a minimum, then when the inequalities approach infeasibility $g_i(x) \to 0$, then $\log(-g_i(x)) \to -\infty$. As a result, $-\log(-g_i(x)) \to \infty$, and thus also the problem is going to infinity. Hence, violating the inequality constraints of the original problem (i.e., $g_i(x) > 0$) will be avoided as infinity is the worst objective function value when minimising. On the other hand, while the solution is feasible it is also measured how close the solution is from violating the constraints. Resultantly, the algorithm will search points only within the interior of the feasible region when iterating in finding an optimum solution.

As the iterations proceed, the value of t is gradually increased so that the log barrier approximation of the strict inequality constraints improves. As $t \to \infty$, the original problem is approximated with high accuracy. At every iteration, the problem is solved by checking whether the KKT conditions [95] for the barrier problem are satisfied within a predefined constraint tolerance, ϵ. This way, a search direction for the next iteration is

[13] The advantage of using a logarithmic barrier is the differentiability and the useful property that $ln(-g_i(x))$ is undefined for $g_i(x) > 0$.

[14] this parameter controls how much weight is given to the barrier; a large value implies staying far away from the boundaries.

[15] Note that an equivalent representation can be provided when introducing slack variables, $\log(s_i)$ with $g_i(x) + s_i = 0$. The slack variables are restricted to be positive so that the iterates remain in the interior of the feasible region, $s \geq 0$ [93].

computed [46]. Once the search direction is found, the appropriate step size α for increasing the barrier parameter needs to be determined, where $t_{k+1} = \alpha t_k$. This way, the barrier method follows a central path so that t is not increased to drastically as that would result in numerical instability. The central path associated with problem (29) is the set of points $x^*(t)$ that are strictly feasible[16] with $t > 0$. However, tracing the central path is a computational intense process. Instead, it can be approximated using a step mechanism, such as Newton's method for solving NLPs [94]. This process of (1) solving the problem with the KKT conditions, (2) using the solution x^* as starting point for the next iteration, and (3) increasing t, repeats until the constraints are approximated close enough. Ultimately, by solving the barrier method (30), then effectively the original problem (29) is solved as basically all inequality constraints $g_i(x) \leq 0$ of the original problem would be satisfied.

That is where the useful property of IPMs comes into play. It can be predefined how close to approximate the boundary of the feasible region (i.e., the union of the constraints), how close to approach infeasibility but the interior point is never left. In other words, the inequality constraints can be satisfied with high precision when employing IPM. Furthermore, IPM can be applied to nonconvex constrained optimisation problems. However, only local minima can be found. A more detailed explanation on IPMs is provided in [46], [96], [97].

4.3.3 The Solver Output

The solver iterates in finding a feasible solution until the objective no longer decreases in either direction. This implies that a local minimum for the cost function is found. The iterations of finding a feasible objective function are plotted. A random illustration of such a plot is depicted in Figure 8. This shows that the solver finds decreasing cost values as the iterations proceed. If the objective solution is infeasible (i.e., constraints are violated) for an iteration, this is indicated with red dots in the graph. More specifically, the tolerance in constraint violation is set at 'TolCon = 1e-4', implying that a solution is regarded infeasible when the constraints are violated with more than this value. The variables of this problem are considered in units [kWh], thus a smaller value than TolCon = 1e-4 is not required because it would reduce the flexibility of the solver. However, choosing a larger value could lead to less accurate solutions that violate the boundary conditions too much. Furthermore, if no feasible solution at all can be found, the solver is forced to stop and to output the results after 9000 iterations. This amount of iterations can be customised.

[16] $x^*(t)$ is strictly feasible if it satisfies, $h(x^*(t)) = 0$ and $g_i(x^*(t)) < 0$, with $i = 1, ..., m$.

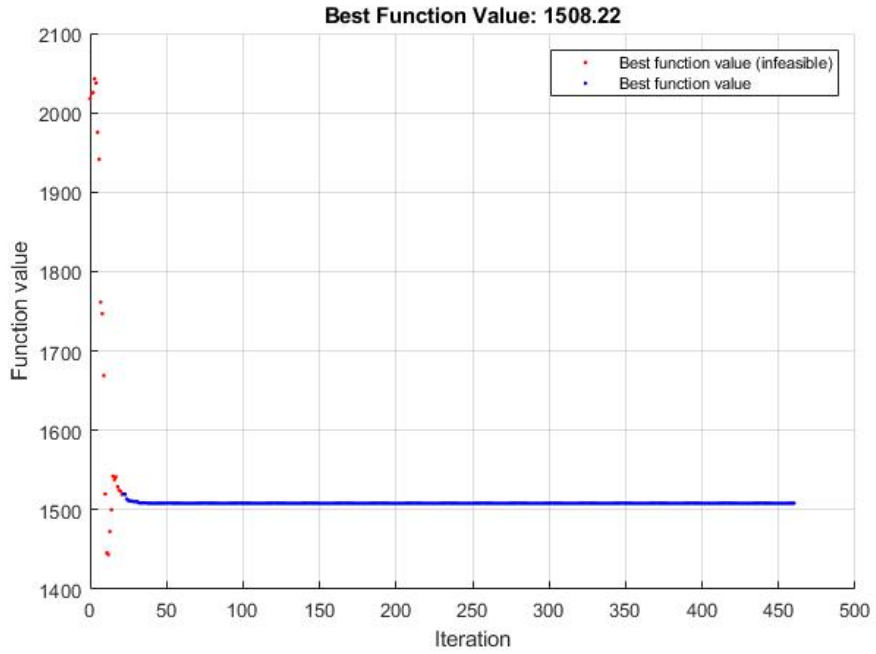

Figure 8: An illustration of the solution for the objective returned by the solver. The objective considers the summation of the costs over the time horizon. The solver iterates in finding a solution until the objective no longer decreases in either direction. This implies a local minimum is found. If the objective solution is infeasible (i.e., constraints are violated) this is indicated with red dots.

Once the solver has found a feasible solution for a two-day ahead schedule, the solver returns the corresponding minimised objective value (i.e., the summation of costs over the time horizon) and the setpoints for all optimisation variables over the time horizon. This implies that each optimisation variable has $T = 48$ setpoints. The first 24 setpoints are written to an excel interface file such that the company can easily extract this control data. If the company wants to run the solver for the following 48 hours, simply the forecast data and initial conditions have to be updated in this excel interface. The initial conditions of the optimisation variables are the setpoints at timestep 24 of the previous solution. Subsequently, when rerunning the code, the solver will determine the new setpoints based on the updated initial conditions and forecast.

5 Algorithm Verification

This section will answer the research question *"Which case scenarios verify the model?"*. Verification is performed to check that the algorithm is working properly. To this end, the basic code where the linear dependencies are excluded will be considered. Verification is performed by simulating several simplistic scenarios and comparing the results of the solver with the hypothesis. If the results match the hypothesis, this implies that the code is operating as expected. If the result diverges, it either means that the code is operating differently than desired or that the hypothesis is incorrect. The following scenarios are considered:

1. Scenario I: Varying heat demand and gas price.
   (a) Scenario I.A: low demand and low gas price, high demand and high gas price.
   (b) Scenario I.B: low demand and high gas price, high demand and low gas price.
2. Scenario II: Varying CHP electricity sales price.
3. Scenario III: Varying input from the waste and biomass furnace.

These scenarios will be tested on the basis of average winter input data and device data as heat supply and demand are most substantial during the cold winter months. The scenarios only analyse inputs that might also change in practice. The relevant input variables will be adjusted per scenario to study the algorithm behaviour, while all other variables and cost factors are unaffected. Hence, before simulating these scenarios, the basic model has to be introduced as a reference for comparison.

5.1 Base Case

In Table 1, the input variables, cost factors and coefficient values considered in the base model are introduced. Furthermore, the lower and upper bounds considered for the optimisation variables are displayed in Table 2. Even though it is not possible to adjust a device's efficiency or capacity, these are displayed in the tables for clarity.

The forecast input variables (heat demand, and furnaces) are considered to be static over the time horizon to simplify the base testing. In addition, the linear efficiencies η and the linear state dependent local demand p^{LD} are assumed to be constant during verification. However, the linear relationship for p^{CHP} is included in the base model as the outputs of the CHP unit are coupled and hence, this relation cannot be simplified. This relation is derived from historical company data, see subsubsection 6.1.2. Furthermore, one overall boiler with one overall efficiency (based on aggregating historical company data) is assumed to simplify the verification procedure. Later, when validating the model, the more detailed situation of A2A's DH plant will be incorporated in the model including these linear variable and efficiency relations and distinguishing between the individual boilers.

Table 1: The static cost factors, input variables, and coefficients in the base case. As mentioned before, $c_{\text{ts}} = 0$ because A2A is not interested in having back-up energy. Also, $c_{\text{share}} = 0$ because to simplify the verification one overall boiler production is assumed. The artificial cost factor c_{diff} is chosen such that it does not influence the outcome for the cost function and optimisation variables but merely returns smooth and stable results. Furthermore, the artificial cost factor c_δ is chosen large to prevent dissipation as this implies loss of potential revenues. As a last remark, the company did not provide data on the electricity price c_p. Therefore, this value is derived from [98].

Costs	**[€/MWh]**
c_g	89.38
c_p	188
c_{out}	74.5
c_{ets}	17.56
c_{tee}	18.813
c_δ	10^6
c_{ts}	0
c_{diff}	10^1
c_{share}	0

Inputs	**[MWh]**
h^{WF}	9.632
h^{BF}	4.087
h^{D}	39.133
p^{LD}	0.374
ϵ^{GB}	0.0133

Coefficients	**[dmnl]**
η^{CHP}	0.44
η^{GB}	0.93
γ^{GB}	$3.414 \cdot 10^{-3}$

Table 2: The minimum bounds (left table) and maximum bounds (right table) of the optimisation variables. Note that in the proposed model the storage level W^{TS} is normalised. Hence, $W_m^{TS} = 0$ and $W_M^{TS} = 1$ with the initial storage level set at $W^{TS}(0) = 0$.

Lower bound	**[MWh]]**
h_m^{CHP}	9.766
h_m^{GB}	0
W_m^{TS}	0
h_m^{TS}	-8
h_m^{δ}	0

Upper bound	**[MWh]**
h_M^{CHP}	15.387
h_M^{GB}	46
W_M^{TS}	20
h_M^{TS}	8
h_M^{δ}	23.129

Results: The solution for the optimisation variables at each time instant for the base model can be viewed in Figure 9. It is clear that the demand is greater than the minimum production rate. The minimum production is the sum of the furnaces, minimum CHP and minimum boiler operation. As a result, additional production is required to suffice demand. The thermal energy is produced by the GB as this device operates with substantial better efficiency than the CHP (see Table 1). This efficiency outweighs the more expensive operation of the GB. When disregarding the efficiencies and viewing the unitary cost factors, the boilers are more expensive to operate because of the electricity purchase cost c_p, and the lost income from CHP electricity sales c_{out} after correction for the fee and grant on CO2 emissions. However, as the boilers produce more efficiently, the total boiler costs are in fact lower than CHP costs. More specifically, for this base model the total boiler costs are €37,048, CHP costs are €54,042, and after correction for electricity sales the CHP costs are €43,134. Resultantly, the total cost equals €80,182. Here, the CHP is operated at its minimum production rate. Note that at the minimum rate, the CHP can easily suffice the local electricity demand (see linear relation in subsubsection 6.1.2): $p_m^{CHP}(h_m^{CHP}) = p_m^{CHP}(9.766) = 6.475 > p^{LD} = 0.374[MWh]$.

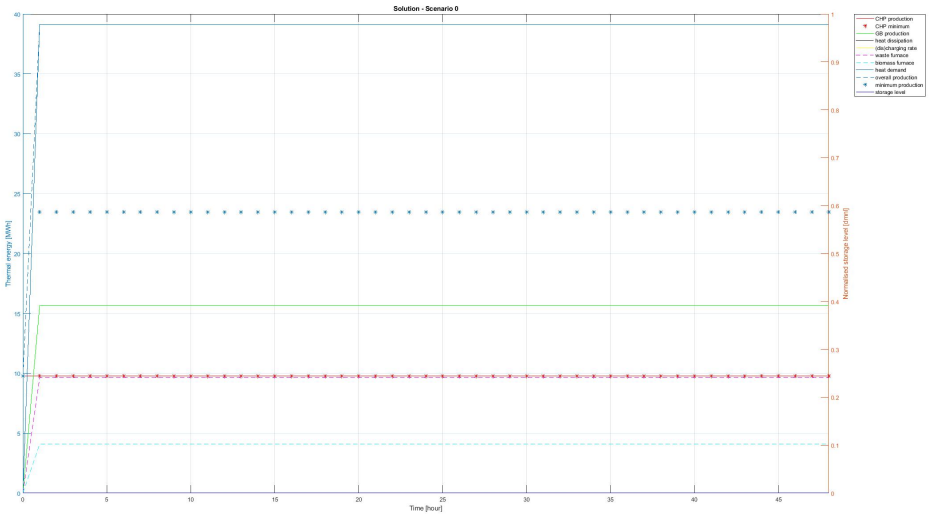

Figure 9: The feasible solution for the optimisation variables returned by the solver at each time instant for the base model. Note that the value for the normalised storage level $W^{TS} \in [0, 1]$ can be read off from the y-axis on the RHS. The associated total cost equals €80,182. It is possible to zoom in, to better display the graphs.

5.2 Scenario I.A

Scenario I.A: Evaluation of the storage dynamics. This is performed by considering a varying demand and gas purchase rate throughout the day. The algorithm solves the optimisation problem for a two-day ahead schedule in which the variables will have low values during the first half of both days, while these values will be high during the second half of both days (Table 3). The low and high demand values are taken as the minimum and maximum of the average winter data provided by A2A. The price is assumed to deviate with twice its base value. For simplicity, the values are held constant during each of the four half days. For this scenario, all other input variables and the remaining cost factors are unaffected.

Table 3: The values assigned to the heat demand h^D and gas purchase rate c_g at each timestep k over the time horizon of 48 hours, in scenario I.A.

Daypart	**k$^{\text{th}}$-timestep**	**h$^{\text{D}}$[MWh]**	**c$_{\text{g}}$ [€/MWh]**
1	$k = 1, \ldots, k = 12$	21.713	89.38
2	$k = 13, \ldots, k = 24$	59.536	178.76
3	$k = 25, \ldots, k = 36$	21.713	89.38
4	$k = 37, \ldots, k = 48$	59.536	178.76

Hypothesis I.A: *It is expected that the storage tank will be filled during the first half of each day (i.e., dayparts 1 and 3), even though demand is low in these periods. This is predicted because the purchase price is substantially lower as opposed to the second half of the days (i.e., dayparts 2 and 4). In addition, it is predicted that during dayparts 2 and 4, when both demand and costs are high, the storage tank will be discharged as it is more cost-effective to withdraw energy from the storage than to produce at a high purchase rate.*

Results I.A: The results in Figure 10 are in line with the hypothesis. The storage tank is indeed filled during the first half of each day, i.e., $\{h^{TS} \geq 0 | k \in [0, 12], k \in [25, 36]\}$ and $W^{TS}_{k=12} = W^{TS}_{k=36} = 1$, and emptied during the second half of each day when the gas price is substantially higher, i.e., $\{h^{TS} \leq 0 | k \in [13, 24], k \in [37, 48]\}$ and $W^{TS}_{k=24} = W^{TS}_{k=48} = 0$.

Apart from discharged thermal energy, also additional heat production is required to meet the demand during dayparts 2 and 4. The solver decided to maximise GB production rather than CHP production during these high-demand dayparts because the GB has a greater efficiency and is thus more cost effective. However, also CHP production is seen during these dayparts because $h^{CHP}_m = 9.766$ [MWh]. The GB production is curved because it is scaled up and back in accordance with the discharging rate during dayparts 2 and 4. Discharging happens in a smooth fashion due to the artificial penalty installed on (dis)charging differences in the cost function (17). The tank is fully emptied in the dayparts with high demand as this is more cost effective than upscaling CHP production. In dayparts 1 and 3 with low demand, there is sufficient production surplus due to the minimum CHP bound and fixed furnace inputs being greater than demand: $h^{CHP}_m + h^{GB}_m h^{WF} + h^{BF} = 9.766 + 0 + 9.632 + 4.087 = 23.485 > h^D = 21.713$. Hence, the storage tank is being charged with $h^{TS} > 0$. This is also cost-effective as during dayparts 2 and 4 where the gas price is high, there is less production (and thus less energy purchases) needed due to the storage being emptied. In fact, there is even a small amount of heat excess during dayparts 1 and 3 because the production surplus is greater than what can be charged.

Furthermore, the solver found a higher feasible objective solution as opposed to the base case. This is reasonable as the gas price is substantially greater during dayparts 2 and 4, and also total demand (and hence total production) over the time horizon is greater compared to the base scenario. This results in a higher overall cost value of €147,297.

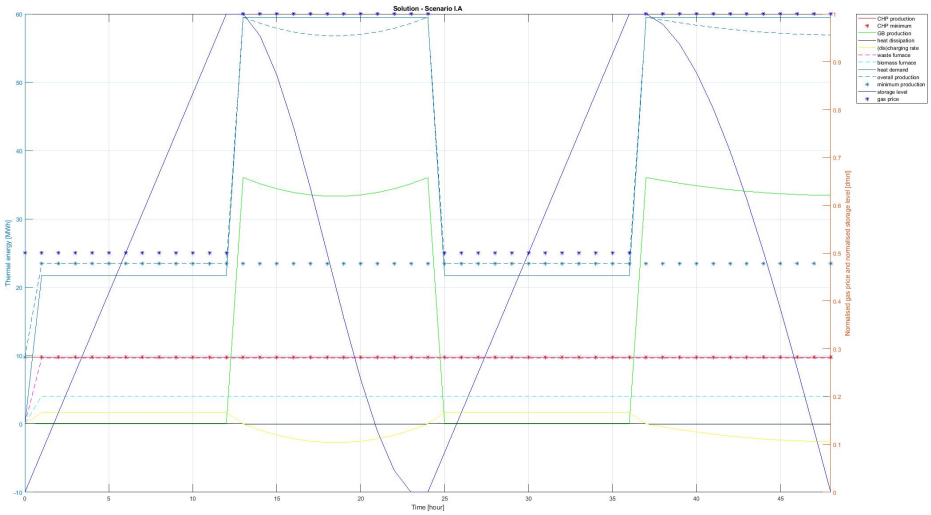

Figure 10: The solution for the optimisation variables returned by the solver at each time instant for scenario I.A. The values for the the normalised storage level and gas price rate can be read off from the y-axis on the RHS. The gas price is displayed in a normalised fashion, similar as for the storage level. Hence, both $W^{TS}, c_g \in [0, 1]$. The associated total cost equals €147,297. It is possible to zoom in, to better display the graphs.

5.3 Scenario I.B

Scenario I.B: Evaluation of the storage dynamics. In the mornings heat demand is high and gas price is low, while in the evenings demand is low and price is high (Table 4). The low and high demand values are taken as the minimum and maximum of the average winter data provided by A2A. The price is assumed to deviate with twice its base value. For simplicity, the values are held constant during each of the four half days. All other input variables and the remaining cost factors are unaffected.

Table 4: The values assigned to the heat demand h^D and gas purchase rate c_g at each timestep k over the time horizon of 48 hours, in scenario I.B.

Daypart	**kth-timestep**	**h^D[MWh]**	**c$_g$ [€/MWh]**
1	$k = 1, \ldots, k = 12$	59.536	89.38
2	$k = 13, \ldots, k = 24$	21.713	178.76
3	$k = 25, \ldots, k = 36$	59.536	89.38
4	$k = 37, \ldots, k = 48$	21.713	178.76

Hypothesis I.B: *It is expected that there will be a production surplus by upscaling the GB during dayparts 1 and 3, when the gas price is low, such that not only demand is met but also the storage tank is filled. This is predicted because the gas purchase price is substantially lower than in dayparts 2 and 4. During these dayparts, when demand is low but price is high, the storage tank is emptied to suffice demand. This is expected as it is more cost-effective to withdraw energy from the storage than to produce at a (high) purchase rate. Consequently, during dayparts 2 and 4, production will be scaled back more than it would have been without a storage supply.*

Results I.B: As explained in scenario I.A, it is more cost effective to operate the GB in terms of efficiency despite the greater unitary cost factors. Hence, the boilers have a greater share in production to meet demand. In addition, the CHP is operated at its minimum rate which is sufficient to suffice demand.

Apart from that, the results depicted in Figure 11 seem not to be in line with the hypothesis. The storage tank is filled during the dayparts where the gas price is high and is, in fact, emptied when the gas price is low (with the exception of daypart 1 since the initial state of charge is zero). However, the explanation to this is rather logic because the fixed heat input from the furnaces is $h^{BF} + h^{WF} = 13.719$ [MWh] (see Table 1), and the minimum CHP operation is $h_m^{CHP} = 9.766$ [MWh] (see Table 2). These are exactly the values during the dayparts where the gas price is high and demand is low. This implies that when the plant operates at the minimum feasible rates, there is still a production surplus: $h^{BF} + h^{WF} + h^{CHP} = 23.485 > h^D = 21.713$ [MWh]. As a result, the production surplus is added to the storage tank with $h^{TS} = 1.6667$ [MWh]. Note that this charging rate is smaller than the actual production surplus of 1.772 because during dayparts 2 and 4 the total surplus is greater than what can be stored in the tank, and hence, $h^{\delta} > 0$. Accordingly, the stored energy is used in daypart 3, since there will be a production surplus in day part 4 anyway and there is no need to have some back-up energy in the meantime.

This explanation for having a reversed behaviour from what is stated in the hypothesis can be demonstrated by rerunning this scenario with an adjusted 'low' demand value, such that production above the minimum feasible rates is required with $h^D = 31.713$. The

results are depicted in Figure 26 of Appendix A. Indeed, the storage is fully charged when the gas price is low, so that it can be emptied in the period where the gas price is high to ensure demand is still being met in a cost-effective manner. Resultantly, there is no excess heat above the storage capacity and hence, $h^{\delta} = 0$. To ensure charging of the tank, GB production is increased which also causes the total costs to increase as more gas has to be purchased when the overall demand is greater, compared to the initial run of scenario I.B.

Furthermore, the objective solution of the original run of scenario I.B is €109,614 which is less than the costs incurred in scenario I.A. This is reasonable as demand is low in the periods where the gas price is high. Resultantly, production is substantially lower in the high gas price periods as opposed to scenario I.A.

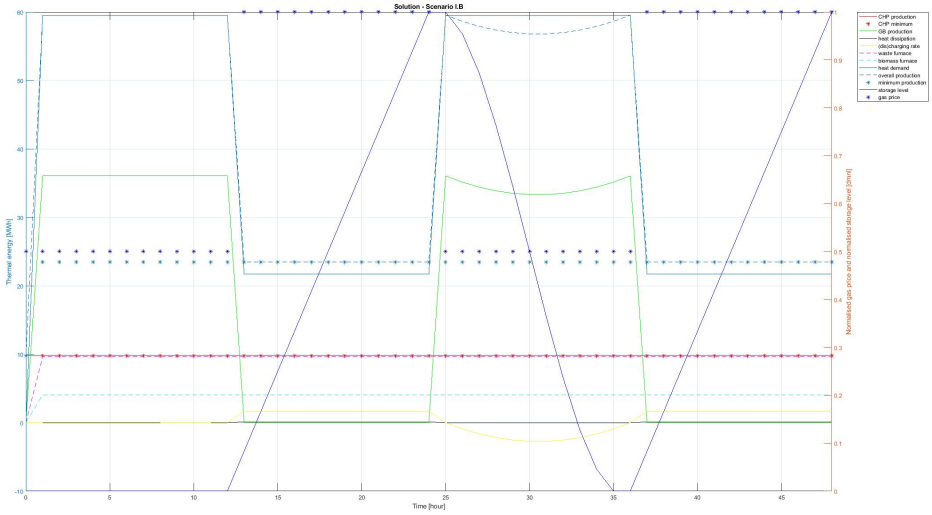

Figure 11: The solution for the optimisation variables returned by the solver at each time instant for scenario I.B. Note that the values for the gas price and the storage level can be read off from the y-axis on the RHS. The gas price is displayed in a normalised fashion, similar as for the storage level. Hence, both $W^{TS}, c_g \in [0, 1]$. The associated total cost equals €109,614. It is possible to zoom in, to better display the graphs.

5.4 Scenario II

Scenario II: Test how the model behaves to a varying electricity sales price, c_{out}. In the mornings the price is low and in the evenings the price is high as depicted in Table 5. The price is assumed to deviate with twice its base value. All other variables are similar to the base case.

Table 5: The values assigned to the electricity sales price c_{out} at each timestep k over the time horizon of 48 hours, in scenario II.

Daypart	**k$^{\text{th}}$-timestep**	**c_{out} [€/MWh]**
1	$k = 1, \ldots, k = 12$	74.5
2	$k = 13, \ldots, k = 24$	149
3	$k = 25, \ldots, k = 36$	74.5
4	$k = 37, \ldots, k = 48$	149

Hypothesis II: *It is expected that the solver will maximise CHP production during dayparts 2 and 4 when electricity sales are more profitable. The additional CHP heat production will be added to the storage tank as demand is held constant throughout the dayparts. In addition, during dayparts 1 and 3, CHP production is scaled back to its minimum. In conjunction with this, it is also expected that costs will be minimised to a greater extent when the revenue will be increased.*

Results II: Indeed, the CHP produces at its maximum rate when the sales price is high. However, no production surplus is created. Instead, boiler production is scaled back to ensure cost effectiveness of less energy purchases and the maximum CHP production does not result in a surplus. As a result, the storage behaviour is zero over the time horizon. When the sales price is low, the CHP operates at its minimum and instead, GB production is maximised as its operation is most efficient. There is also no heat dissipation as demand can easily be met.

Lastly, it can be concluded that the total costs of €69,810 for this scenario are lower than for the base case (and also compared to scenario I.A and I.B). However, this is not due to additional revenues as was stated in the hypothesis. On the contrary, the cost reduction is simply the consequence of a lower overall heat demand which results in less production and hence, less gas purchases. Also, the overall gas purchase price is lower as opposed to scenario I.A and I.B.

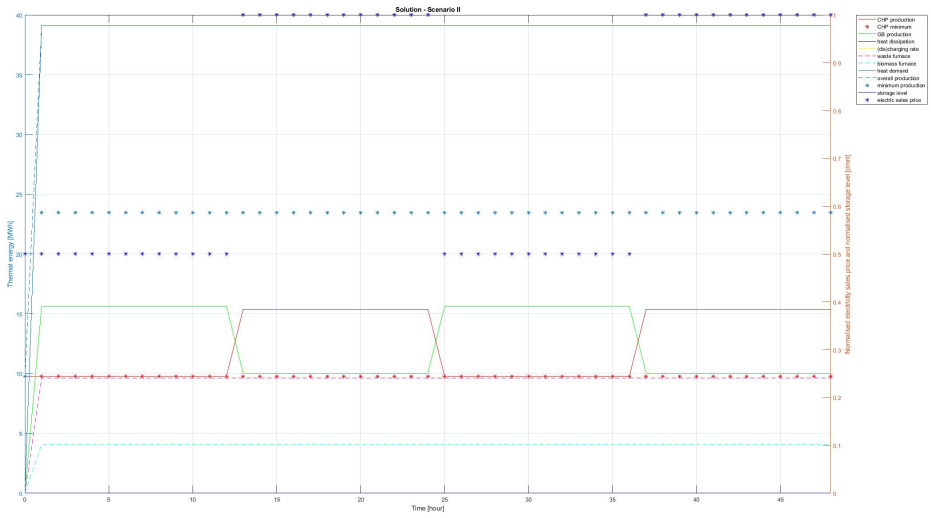

Figure 12: The solution for the optimisation variables returned by the solver at each time instant for scenario II. Note that the values for the electricity sales price and the storage level can be read off from the y-axis on the RHS. The electricity sales price is displayed in a normalised fashion, similar as for the storage level. Hence, both $W^{TS}, c_{out} \in [0, 1]$. The associated total cost equals €69,694. It is possible to zoom in, to better display the graphs.

5.5 Scenario III

Scenario III: Test how the model behaves to a varying input from the furnaces, h^{BF} and h^{WF}. In the mornings the input from the furnaces is low and in the evenings the input is high as depicted in Table 6. To ensure realistic values, the low and high furnace values

are taken as the minimum and maximum of the average winter data provided by A2A. All other variables are similar to the base case.

Table 6: The values assigned to the furnaces h_{BF} and h_{WF} at each timestep k over the time horizon of 48 hours, in scenario III.

Daypart	**kth-timestep**	**h^{BF} [MWh]**	**h^{WF} [MWh]**
1	$k = 1, \ldots, k = 12$	2.578	7.857
2	$k = 13, \ldots, k = 24$	4.672	10.521
3	$k = 25, \ldots, k = 36$	2.578	7.857
4	$k = 37, \ldots, k = 48$	4.672	10.521

Hypothesis III: *It is expected that, compared to the base case, the solver will downscale GB production during the dayparts where the input from the furnaces is high. The CHP operation will remain unaffected by producing at the minimum, similar to the base case. Furthermore, it is expected that the increased furnace input will not result in a production surplus. Consequentially, the storage tank will not be used in this scenario. Related to this, it is also expected that costs will be minimised to a greater extent as production can be scaled back, leading to fewer gas purchases.*

Results III: As shown in Figure 13, the behaviour corresponds to the hypothesis. The furnace inputs are indeed not substantially large that a production surplus is created. In fact, substantial GB production is required to meet demand (next to minimum CHP operation). Furthermore, boiler production is scaled accordingly with the furnace inputs. Overall production meets demand accurately over the time horizon, which is reflected in zero heat dissipation. However, next to furnace inputs also additional production is required to meet demand. This result in greater costs as opposed to the base case because total furnace input in the base case is $h^{WF}(1:T) + h^{BF}(1:T) = 658.512$ [MWh], while the total furnace input for this scenario equals 615.072 [MWh]. Hence, more additional production is required, resulting in a total cost of €82,324.

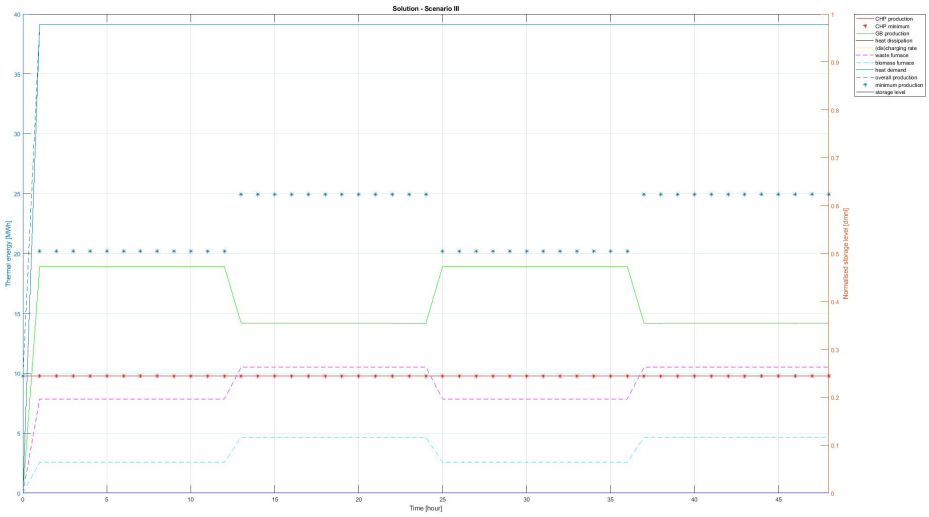

Figure 13: The solution for the optimisation variables returned by the solver at each time instant for scenario III. Note that the value for the normalised storage level $W^{TS} \in [0, 1]$ can be read off from the y-axis on the RHS. The associated total cost equals €82,324. It is possible to zoom in, to better display the graphs.

6 Algorithm Performance

This section will answer the research question *"What is the performance of the designed algorithm compared to A2A's historical data and what conclusions are drawn from these results?"*. This is done by means of backtesting. However, first an elaboration on the integration of linearly dependent company data will be provided. Secondly, tuning of the artificial cost factors in the objective function is explained. Thereafter, the backtest can be performed.

6.1 Integration of Linearly Dependent Company Data

During the algorithm verification in section 5, all variables where assumed to be constant. However, a couple of these assumptions have to be relaxed before the model can be validated. More specifically, these variables are in fact related to the optimisation variables. These state dependent relationships where derived from historical company data[17].

Apart from the variable relationships described below, the remaining model variables introduced in subsection 3.2 that cannot be optimised (thermal storage dissipation, and device operating constraints) are loaded from company excel data as constants. In addition, the hourly external heat input from the furnaces and the hourly heat demand are also loaded from excel data but these are forecast and updated with each iteration of the code. The forecast is provided by A2A.

6.1.1 Local electricity demand

The electrical consumption of A2A's plant is dependent on the degree of production, i.e., $p^{LD}(h^{CHP})$. This relation was extracted from monthly historical data, provided in Figure 14a. Subsequently, the plotted datapoints were curve fitted. A linear trendline was the best approximation of the Excel options. The linear equation displayed in Figure 14a is inputted to the solver. A minimum amount of electric consumption is required irrespective of the production rate to keep the plant in operation. Logically, more electricity consumption is required when the plant increases its rate of operation.

6.1.2 Electricity production of CHP

As explained in subsection 3.2, both outputs of the CHP are coupled. In other words, the CHP electricity production is related to the CHP heat production, $p^{CHP}(h^{CHP})$. This relation was best approximated by linearly curve fitting the historical data, displayed in Figure 14b. Note that, despite the negative y-intercept of -6173, this relation is robust as it is defined within the operating range of the CHP. In other words, the CHP heat output (and also the power output) is constrained to be larger than zero. More specifically, $h_m^{CHP} = 9766[kWh]$ and hence, the electricity production can not become negative. It is reasonable that the relation is positive linear: when the heat production increases, this implies that also more electricity is produced as the one is the result of the other.

[17] A disclaimer regarding the data fitting: the data accuracy differs per variable. For instance, the local electricity demand p^{LD} and the electricity consumption of each boiler p_i^{GB} were derived from twelve monthly data points. Whereas the CHP electricity production p^{CHP} and the thermal efficiency of the CHP η^{CHP} were approximated from 725 hourly datapoints of the month January 2022. The thermal efficiency of each boiler η_i^{GB} was determined from three to four datapoints, without specifying which month is considered

6.1.3 Efficiency of CHP

The operating efficiency of the CHP device varies with the degree of loading, $\eta^{CHP}(h^{CHP})$. Once again, this relation was approximated from historical company data. This is depicted in Figure 14c. Note that the thermal efficiency decreases with increasing thermal production rate. This is because the electrical production process becomes more efficient when the degree of electrical loading increases [9]. As a consequence, the energy input is converted into electrical power to a larger extent as depicted in Figure 14d. This leaves less room for thermal energy production.

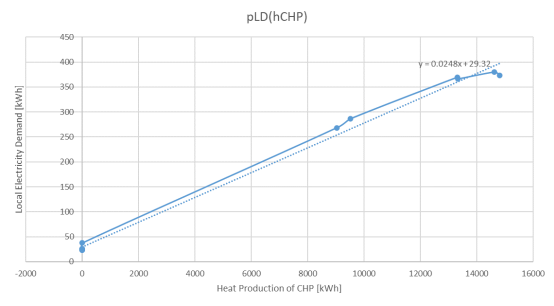

(a) Plot of datapoints relating the local electricity consumption with the CHP heat production. In the summer months the CHP is shut down.

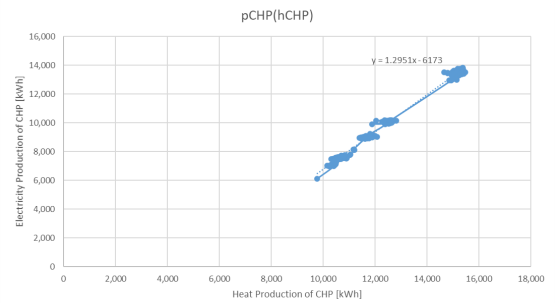

(b) Plot of datapoints relating the electricity and thermal production of the CHP.

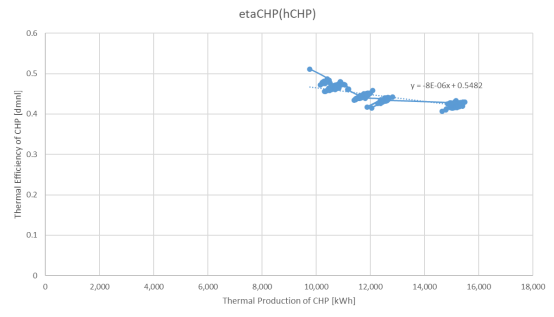

(c) Plot of datapoints relating the thermal efficiency of the CHP to the thermal CHP production.

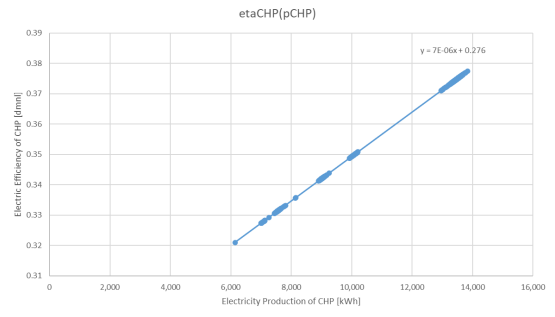

(d) Plot of datapoints relating the electric efficiency of the CHP to the power production.

Figure 14: Variables and efficiencies linearly dependent on the amount of CHP production. y curves of the individual boilers that are assumed to be linearly dependent on the thermal production. To more clearly view the graphs, please zoom in.

6.1.4 Efficiency of GB

Also the operating efficiency of each boiler is dependent on the degree of loading, i.e., $\eta_i^{GB}(h_i^{GB})$. These relationships were derived from historical company data, the graphs are depicted in Figure 15. The efficiency increases with increasing production, as is customary. Some of these curves are not as linearly as expected but the curves were also derived from two to four historical data points. Due to this lack of data accuracy, it is assumed that still all efficiency curves are linear.

6.1.5 Electricity consumption of GB

Lastly, also a relation for the electrical consumption of each boiler was derived from historical company data. This consumption depends on the degree of loading, i.e, $p_i^{GB}(h_i^{GB})$. These relations are depicted in the graphs of Figure 16. Due to time constraints and lack

of extensive data to derive accurate relations[18], the model will assume a linear relation between the electricity consumption and heat production of each boiler. Even though, the graphs in Figure 16 clearly show that the relations are not necessarily linear.

In general, it is reasonable that device components require more electrical consumption when operating at a higher rate, to scale the activity of for instance pumps and valves accordingly. Note that also a fixed amount of electrical consumption is required, irrespective of the degree of loading, to ensure the boilers are maintained in operation. This pattern will also be reflected in the electricity purchases, a fixed cost and a varying cost that is proportional to the degree of boiler activity.

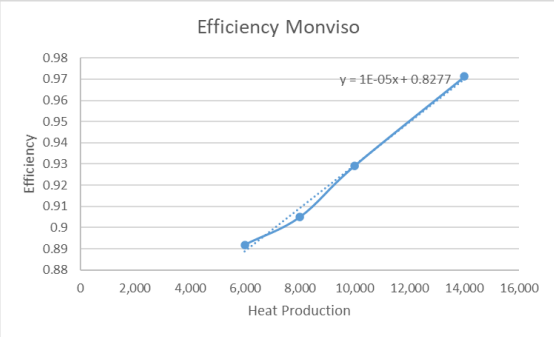

(a) Plot of datapoints relating the efficiency of boiler 1, called 'Monviso', to its thermal production.

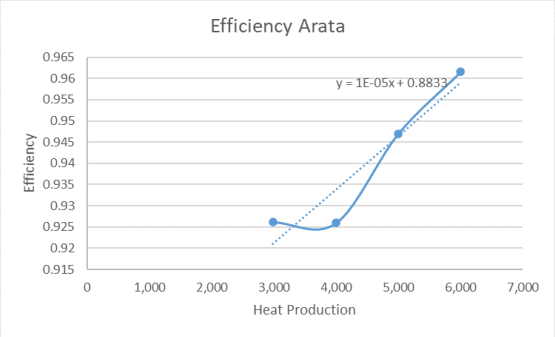

(b) Plot of datapoints relating the efficiency of boiler 2, called 'Arata', to its thermal production.

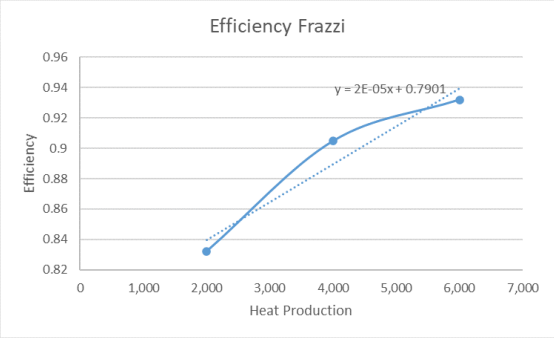

(c) Plot of datapoints relating the efficiency of boiler 3, called 'Frazzi', to its thermal production.

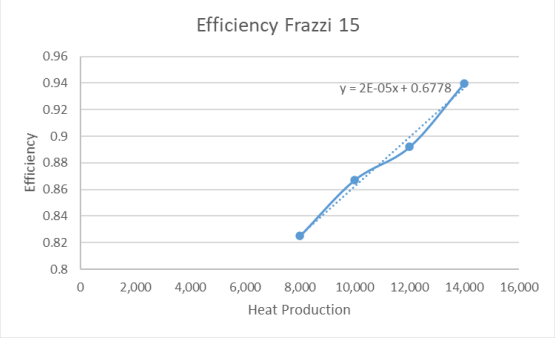

(d) Plot of datapoints relating the efficiency of boiler 4, called 'Frazzi15', to its thermal production.

Figure 15: Efficiency curves of the individual boilers that are assumed to be linearly dependent on the thermal production. To more clearly view the graphs, please zoom in.

[18]In the summer there hardly is boiler activity, a fixed amount of electricity consumption would be expected. However, a low but slightly fluctuating consumption profile is noticed. Whereas in the winter, the consumption of the boilers is more substantial. However, the curves were derived from limited data availability, on the basis of 12 monthly datapoints.

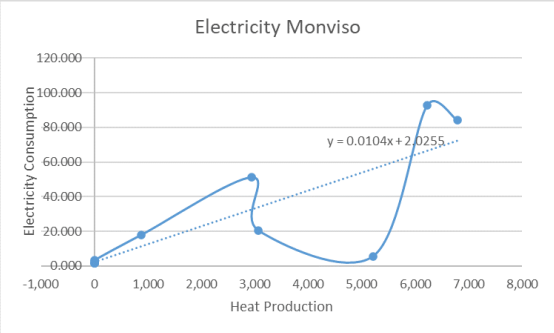

(a) Plot of datapoints relating the electricity consumption of boiler 1, called 'Monviso', to its thermal production.

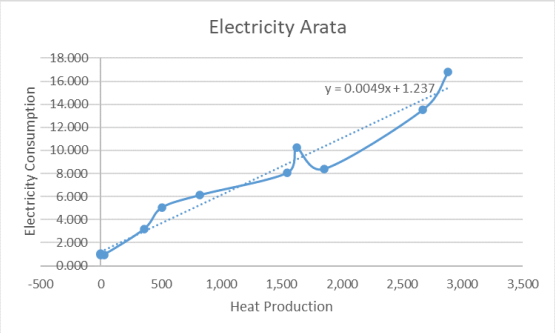

(b) Plot of datapoints relating the electricity consumption of boiler 2, called 'Arata', to its thermal production.

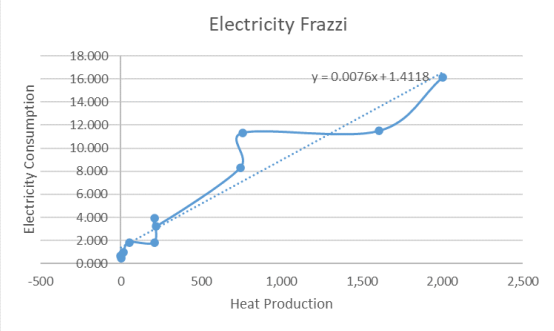

(c) Plot of datapoints relating the electricity consumption of boiler 3, called 'Frazzi', to its thermal production.

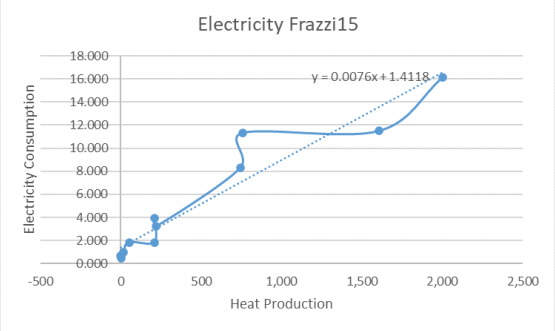

(d) Plot of datapoints relating the electricity consumption of boiler 4, called 'Frazzi15', to its thermal production.

Figure 16: Electricity consumption curves of the individual boilers that are assumed to be linearly dependent on the thermal production. The more frequently a boiler is operated, the greater the electricity consumption. The historical electricity consumption data does not correct for this frequency of use. It should be noted that the boilers are hardly operated in the summer months. To more clearly view the graphs, please zoom in.

6.2 Tuning the Artificial Cost Factors

As a final step before validating the model, the weights associated with the artificial cost terms have to be tuned. A value for these terms was already provided during the verification phase in section 5. However, with the integration of the state dependent relations and consideration of individual boilers, the model has slightly adjusted and hence, re-tuning is required.

Table 7: The selected weights for the artificial cost terms.

Cost term	**[€/kWh]**
c_{ts}	0
c_{δ}	10^{12}
c_{diff}	10^{-1}
c_{share}	10^{-1}

The cost term associated with maximising the storage level is set to zero, $c_{ts} = 0$, as the company's operation do not require a minimum storage level for back-up energy since a production shortage is not likely when relying on fossil fuels. Whereas the weight associated with thermal energy dissipation, c_{δ}, is chosen substantially large as the solver should be discouraged by all means to waste energy and to ensure matching of supply and demand (see Table 7). In fact, it should be significantly larger than c_{share} as this term considers four optimisation variables and in principal will always be larger (if weight factors are selected in the same range).

The third weight, c_{diff}, penalises the changes in the (dis)charging rate over the time horizon. This cost factor is required to ensure smooth non-fluctuating results for the optimisation variables. If the objective would not account for storage usage, then the solver is free to select the storage behaviour (and thus device operation required to charge the storage) as long as demand does not approach or exceed total production capacity. When in that case the gas price varies, it does become interesting to operate the storage in a cost-effective manner. The pitfall here is that within the company model the gas price is fixed. For that reason, an artificial cost is installed on the storage. However, this weight should be considerably small compared to the other weights, so that flexibility in storage usage is maintained and the solver is still focused on optimising the variables related to the actual costs. This process involved trial and error before a suitable value was found: a weight small enough that it does not affect the outcome behaviour of the optimisation variables or the total cost but merely smooths the output. The iteration results of this trial and error process are displayed in Table 8. A value of $c_{\text{diff}} = 1.00E-01$ resulted in the lowest cost value without affecting the dissipation value. Also other optimisation variables were not affected.

Table 8: The iteration results in finding a suitable value for c_{diff}.

c_{δ}	c_{diff}	costs	sum(h^{δ})
$1.00E+12$	$1.00E-02$	162317	$-1.03E+03$
$1.00E+12$	$1.00E-01$	161986	$-1.03E+03$
$1.00E+12$	$1.00E+00$	166194	$-1.03E+03$

Similar reasoning applies to selecting an appropriate weight for the boiler heat produc-

tion sharing c_{share}: the weight should not be too large to affect the total boiler production to be significantly greater or smaller than demand but at the same time, it should be large enough to actually enforce equal boiler sharing in relation to the frequency of operation. The iteration results of this trial and error process are displayed in Table 9. A value of $c_{\text{diff}} = 1.00E-01$ resulted in the lowest cost value without affecting the dissipation value. Note that there is a trade-off between dissipation and boiler sharing: if the penalty on dissipation would be reduced, then this would result in a lower sum of violating the weighted boiler sharing constraints but at the same time the summed value of dissipated heat would increase substantially. It is considered more important to match demand and supply, than it is to approximate the weighted boiler sharing production.

Table 9: The iteration results in finding a suitable value for c_{share}.

c_δ	c_{share}	c_{diff}	costs	sum(sharing constraints)	sum(h^δ)
1.00E+12	1.00E+03	1.00E-01	162925	8.77E+05	-8.48E-07
1.00E+12	1.00E+02	1.00E-01	162925	8.77E+05	-8.59E-08
1.00E+12	1.00E+01	1.00E-01	162925	8.88E+05	-9.55E-09
1.00E+12	1.00E+00	1.00E-01	162887	1.88E+06	-1.60E-09
1.00E+12	1.00E-01	1.00E-01	162418	1.06E+07	-3.65E-10
1.00E+12	1.00E-02	1.00E-01	163123	8.54E+07	-1.96E-11

6.3 Model Validation

The procedure of backtesting is used to validate the model. Historical demand forecast data from February 2022 (with the exclusion of week 1 as in this week the CHP plant malfunctioned[19]) is fed to the solver and the simulation results are compared with the actual historical data. If the simulation and actual results are broadly similar and if the solver returns lower total costs, the model is considered to be valid. Before proceeding, a disclaimer regarding the accuracy of A2A's historical operational data should be mentioned.

6.3.1 Accuracy of Historical Operational Data

A couple of limitation regarding the historical data accuracy:

1. Previously, the company also managed the production by means of a solver. However, sometimes the operators decide to manage the devices differently from what the solver suggested to be the optimum, due to their operational experience (such as, which devices are in the geographic proximity to the demand, controlling the CO2 emissions per site, etc.). Therefore, it would be preferable to compare our solver results with the historical optimal results of A2A's solver. However, the company no longer has access to the solver data due to expiration of the license. A2A could only provide the historical data of how the operators decided to manage the devices.
2. Secondly, the sensors on the storage tank are defective. Consequently, there is no reliable record of the amount of energy stored and withdrawn from the storage units. Therefore, when comparing the simulation with the actual results, the storage tank is not considered.
3. Lastly, when analysing the historical company results, the data seem to be ambiguous because there are production shortfalls on a fairly regular basis. This is notable

[19] When there is no production, there are also no energy purchases. Hence, it would be an unfair comparison.

because at these time instants, the devices are not operating close to the maximum capacity to meet demand. This could be due to a number of reasons: (1) the data is incorrect due to, for example, malfunctioning storage tank sensors, (2) incorrect demand forecasting, (3) the proposed model does not match A2A's reality, or (4) the results are correct but the company is managing the operations inefficiently.

6.3.2 Backtest Set-up

The minimum and maximum bounds for the devices in the month February are provided in Table 10. Note that the minimum heat production of the CHP varies per month, the other bounds are irrespective of time.

Table 10: The bounds of the optimisation variables for the month February, 2022. In the proposed model the storage level W^{TS} is normalised. Hence, $W_m^{TS} = 0$ and $W_M^{TS} = 1$ with the initial storage level set at $W^{TS}(0) = 0$.

Lower bound	**[kWh]]**
h_m^{CHP}	11,716
$h_{1,m}^{GB}$	0
$h_{2,m}^{GB}$	0
$h_{3,m}^{GB}$	0
$h_{4,m}^{GB}$	0
W_m^{TS}	0
h_m^{TS}	-8,000
h_m^{δ}	0

Upper bound	**[kWh]**
h_M^{CHP}	15,387
$h_{1,M}^{GB}$	6,000
$h_{2,M}^{GB}$	12,000
$h_{3,M}^{GB}$	14,000
$h_{4,M}^{GB}$	14,000
W_M^{TS}	20,000
h_M^{TS}	8,000
h_M^{δ}	10,500

Company Experience: In the hours when demand is low, generally during the night, the minimum generation of thermal energy from the CHP and the external input from the biomass and waste plants is greater than the demand. To avoid heat dissipation, the excess heat is stored in the tank. Whereas, in the hours when demand is high, usually early in the morning, the tank is discharged and if necessary, the boilers supplement the remaining supply. Apart from that, regarding the February data, the first two weeks in February were normal cold weeks, while the other two weeks were uncommonly warmer for February.

Backtesting Procedure: The demand forecast for a two-day ahead schedule is inputted to the solver and an hourly solution for the optimisation variables is provided. For each optimisation step, the solver outputs $T = 48$ setpoints per optimisation variable. In practice, the company would implement the first 24 setpoints and thus these 24 setpoints are compared with the actual data. Subsequently, the time window shifts one day ahead per iteration with the demand forecast of day two of the previous iteration being updated and the forecast of the new day (i.e., day three) being added[20]. In addition, the initial condition of the optimisation variables are updated with each iteration by taking the value of the final implemented setpoint of the previous iteration (i.e., at T = 24). Apart from demand forecast, also the heat supply from the furnaces is provided by A2A. However, this data is provided just once without any updates. This procedure is repeated for all days in February: (1) input the (updated) forecast data, (2) update the initial conditions, (3) solve the problem for $T = 48$ timesteps, and (4) implement the first 24 setpoints.

[20]This implies that for each day the demand is predicted twice as there is a two-day ahead forecast and an updated one-day ahead forecast. The results of this updated one-day ahead forecast are implemented by the company.

This algorithm is summarised in algorithm *alg.* (1). Therefore, this backtesting procedure opts for a MPC-like approach as it uses a receding horizon approach and uses the final setpoint of the previous iteration as initial condition. However, the MPC framework usually implements just one setpoint and thus updates the data and solution per timestep more frequently. Whereas for the case of A2A, 24 setpoints are being implemented at once. Hence, it is not an actual MPC framework.

Algorithm 1: Algorithm for backtest simulations

```
Data: Demand forecast data, furnace data
Result: Optimised hourly device variables.
initialise x_0 ≥ 0;
days = length(February);
T = 48;
for i = 1 : days do
    if i == 1 then
        for k = 1 : T do
            Load furnace data h^WF, h^BF;
            Load demand forecast h^D;
            Solve problem (19)|_{k=1}^{T};
        end
        Implement x(1 : 24, i)
    else
        Update x_0 = x(24, i − 1);
        for i = 1 : T do
            Load furnace data h^WF, h^BF;
            Update demand forecast h^D;
            Solve problem (19)|_{k=1}^{T};
        end
        Implement x(1 : 24, i)
    end
end
```

Two experiments are conducted for the proposed company model,

1. Perform the backtest of simulations for company data in the month February, 2022.
2. Compare the simulation results and costs in experiment (1) with actual historical plant data. This will be elaborated in the following section.

6.3.3 The Backtest

When analysing the demand profile, it appears to be cyclical as visualised in Figure 17. In conjunction with this, the results for each day also evolve according to the same general pattern since production is matched to demand. Therefore, it is decided to address here the results of one specific day as analysis of the other days will lead to comparable results[21]. Specifically, the first day of the second week will be analysed as this was a normal cold February week.

[21] On request comparison results of all days can be provided, sissing.marleen@gmail.com.

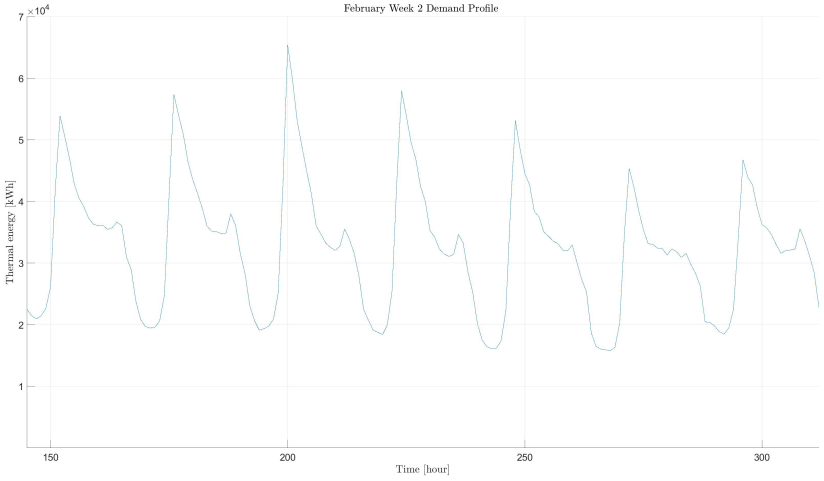

(a) Plot of demand profile of second week of February, 2022.

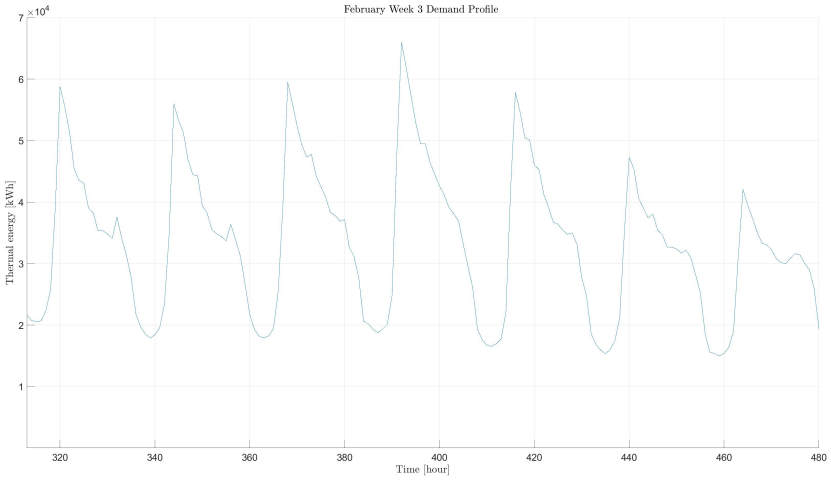

(b) Plot of demand profile of third week of February, 2022.

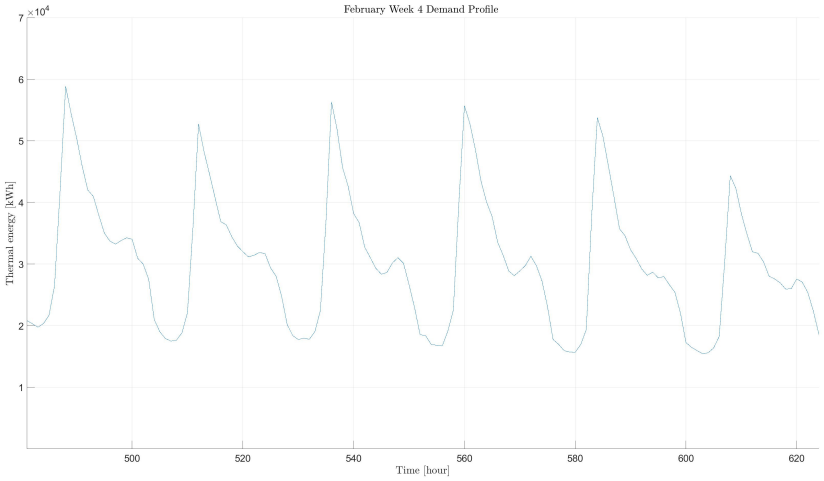

(c) Plot of demand profile of fourth week of February, 2022.

Figure 17: Visualisation of cyclical demand profile for the month February, 2022. To view the graphs more clearly, please zoom in.

Matching of Supply and Demand

When comparing the matching of supply and demand in Figure 18, it is notable that the simulation matches production and demand quite precisely for each time instant. Only for the first couple of hours there is a small production surplus, which is translated in a positive dissipation value to close the gap between production and demand. Dissipation occurs because the maximum charging rate is less than the minimum production: $h_M^{TS} < h^{BF} + h^{WF} + h_m^{CHP} + \sum_{i=1}^{4} h_{i,m}^{GB}$ (see Table 10). The input of the furnaces varies per timestep. On the other hand, the historical results show that the actual production has difficulty tracking demand, quite frequently production under- or overshoots the demand. These fluctuations are reflected in the dissipation, $h_{\text{A2A}}^{\delta} \neq 0$. These fluctuations may be caused due to the defective storage sensors, which result in incorrect recordings of h^{TS} or indicate the actual operational situation. In addition, there seems to be a shift in matching demand and supply when analysing the actual results of A2A, as the production lags demand by a timestep. However, when the production profile is shifted by one timestep to the left, there is still a substantial mismatch. Possibly, this mismatch could be caused by the faulty storage sensors, but this is a conjecture.

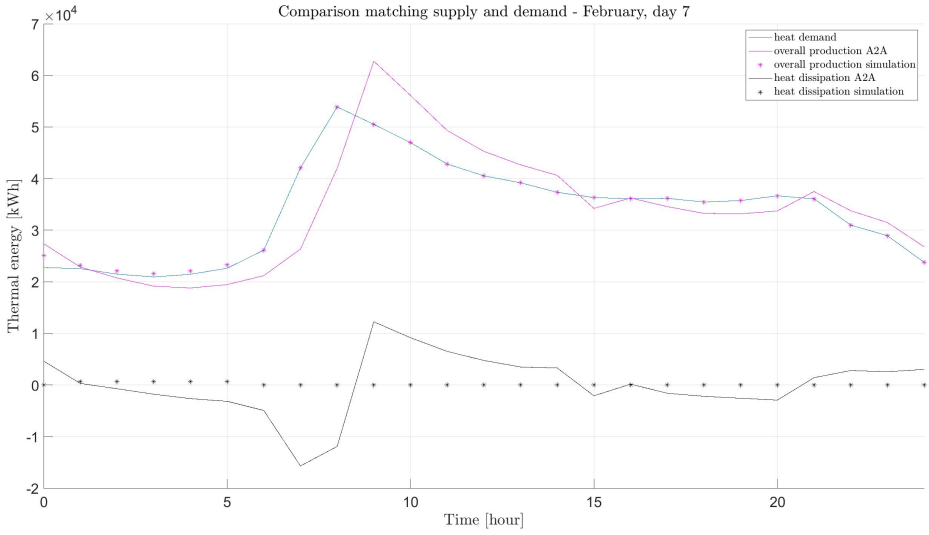

Figure 18: Visualisation of matching supply and demand for both the actual results and simulations results of day 7 in February, 2022. The total hourly production is the sum of $h^{CHP} + \sum_{i=1}^{4} h_i^{GB} + h^{BF} + h^{WF} - h^{TS}$. The hourly dissipation h^{δ} reflects the imbalance between production and demand, where $h^{\delta} < 0$ implies a production shortage and $h^{\delta} > 0$ implies excess heat.

Heat Production of the Devices

Figure 19 zooms more closely in on the heat produced to match supply to the demand. The production by the CHP and by each of the four boilers is considered. The (dis)charging rate is not included in here as there is no reliable record for the actual results of A2A. In Figure 19, the gap between simulated production and demand is closed by the supply from the furnaces and the storage tank (not depicted). Whereas the gap between actual production and demand is (partly) closed by the supply from the furnaces and the storage tank, for as far the latter is recorded correctly. It can be observed that the company does indeed respond to a change in demand with an operational lag. Especially, around peak demand in the morning. On the other hand, the simulations respond in advance to a change in demand. This indicates that the simulations track demand using the storage tank: more production (compared to the actual data) before demand increases to generate

back-up energy in the tank, and less production when there is an actual increase in demand because the tank is discharged.

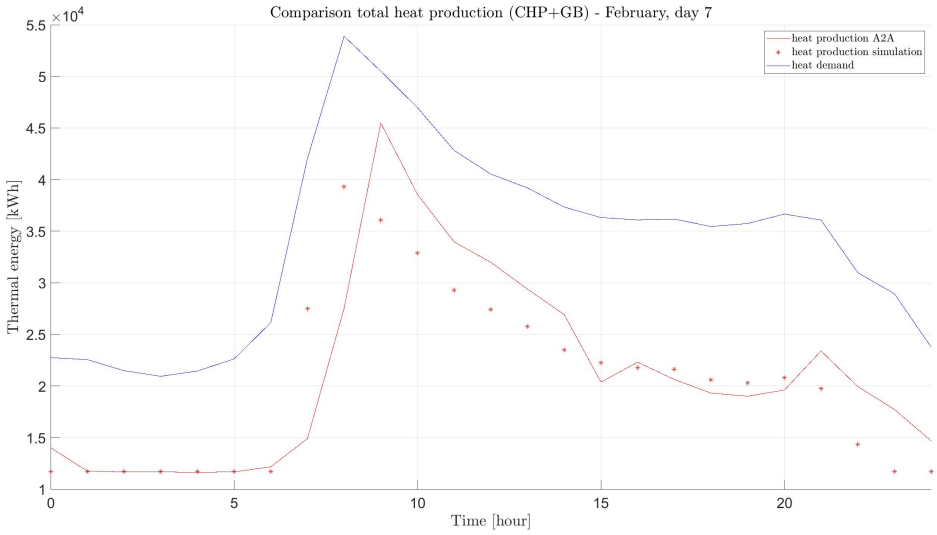

Figure 19: The amount of produced heat ($h^{CHP} + \sum_{i=1}^{4} h_i^{GB}$) for both the actual results and simulations results of day 7 in February, 2022.

Demonstration of Storage Tank Usage

By showing a plot of only simulation results, it can be demonstrated that indeed the storage tank is employed in the event of an imbalance between production and demand. When viewing Figure 20, the tank is filled in the mornings, when there is valley filling due to the minimum production being greater than demand. During day time, when demand is high, the tank is gradually discharged with total production graph slightly below demand. This results also in peak shaving of the boiler devices, displayed by the green graph in Figure 20. To view the individual boiler graphs view Figure 22. Therefore, it seems that production is always operating in a comfortable way not too much stressing the devices. Note that it is possible to fully discharge the tank as the solver considers also the demand profile for the next day[22]. Furthermore, boiler production is scaled up when demand increases as these operate with greater efficiency than the CHP. However, around $T = 8$ CHP production is scaled up because of a too costly violating of the boiler sharing as boiler 1 (Arata) is already operating at maximum capacity (view Table 10 and Figure 22).

[22]The control horizon is 24 timesteps, while the prediction horizon is 48 timesteps.

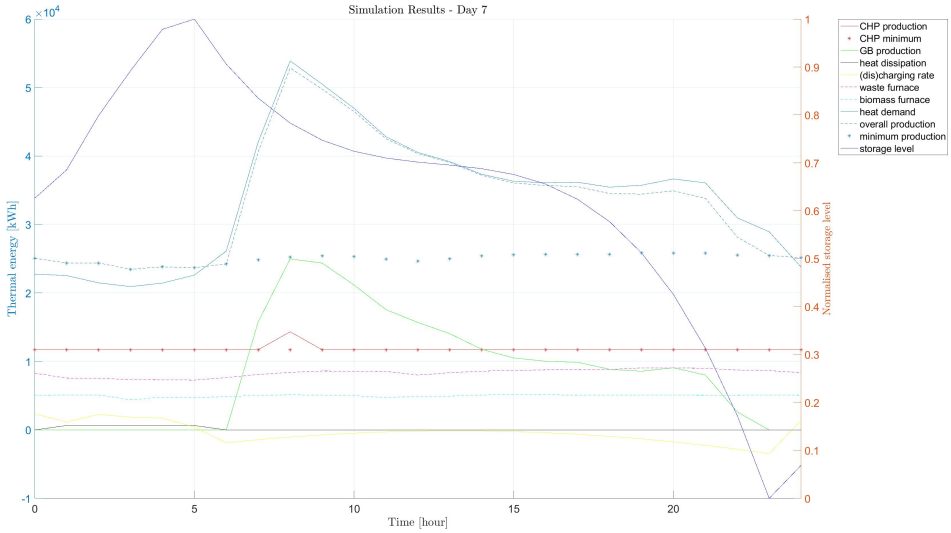

Figure 20: The simulation results of day 7 in February, 2022. This figure shows how the storage tank mitigates an imbalance between production and demand. Note that the green graph represent the total summed boiler production, $\sum_{i=1}^{4} h_i^{GB}$. To view the graph more clearly, please zoom in.

Individual Boiler Operation

Regarding the operation of the individual boilers, when comparing the simulated results of Figure 22 with the actual results of Figure 21, it is shown that the simulations make the individual boilers operate more comfortably and attempt to meet the enforced weighted boiler sharing. Whereas the actual results show more fluctuating behaviour for the boilers, alternating between scaling up and scaling down production. Moreover, total simulated boiler production is also considerably lower when the peak demand occurs at $T = 8$ which can be explained by the use of the storage tank, since the same minimum CHP operation and furnace inputs is considered in both the simulated and actual situation. However, the overall pattern of total boiler operation is similar for the simulation and actual case.

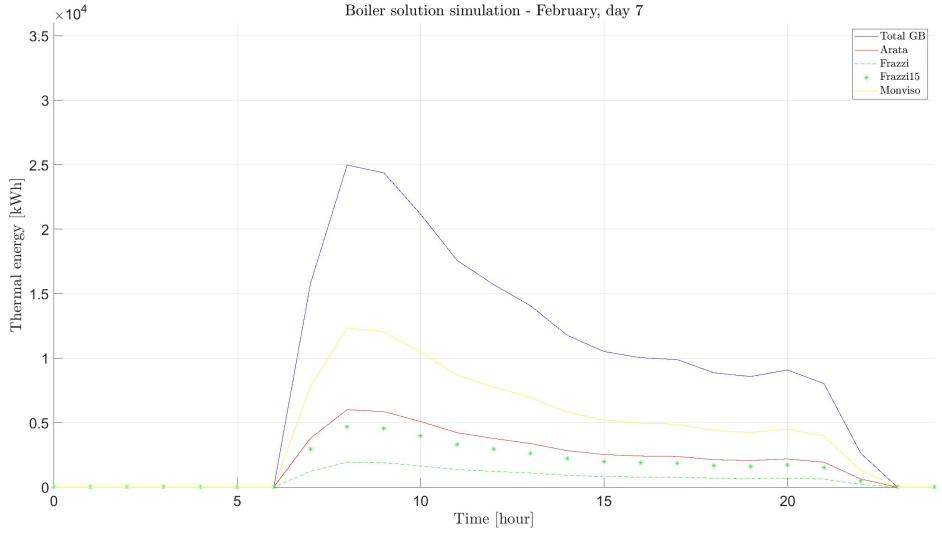

Figure 21: Plot of actual individual boiler results for day 7 of February, 2022. To view the graph more clearly, please zoom in.

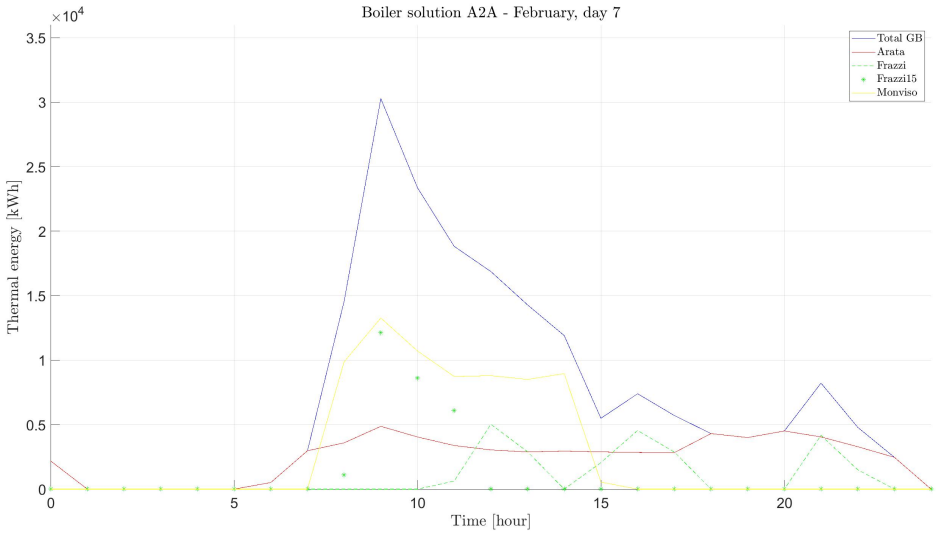

Figure 22: Plot of simulated individual boiler results for day 7 of February, 2022. To view the graph more clearly, please zoom in.

Energy Inputs and Outputs

When analysing the energy inputs and outputs, it is notable that the company operates the CHP to a greater extent compared to the simulation results. Instead, the simulations operate the boilers more. This is reflected in twofold: (1) greater amount of gas input for the actual results as depicted in Figure 23a because the CHP operates with a lower thermal efficiency than the boilers, and (2) the greater amount of electricity output caused by CHP production which is depicted in Figure 23c. More specifically, the hourly gas input for the actual results is substantially greater from $t = 9$ until the end of the day, even though the differences in total production between simulation and actual results, as depicted in Figure 18, is smaller. In fact, actual production is below simulated production between hours $t = 15$ and $t = 20$. However, the actual gas input is greater at these timesteps. This indicates that when peak demand occurs at $t = 8$, the company increases CHP operation considerably while the simulation increases boiler operation. This is also reflected in a steep increase in electricity output at $t = 8$ for the actual results, depicted in Figure 23c.

Furthermore, the electricity input depicted in Figure 23b reflect the boiler usage. During the first half of the day the simulation operates the boilers to a greater extent, while during peak demand the simulated boiler operation is below the actual operation. During the rest of the day, the operation of the simulated boilers is reduced more gradually compared to the actual results.

It seems that the company uses less of the storage tank since both CHP and boiler operation increases during peak demand. While in the simulation results only the boiler operation increases during peak demand with similar values (see Figure 21 and Figure 22). This indicates that in the simulations, instead of increased CHP production, the tank is discharged.

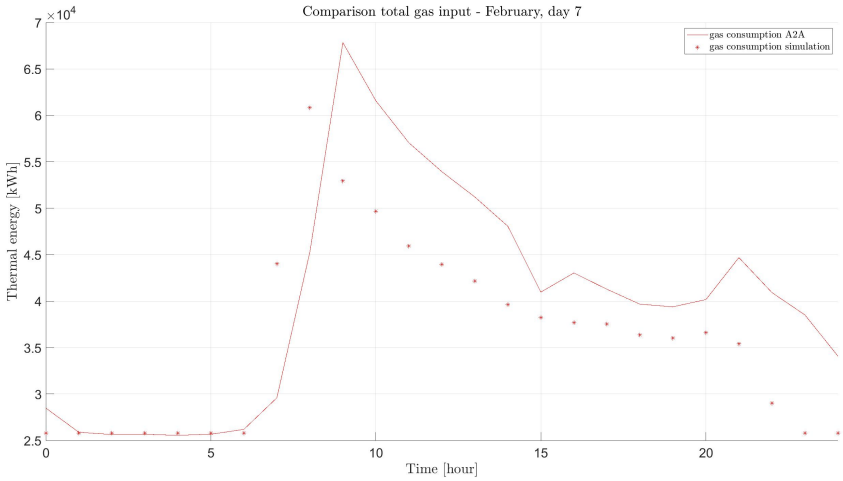

(a) Plot of hourly gas input for both the actual results and simulations results of day 7 in February, 2022.

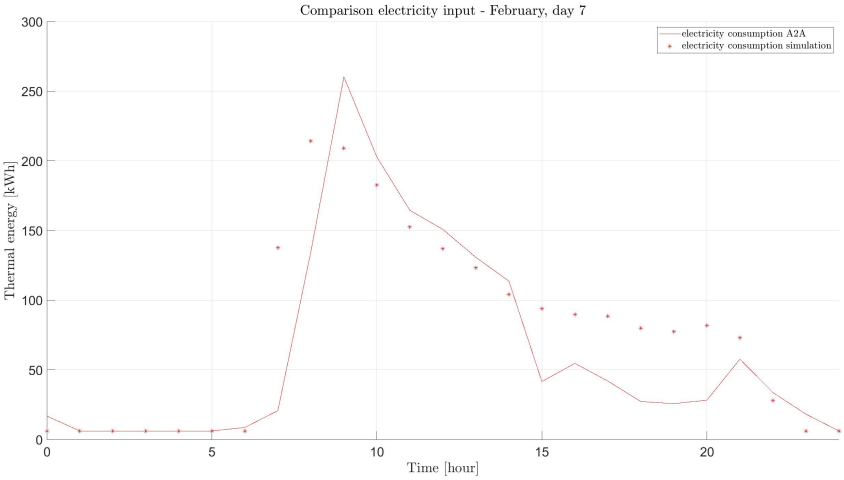

(b) Plot of hourly power input for both the actual results and simulations results of day 7 in February, 2022.

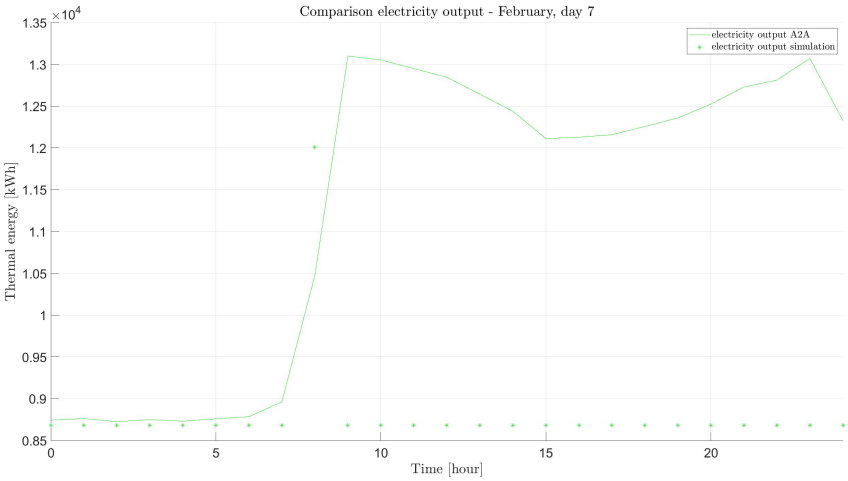

(c) Plot of hourly power output for both the actual results and simulations results of day 7 in February, 2022.

Figure 23: Visualisation of comparison results for the energy inputs and outputs for day 7 of February, 2022. To view the graphs more clearly, please zoom in.

Cost Comparison

When comparing the estimated hourly costs shown in Figure 24, it can be seen that these graphs are related to each other in the same way as the gas inputs for the simulation and actual results (see Figure 23a). This is reasonable because the gas purchases substantiate a significantly larger part of the total cost than the purchase and sale of electricity. Only a small amount of electricity is needed to operate the boilers and, moreover, the sale of electricity is less extensive than the purchase of gas.

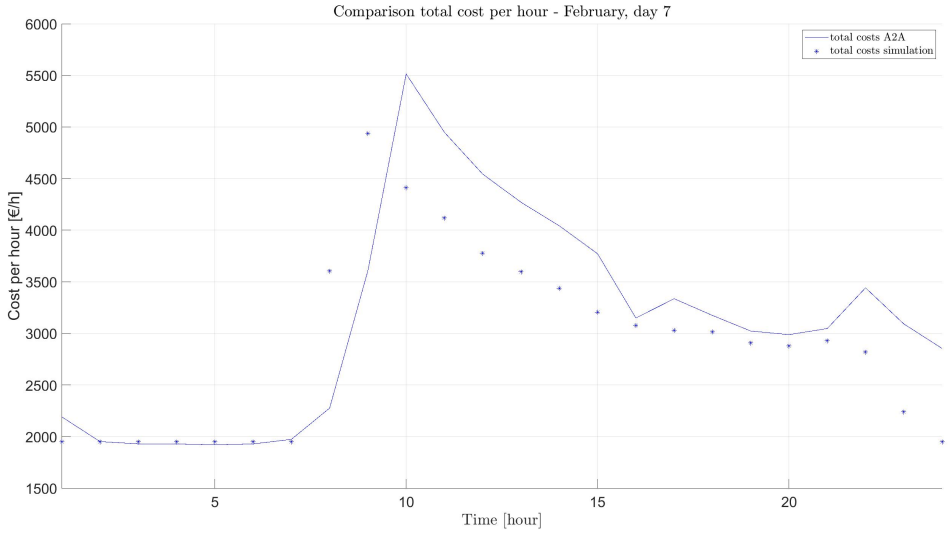

Figure 24: Plot of total hourly cost for both the actual results and simulations results of day 7 in February, 2022. In fact, the hourly actual cost is estimated from historical operational data using the same cost function (17) as for the estimated simulation costs.

When zooming out, looking at the estimated daily costs for weeks 2, 3 and 4, it fluctuates whether the actual data or the simulated data results in lower daily costs. These results are depicted in Figure 25. However, when summing the differences between simulation and actual cost for each day, it appears that the simulations lead to a cost reduction of 1.7%. In total, the cost savings are €24196 for the month February. This is a promising outcome, even though the cost analysis considers the results of only one month and more specifically, the results for the demand profile in winter period. Especially, when taking into account the frequent production shortages of the actual results (negative dissipation results as depicted in Figure 18) which imply less energy purchases. These productions shortages (i.e., not fulfilling demand) are not reflected in the costs. Moreover, the cost calculation does not account for excess heat dissipated into the air which in fact, imply lost revenues. In the actual company results, dissipation of excess heat appears on a regular basis (see Figure 18).

Despite these production shortfalls and the dissipation of excess heat for the actual company results (both not considered in the cost calculation), the simulated results still lead to a cost reduction. Furthermore, the company is already operating close to an optimum since the actual historical company data is also based on solver results. Thus, the proposed model shows better results than actual data that are already close to an optimum.

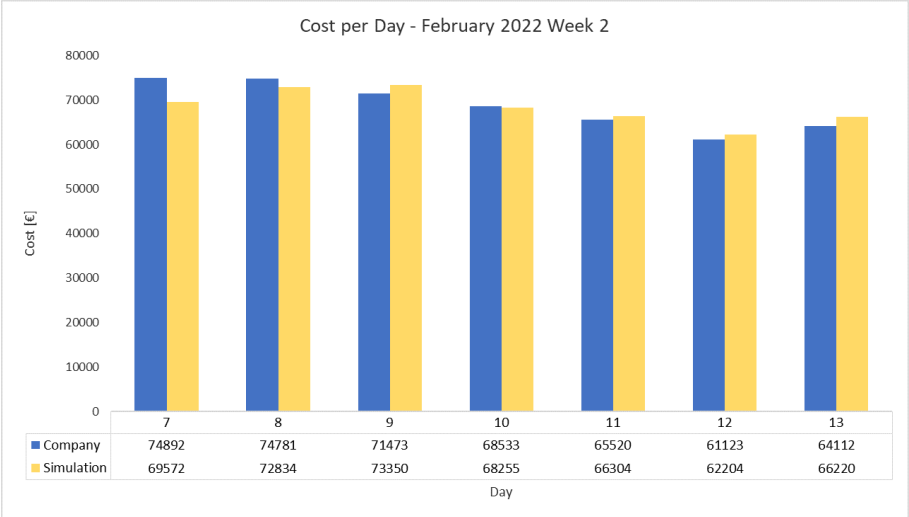

(a) Overview of estimated daily cost for week 2 of February, 2022.

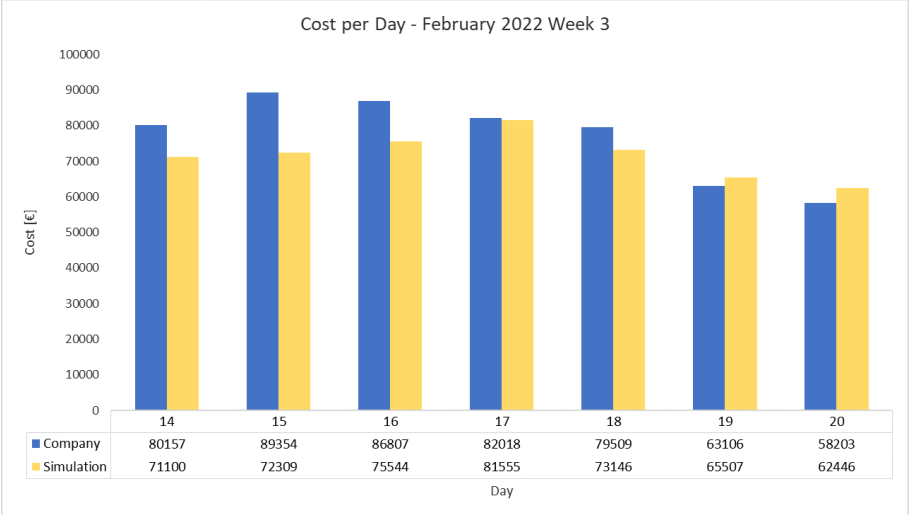

(b) Overview of estimated daily cost for week 3 of February, 2022.

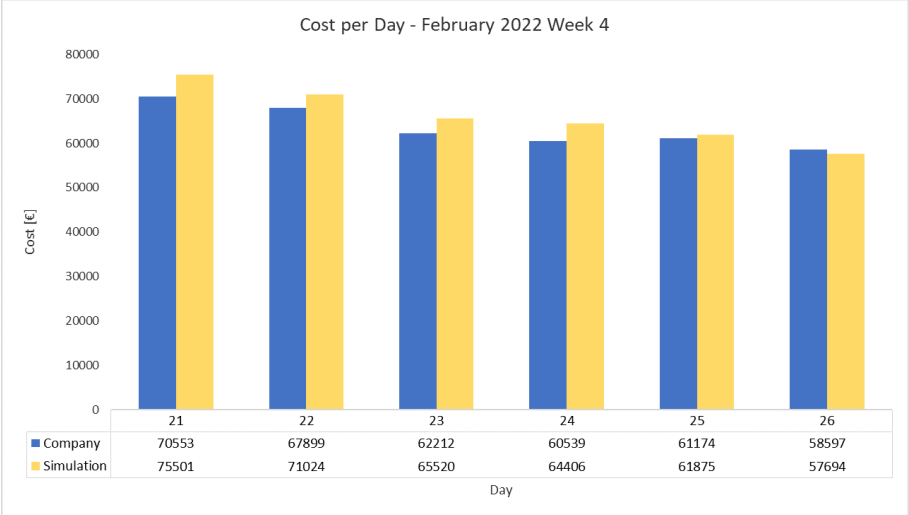

(c) Overview of estimated daily cost for week 4 of February, 2022.

Figure 25: Estimated daily cost of the simulations and actual data for weeks 2, 3, and 4 of February, 2022. The daily cost is computed with cost function (17). The results do not include day 27 and 28 of February because no demand profile is provided for these days. To view the graphs more clearly, please zoom in.

6.4 Discussion of Results

The proposed model anticipates demand by using the storage tank: pre-charging before a peak demand is expected, and gradually discharging when demand is high (see Figure 20). In this way, the demand profile is accurately tracked using both the production devices and the storage tank. Furthermore, the proposed model operates the devices more cost-effectively as upscaling boiler production is preferred over the less efficient CHP production. While the actual results show a more substantial CHP production in sufficing demand, compared to the simulation results. Moreover, actual production seems to lag behind demand and it is often the case that actual production under- or over-shoots demand (see Figure 18). The company has indicated that the storage sensors are defective. This might influence the actual results or at least, affect the accuracy of the comparison.

Furthermore, when focusing on the simulation results, it is noteworthy that the proposed model operates the storage tank and production devices in a comfortable way, not overloading the devices. Indeed, as expected, the storage tank is employed in the event of an imbalance between production and demand. Consequently, the proposed model adjusts production earlier to a change in demand as it accounts for future timesteps. In this way, the storage tank is charged prior to the peak demand.

Lastly, when comparing the estimated costs, it appears that the proposed model leads to a substantial cost saving of 1.7% (i.e., a cost reduction of €24196) for February. This cost reduction is relative to historical operating data that is already close to an optimum. Furthermore, the actual operating data show production shortages on a frequent basis, implying less energy purchases and thus, lower estimated costs. Even in this situation the proposed model leads to cost savings.

The cost calculation could be improved by including lost revenues from dissipated excess heat and penalising production shortages because then demand is not met. This would result in a fairer cost comparison since the actual results regularly show these phenomena (see Figure 18). Consequently, if these factors are also considered in the cost calculation, it is expected that this would result in further operational cost reductions by the proposed model since dissipation and production shortages hardly ever occur in the simulation results. Although the proposed model is promising, it should be noted that the conclusions are based on a one-month data comparison and on the demand profile in the winter period, while the demand and production for thermal energy is different in the summer.

7 Concluding Remarks

In this section, first the limitations of this research are discussed. Thereafter, options for further research are suggested which result from the limitations of this thesis. The section is finalised with the conclusion reflecting on the research goal and research questions stated in section 1.2, including an advise to the company.

7.1 Limitations

First, it should be noted that the company data is indistinct due to faulty storage sensors which limits the accuracy of the backtest and thus the assessment of the proposed model's performance. In addition, the cost calculation does not reflect the true cost as it does not take into account the lost revenue due to excess heat dissipated into the atmosphere, nor the consideration of a penalty if demand is not met. This would result in a fairer comparison, as these phenomena are observed in the analysis of actual company data. In addition, the model has only been tested for a demand profile in the winter period, while the demand profile and operations will be different for the hot summer months.

Also, parameter tuning of the artificial cost factors is done by means of trial and error as explained in section 6.2.

Furthermore, a number of model simplifications are assumed. The grid connections, heat distribution network, and consumer behaviour are excluded from the model. Also, a (dis)charging efficiency is neglected while it could be investigated in practice whether this is indeed justified. Moreover, once the CHP is activated in the winter period, it is kept in operation because it is an inefficient process and requires transmission time to alternately turn the CHP on and off. This dynamic is included in a limited way by assuming a lower bound greater than zero for CHP operation, while it could be modelled in more detail. In addition, the prioritisation of boiler operation is approximated but not exactly represented. The model prioritises the probability that each boiler will be operated (based on operating frequency) but this gives no assurance that the operator will also decide this way. Thus, this is a simplified approximation of the real situation.

At this moment, a centralised optimisation approach is used. This works out for the consideration of a single heating plant, yet when considering multiple heating plants computational time might become a problem.

The final recognised limitation is that the proposed model minimises the operational costs locally, but global optimality cannot be guaranteed due to the nonlinearity inherent in the objective cost function.

7.2 Further Work

As a first option for further research, the actual operational data should be recorded with more accuracy by replacing the storage sensors. In addition, the cost calculation should consider also the aspects of excess heat dissipation and not meeting demand due to production shortages. Moreover, the proposed model should be tested for multiple months, especially to incorporate seasonal (weather) changes. This would lead to a fairer comparison of the proposed model with the company's actual situation.

As explained in section 6.2, the factors associated with the artificial cost terms were fitted by means of trial and error. While more sophisticated methods are in place as well, such as genetic algorithms which are used to optimise model parameters[99] [100].

Apart from a fairer backtest, the model could also better approximate reality in a couple of ways. First of all, the geographical location of demand could be recorded by installing additional sensors in the network. This way, the prioritisation of boiler operation is better captured. In addition, the storage dynamics could be included with more detail by considering a storage efficiency. This requires the introduction of separate variables for charging and discharging to account for the individual efficiencies as explained in subsubsection 3.2.2, as well as the introduction of binary variables to ensure both cannot happen simultaneously. Ultimately, this would translate the problem into a mixed-integer program. As explained in section 2, a MIP would result in better solutions but also require more computational time. Furthermore, the difficulty and delay in scaling CHP production could be incorporated in the model by introducing constraints for ramping up and down CHP production [18]. Similarly, such constraints could also be considered to better represent the boiler operation.

Currently, with each 24 setpoints the solution is updated. However, if instead the solution was updated for each setpoint and system feedback is incorporated, the model would be able to respond quicker to disturbances or changes in actual demand. This approach is referred to as model predictive control (MPC) [70]. An MPC framework may reduce the costs to a greater extent compared to a day-ahead optimisation strategy but also requires more computational power [9]. In order to implement this framework, the demand profile should be updated more frequently.

Furthermore, the proposed model only considers the district heating plant while in reality this plant is part of a broader heating network. The scalability of the solver will be limited when also considering other elements of the heating network (transportation, grid connectionts, etc.) or the whole network in the model. At a certain point, the computational power of the solver will be too limited because optimisation in a centralised fashion is considered. Therefore, the model should optimise in a distributed fashion when considering the district heating network, as explained in section subsection 2.3.

As a final suggestion for further work, this thesis focused on optimising the operational side of the system: energy generation and storage. The consideration of controllable load and storage devices in the model provides more flexibility in matching supply and demand. While it is also possible to manage the demand side by incorporating policies such as smart energy tariffs to foster certain consumption behaviour. If it is possible to control the demand response, this would for instance improve the reliability of demand predictions [101] [102].

7.3 Conclusion

In section 1.1 the problem was defined as the limitation of insight regarding the design of an optimal operating scheme to minimise costs and energy waste for A2A's DH plant. First, the literature review introduced the major system components, applicable control methods, and theories used for the problem. Based on this, it was decided to approach A2A's DH plant as an energy hub. This led to the research goal of designing a control strategy aimed at hourly operational optimisation for a two-day ahead demand profile, including supply and demand matching.

The operational topology of A2A's DH plant was configured. Subsequently, this was translated into a mathematical model that describes the energy balancing relations, including the storage dynamics, and defines the capacity constraints. Using these equality and inequality constraints, cost values could be assigned to the different operations to formulate the objective cost function. Along with the actual operational costs, a number of artificial terms were introduced to enforce certain behaviour. These artificial cost factors are designed to discourage fluctuating (dis)charging behaviour over the time horizon thereby reinforcing gradual up- and downscaling of device usage, preventing excess heat dissipation, and fostering the weighted distribution of heat production across the boilers.

The proposed model is controlled using an interior point method with logarithmic barrier function following a central path (explained in section 4.3). This method allows specifying how precisely the formulated constraints should be satisfied. The operations are controlled with a two-day ahead optimisation strategy using demand profile predictions. The working of the algorithm was verified by testing the behaviour of the proposed model under simplistic case scenarios.

Eventually, the performance of the model was validated with backtesting. Simulations were performed on historical demand profile data provided by the company. The simulated results were compared with the actual operational data of that demand profile. It was found that the proposed model tracked demand more accurately, so that supply and demand were better matched. In addition, the model anticipated the demand profile and balances the thermal energy flows by using the storage tank. At the same time, this resulted in comfortable operations that did not overload the devices and thus, operational lifetime. Ultimately, the proposed model shows an improved operation compared to the current situation of A2A as costs are reduced.

For these reasons, the company is advised to optimally operate the devices using the proposed model as it leads to lower operational costs and improves operational performance. On top of integrating this proposed model into A2A's daily operational activities, it is also recommended to invest in sensors. Firstly, to repair the storage sensors so that the storage profile can be accurately recorded and used by the proposed model. Secondly, sensors should be installed on a larger scale throughout the network to get more detailed as well as more frequent data updates. This would provide opportunities to move from a two-day ahead optimisation strategy to feedback integration using model predictive control optimisation, which could improve results but also requires more computational power. This could lead to further reductions in operational costs as the model could respond more quickly to disturbances or changes in the system or demand profile. In addition, this also allows to identify where demand is coming from geographically, so that boiler operation can be adjusted accordingly by the model.

Returning to the goal defined in section 1.2, a control strategy employing two-day ahead operational optimisation based on demand forecast was successfully designed. Operational costs are minimised while demand is met. Further research could focus on expanding the proposed model by incorporating a MPC framework, considering the storage dynamics in more detail by translating the model into a mixed integer problem, and optimising in a distributed fashion so that the entire district heating network can be considered in the model, including demand-side management.

References

[1] Benjamin K Sovacool, Scott Victor Valentine, Malavika Jain Bambawale, Marilyn A Brown, Terezinha de Fátima Cardoso, Sayasat Nurbek, Gulimzhan Suleimenova, Jinke Li, Yang Xu, Anil Jain, et al. Exploring propositions about perceptions of energy security: An international survey. *Environmental science & policy*, 16:44–64, 2012.

[2] Stefan Pfenninger, Adam Hawkes, and James Keirstead. Energy systems modeling for twenty-first century energy challenges. *Renewable and Sustainable Energy Reviews*, 33:74–86, 2014.

[3] Martin Geidl and Goran Andersson. A modeling and optimization approach for multiple energy carrier power flow. In *2005 IEEE Russia Power Tech*, pages 1–7. IEEE, 2005.

[4] K Hemmes, JL Zachariah-Wolf, M Geidl, and G Andersson. Towards multi-source multi-product energy systems. *International Journal of Hydrogen Energy*, 32(10-11):1332–1338, 2007.

[5] Mohammad Mohammadi, Younes Noorollahi, Behnam Mohammadi-Ivatloo, and Hossein Yousefi. Energy hub: From a model to a concept–a review. *Renewable and Sustainable Energy Reviews*, 80:1512–1527, 2017.

[6] Enerdata. Global - energy statistics yearbook, 2022. `https://energydata.info/dataset/key-world-energy-statistics-enerdata` [accessed: 14 March 2022].

[7] Faeze Brahman, Masoud Honarmand, and Shahram Jadid. Optimal electrical and thermal energy management of a residential energy hub, integrating demand response and energy storage system. *Energy and Buildings*, 90:65–75, 2015.

[8] Marie Münster, Poul Erik Morthorst, Helge V Larsen, Lars Bregnbæk, Jesper Werling, Hans Henrik Lindboe, and Hans Ravn. The role of district heating in the future danish energy system. *Energy*, 48(1):47–55, 2012.

[9] Jonathan Reynolds, Muhammad Waseem Ahmad, and Yacine Rezgui. District heating energy generation optimisation considering thermal storage. In *2018 IEEE International Conference on Smart Energy Grid Engineering (SEGE)*, pages 330–335. IEEE, 2018.

[10] Behrang Talebi, Parham A Mirzaei, Arash Bastani, and Fariborz Haghighat. A review of district heating systems: modeling and optimization. *Frontiers in Built Environment*, 2:22, 2016.

[11] Ioan Sarbu, Matei Mirza, and Emanuel Crasmareanu. A review of modelling and optimisation techniques for district heating systems. *International Journal of Energy Research*, 43(13):6572–6598, 2019.

[12] Yang Cao, Wei Wei, Jianhui Wang, Shengwei Mei, Miadreza Shafie-khah, and Joao PS Catalao. Capacity planning of energy hub in multi-carrier energy networks: A data-driven robust stochastic programming approach. *IEEE Transactions on Sustainable Energy*, 11(1):3–14, 2018.

[13] Sijia Geng, Maria Vrakopoulou, and Ian A Hiskens. Optimal capacity design and operation of energy hub systems. *Proceedings of the IEEE*, 108(9):1475–1495, 2020.

[14] Jijun Zhou, Song Deng, WD Turner, DE Claridge, and JS Haberl. Improving boiler efficiency modeling based on ambient air temperature. In *Thirteenth Symposium on Improving Building Systems in Hot and Humid Climates*. Energy Systems Laboratory (http://esl. tamu. edu), 2002.

[15] Roel J Wieringa. *Design science methodology for information systems and software engineering*. Springer, 2014.

[16] Jiakun Fang, Qing Zeng, Xiaomeng Ai, Zhe Chen, and Jinyu Wen. Dynamic optimal energy flow in the integrated natural gas and electrical power systems. *IEEE Transactions on Sustainable Energy*, 9(1):188–198, 2017.

[17] Meryem Terhan and Kemal Comakli. Energy and exergy analyses of natural gas-fired boilers in a district heating system. *Applied Thermal Engineering*, 121:380–387, 2017.

[18] Hrvoje Dorotić, Tomislav Pukšec, and Neven Duić. Analysis of displacing natural gas boiler units in district heating systems by using multi-objective optimization and different taxing approaches. *Energy Conversion and Management*, 205:112411, 2020.

[19] Xuezhi Liu and Pierluigi Mancarella. Modelling, assessment and sankey diagrams of integrated electricity-heat-gas networks in multi-vector district energy systems. *Applied Energy*, 167:336–352, 2016.

[20] Martin Geidl and Göran Andersson. Optimal power flow of multiple energy carriers. *IEEE Transactions on power systems*, 22(1):145–155, 2007.

[21] Martin Geidl, Gaudenz Koeppel, Patrick Favre-Perrod, Bernd Klockl, Goran Andersson, and Klaus Frohlich. Energy hubs for the future. *IEEE power and energy magazine*, 5(1):24–30, 2006.

[22] Xinhui Lu, Zhaoxi Liu, Li Ma, Lingfeng Wang, Kaile Zhou, and Nanping Feng. A robust optimization approach for optimal load dispatch of community energy hub. *Applied Energy*, 259:114195, 2020.

[23] Alessandra Parisio, Carmen Del Vecchio, and Alfredo Vaccaro. A robust optimization approach to energy hub management. *International Journal of Electrical Power & Energy Systems*, 42(1):98–104, 2012.

[24] Tengfei Ma, Junyong Wu, and Liangliang Hao. Energy flow modeling and optimal operation analysis of the micro energy grid based on energy hub. *Energy conversion and management*, 133:292–306, 2017.

[25] I González-Pino, E Pérez-Iribarren, A Campos-Celador, J Terés-Zubiaga, and J Las-Heras-Casas. Modelling and experimental characterization of a stirling engine-based domestic micro-chp device. *Energy Conversion and Management*, 225:113429, 2020.

[26] AD Hawkes and MA Leach. Cost-effective operating strategy for residential micro-combined heat and power. *Energy*, 32(5):711–723, 2007.

[27] Risto Lahdelma and Henri Hakonen. An efficient linear programming algorithm for combined heat and power production. *European Journal of Operational Research*, 148(1):141–151, 2003.

[28] Y Chorfi. *Optimal control of a micro gas grid with asynchronous information exchange*. PhD thesis, Faculty of Science and Engineering, 2016.

[29] Gunn Kristine Holst Larsen. Distributed control of a network with multiple electricity producers and consumers. *University of Groningen Library][Host]*, 2014.

[30] Yanjuan Yu, Hongkun Chen, Lei Chen, Cheng Chen, and Jun Wu. Optimal operation of the combined heat and power system equipped with power-to-heat devices for the improvement of wind energy utilization. *Energy Science & Engineering*, 7(5):1605–1620, 2019.

[31] Thomas Nuytten, Bert Claessens, Kristof Paredis, Johan Van Bael, and Daan Six. Flexibility of a combined heat and power system with thermal energy storage for district heating. *Applied energy*, 104:583–591, 2013.

[32] Ralph Evins, Kristina Orehounig, Viktor Dorer, and Jan Carmeliet. New formulations of the 'energy hub'model to address operational constraints. *Energy*, 73:387–398, 2014.

[33] Yunus A Cengel et al. *Introduction to thermodynamics and heat transfer*, volume 846. McGraw-Hill New York, 1997.

[34] Yasuhiro Hamada, Makoto Nakamura, Hideki Kubota, Kiyoshi Ochifuji, Mitsunori Murase, and Ryuichiro Goto. Field performance of a polymer electrolyte fuel cell for a residential energy system. *Renewable and Sustainable Energy Reviews*, 9(4):345–362, 2005.

[35] Arun Kumar and SK Shukla. A review on thermal energy storage unit for solar thermal power plant application. *Energy Procedia*, 74:462–469, 2015.

[36] Elisa Guelpa and Vittorio Verda. Thermal energy storage in district heating and cooling systems: A review. *Applied Energy*, 252:113474, 2019.

[37] Ioan Sarbu and Calin Sebarchievici. A comprehensive review of thermal energy storage. *Sustainability*, 10(1):191, 2018.

[38] Yulong Zhao, Shixue Wang, Minghui Ge, Yanzhe Li, and Zhaojun Liang. Analysis of thermoelectric generation characteristics of flue gas waste heat from natural gas boiler. *Energy Conversion and Management*, 148:820–829, 2017.

[39] Fengguo Liu, Longfeng Zheng, and Rui Zhang. Emissions and thermal efficiency for premixed burners in a condensing gas boiler. *Energy*, 202:117449, 2020.

[40] Janusz Bujak. Mathematical modelling of a steam boiler room to research thermal efficiency. *Energy*, 33(12):1779–1787, 2008.

[41] MC Barma, Rahman Saidur, SMA Rahman, A Allouhi, BA Akash, and Sadiq M Sait. A review on boilers energy use, energy savings, and emissions reductions. *Renewable and Sustainable Energy Reviews*, 79:970–983, 2017.

[42] Yu Huang, Weiting Zhang, Kai Yang, Weizhen Hou, and Yiran Huang. An optimal scheduling method for multi-energy hub systems using game theory. *Energies*, 12(12):2270, 2019.

[43] Vahid Davatgaran, Mohsen Saniei, and Seyed Saeidollah Mortazavi. Optimal bidding strategy for an energy hub in energy market. *Energy*, 148:482–493, 2018.

[44] Qingsen Cai, XingQi Luo, Peng Wang, Chunyang Gao, and Peiyu Zhao. Hybrid model-driven and data-driven control method based on machine learning algorithm in energy hub and application. *Applied Energy*, 305:117913, 2022.

[45] Michał Leśko, Wojciech Bujalski, and Kamil Futyma. Operational optimization in district heating systems with the use of thermal energy storage. *Energy*, 165:902–915, 2018.

[46] Stephen Boyd, Stephen P Boyd, and Lieven Vandenberghe. *Convex optimization*. Cambridge university press, 2004.

[47] Mahmoud Elkazaz, Mark Sumner, and David Thomas. Energy management system for hybrid pv-wind-battery microgrid using convex programming, model predictive and rolling horizon predictive control with experimental validation. *International Journal of Electrical Power & Energy Systems*, 115:105483, 2020.

[48] Zhenning Pan, Tao Yu, Jie Li, Kaiping Qu, and Bo Yang. Risk-averse real-time dispatch of integrated electricity and heat system using a modified approximate dynamic programming approach. *Energy*, 198:117347, 2020.

[49] Somayeh Moazeni, Amir H Miragha, and Boris Defourny. A risk-averse stochastic dynamic programming approach to energy hub optimal dispatch. *IEEE Transactions on Power Systems*, 34(3):2169–2178, 2018.

[50] Hanchen Zhang, Qing Cao, Hong Gao, Peng Wang, Weijiang Zhang, and Nasser Yousefi. Optimum design of a multi-form energy hub by applying particle swarm optimization. *Journal of Cleaner Production*, 260:121079, 2020.

[51] Alaa Farah, Hamdy Hassan, Kenichi Kawabe, and Toshiya Nanahara. Optimal planning of multi-carrier energy hub system using particle swarm optimization. In *2019 IEEE Innovative Smart Grid Technologies-Asia (ISGT Asia)*, pages 3820–3825. IEEE, 2019.

[52] Dirk Den Hertog. *Interior point approach to linear, quadratic and convex programming: algorithms and complexity*, volume 277. Springer Science & Business Media, 2012.

[53] Florian A Potra and Stephen J Wright. Interior-point methods. *Journal of computational and applied mathematics*, 124(1-2):281–302, 2000.

[54] Eduardo F Camacho and Carlos Bordons. Nonlinear model predictive control. In *Model Predictive control*, pages 249–288. Springer, 2007.

[55] Alberto Bemporad and Manfred Morari. Control of systems integrating logic, dynamics, and constraints. *Automatica*, 35(3):407–427, 1999.

[56] Laurence A Wolsey. Mixed integer programming. *Wiley Encyclopedia of Computer Science and Engineering*, pages 1–10, 2007.

[57] Mohammad Chehreghani Bozchalui, Syed Ahsan Hashmi, Hussin Hassen, Claudio A Canizares, and Kankar Bhattacharya. Optimal operation of residential energy hubs in smart grids. *IEEE Transactions on Smart Grid*, 3(4):1755–1766, 2012.

[58] Chengcheng Shao, Xifan Wang, Mohammad Shahidehpour, Xiuli Wang, and Biyang Wang. An milp-based optimal power flow in multicarrier energy systems. *IEEE Transactions on Sustainable Energy*, 8(1):239–248, 2016.

[59] Amirhossein Dolatabadi, Mohammad Jadidbonab, and Behnam Mohammadi-ivatloo. Short-term scheduling strategy for wind-based energy hub: a hybrid stochastic/igdt approach. *IEEE Transactions on Sustainable Energy*, 10(1):438–448, 2018.

[60] Mousa Marzband, Andreas Sumper, José Luis Domínguez-García, and Ramon Gumara-Ferret. Experimental validation of a real time energy management system for microgrids in islanded mode using a local day-ahead electricity market and minlp. *Energy Conversion and Management*, 76:314–322, 2013.

[61] Andrea Lodi. Mixed integer programming computation. In *50 years of integer programming 1958-2008*, pages 619–645. Springer, 2010.

[62] Yurii Nesterov. *Introductory lectures on convex optimization: A basic course*, volume 87. Springer Science & Business Media, 2003.

[63] Frederick S Hillier and Gerald J Lieberman. Introduction to operations research. *Operations Research*, 4(1), 1974.

[64] Nicolas Lefebure, Mohammad Khosravi, Mathias Hudoba de Badyn, Felix Bünning, John Lygeros, Colin Jones, and Roy S Smith. Distributed model predictive control of buildings and energy hubs. *Energy and Buildings*, page 111806, 2022.

[65] Martin Rohden, Andreas Sorge, Marc Timme, and Dirk Witthaut. Self-organized synchronization in decentralized power grids. *Physical review letters*, 109(6):064101, 2012.

[66] Eduardo F Camacho and Carlos Bordons Alba. *Model predictive control*. Springer science & business media, 2013.

[67] Manfred Morari and Jay H Lee. Model predictive control: past, present and future. *Computers & Chemical Engineering*, 23(4-5):667–682, 1999.

[68] David Q Mayne, James B Rawlings, Christopher V Rao, and Pierre OM Scokaert. Constrained model predictive control: Stability and optimality. *Automatica*, 36(6):789–814, 2000.

[69] Jacob Mattingley, Yang Wang, and Stephen Boyd. Receding horizon control. *IEEE Control Systems Magazine*, 31(3):52–65, 2011.

[70] Michele Arnold, Rudy R Negenborn, Goran Andersson, and Bart De Schutter. Model-based predictive control applied to multi-carrier energy systems. In *2009 IEEE power & energy society general meeting*, pages 1–8. IEEE, 2009.

[71] Jorn K Gruber, F Huerta, P Matatagui, and M Prodanović. Advanced building energy management based on a two-stage receding horizon optimization. *Applied energy*, 160:194–205, 2015.

[72] DP Bloomfield and DJ Fisk. The optimisation of intermittent heating for variable efficiency heating systems. *Energy and Buildings*, 3(4):295–301, 1981.

[73] Desti Alkano. *Two-layer distributed optimal control for energy system integration.* PhD thesis, Ph. D. dissertation, University of Groningen, Netherlands, 2016.

[74] CY Zheng, JY Wu, XQ Zhai, and RZ Wang. A novel thermal storage strategy for cchp system based on energy demands and state of storage tank. *International Journal of Electrical Power & Energy Systems*, 85:117–129, 2017.

[75] Mi-Soo Shin, Hey-Suk Kim, Dong-Soon Jang, Sang-Nam Lee, Young-Soo Lee, and Hyung-Gi Yoon. Numerical and experimental study on the design of a stratified thermal storage system. *Applied thermal engineering*, 24(1):17–27, 2004.

[76] Olfa Abdelhak, Hatem Mhiri, and Philippe Bournot. Cfd analysis of thermal stratification in domestic hot water storage tank during dynamic mode. In *Building Simulation*, volume 8, pages 421–429. Springer, 2015.

[77] Nyoman Gunantara. A review of multi-objective optimization: Methods and its applications. *Cogent Engineering*, 5(1):1502242, 2018.

[78] Seyedeh Zahra Mirjalili, Seyedali Mirjalili, Shahrzad Saremi, Hossam Faris, and Ibrahim Aljarah. Grasshopper optimization algorithm for multi-objective optimization problems. *Applied Intelligence*, 48(4):805–820, 2018.

[79] Michael TM Emmerich and André H Deutz. A tutorial on multiobjective optimization: fundamentals and evolutionary methods. *Natural computing*, 17(3):585–609, 2018.

[80] Edward O'Dwyer, Luciano De Tommasi, Konstantinos Kouramas, Marcin Cychowski, and Gordon Lightbody. Prioritised objectives for model predictive control of building heating systems. *Control Engineering Practice*, 63:57–68, 2017.

[81] Arthur Richards and Jonathan How. Mixed-integer programming for control. In *Proceedings of the 2005, American Control Conference, 2005.*, pages 2676–2683. IEEE, 2005.

[82] Francesco Bullo. *Lectures on network systems*, volume 1. Kindle Direct Publishing Santa Barbara, CA, 2019.

[83] Ziang Zhang and Mo-Yuen Chow. Convergence analysis of the incremental cost consensus algorithm under different communication network topologies in a smart grid. *IEEE Transactions on power systems*, 27(4):1761–1768, 2012.

[84] Sundaram Vanka, Martin Haenggi, and Vijay Gupta. Convergence speed of the consensus algorithm with interference and sparse long-range connectivity. *IEEE Journal of Selected Topics in Signal Processing*, 5(4):855–865, 2011.

[85] M Huneault and Francisco D Galiana. A survey of the optimal power flow literature. *IEEE transactions on Power Systems*, 6(2):762–770, 1991.

[86] Rui Li, Wei Wei, Shengwei Mei, Qinran Hu, and Qiuwei Wu. Participation of an energy hub in electricity and heat distribution markets: An mpec approach. *IEEE Transactions on Smart Grid*, 10(4):3641–3653, 2018.

[87] Michael T Heath. *Scientific Computing: An Introductory Survey, Revised Second Edition*. SIAM, 2018.

[88] JS Arora. Arora, j, s. introduction to optimum design, 2012.

[89] Johan Lofberg. Yalmip: A toolbox for modeling and optimization in matlab. In *2004 IEEE international conference on robotics and automation (IEEE Cat. No. 04CH37508)*, pages 284–289. IEEE, 2004.

[90] Mathworks. Choosing the algorithm, 2022. `https://nl.mathworks.com/help/optim/ug/choosing-the-algorithm.html#bsbwxm7` [accessed: 03 March 2022].

[91] Gurobi Optimization. Inc., gurobi optimizer reference manual, 2020.

[92] Mathworks. fmincon, find minimum of constrained nonlinear multivariable function, 2022. `https://nl.mathworks.com/help/optim/ug/fmincon.html` [accessed: 03 March 2022].

[93] Mathworks. Constrained nonlinear optimization algorithms, 2022. `https://nl.mathworks.com/help/optim/ug/constrained-nonlinear-optimization-algorithms.html#brnpd5f` [accessed: 07 April 2022].

[94] Johan Verbeke and Ronald Cools. The newton-raphson method. *International Journal of Mathematical Education in Science and Technology*, 26(2):177–193, 1995.

[95] Anthony L Peressini, Francis E Sullivan, and Jerry J Uhl Jr. *The mathematics of nonlinear programming*. Springer-Verlag, 1988.

[96] Yinyu Ye. *Interior point algorithms: theory and analysis*, volume 44. John Wiley & Sons, 2011.

[97] Tamás Terlaky. *Interior point methods of mathematical programming*, volume 5. Springer Science & Business Media, 2013.

[98] Global Petrol Prices. Italy fuel prices, electricity prices, natural gas prices, 2022. `https://www.globalpetrolprices.com/Italy/` [accessed: 12 February 2022].

[99] John McCall. Genetic algorithms for modelling and optimisation. *Journal of computational and Applied Mathematics*, 184(1):205–222, 2005.

[100] QJ Wang. Using genetic algorithms to optimise model parameters. *Environmental Modelling & Software*, 12(1):27–34, 1997.

[101] Peter Palensky and Dietmar Dietrich. Demand side management: Demand response, intelligent energy systems, and smart loads. *IEEE transactions on industrial informatics*, 7(3):381–388, 2011.

[102] IEEE. *Distributed MPC applied to power demand side control*, 2013.

Appendix A

A Demonstration for Scenario I.B

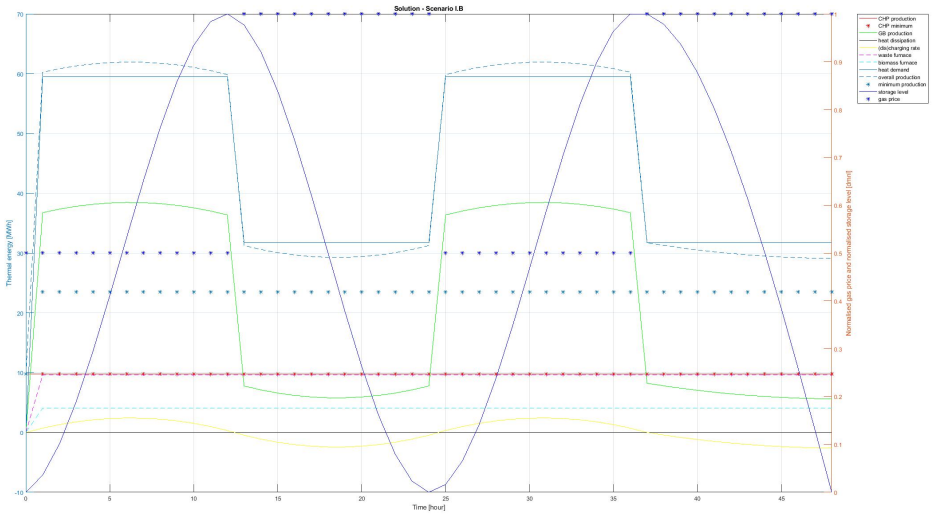

Figure 26: The solution for the optimisation variables returned by the solver at each time instant by rerunning scenario I.B with adjusted demand $\{h^D \in [31.713; 59.536]\}$. Note that the values for the gas price and the storage level can be read off from the y-axis on the RHS. The gas price is displayed in a normalised fashion, similar as for the storage level. Hence, both $W^{TS}, c_g \in [0, 1]$. The associated total cost equals €126,917.